# FIREURISK - DEVELOPING A HOLISTIC, RISK-WISE STRATEGY FOR EUROPEAN WILDFIRE MANAGEMENT

| | |
|---|---|
| **Grant Agreement Number: 101003890**<br>**Call identifier:** H2020-LC-CLA-2018-2019-2020 | |
| **Topic:** | LC-CLA-15-2020<br>Forest Fires risk reduction: towards an integrated fire management approach in the E.U. |
| **Instrument:** | RIA |

# D2.5 – Online modelling tool for extreme fire behaviour and smoke emission and dispersion

| | |
|---|---|
| **Deliverable Identifier:** | D2.5 |
| **Deliverable Due Date:** | 31/03/2024 |
| **Deliverable Submission Date:** | 21/05/2024 |
| **Deliverable Version:** | v.0.5 |
| **Lead partner:** | University of Aveiro |
| **Authors:** | Ana Isabel Miranda, Andrii Bilous, Carla Gama, Carlos Ribeiro, Carlos Viegas, Catarina Afonso, Célia Gouveia, Diogo Lopes, Domingos Xavier Viegas, Dmytro Holiaka, Martin Wooster, Rita |

This project has received funding from the European Union's Horizon 2020 research and innovation programme under grant agreement No 101003890.

| | |
|---|---|
| | Durão, Sergiy Zibtsev, Tobias Osswald, Vadim Bogomolov, Vera Rodrigues, Viktor Myroniuk |
| **Work Package:** | WP2 – Risk reduction to improve protection |
| **Task:** | Task 2.3 - Improve response to reduce risk of high-impact fires name |
| **Dissemination Level:** | ☒ PU: Public<br>☐ CO: Confidential, only for members of the Consortium (including the Commission Services) |

## Revision History

| Version | Date | Edited by | Description |
|---|---|---|---|
| v.0.1 | 15/12/2023 | UAVR | Document Content outline / structure |
| v.0.2 | 27/01/2024 | UAVR | Draft version |
| v.0.3 | 28/03/2024 | UAVR | Complete version formatted according to template |
| v.0.4 | 29/04/2024 | SAFE and AUTH | Complete draft review by WP2 Leader and internal reviewers |
| v.0.5 | 21/05/2024 | UAVR | Final version submitted |

## Quality Control

| Type | Date | Reviewed by | Approved/Comment |
|---|---|---|---|
| Internal | 29/04/2024 | Sébastien Lahaye (SAFE) | Approved with minor changes suggested |
| Internal | 24/04/2024 | Vassiliki Varela (AUTH) | Approved with minor changes suggested |
| Internal (QRB) | 24/05/2024 | Stefan Doerr (SU – QRB) | Approved |

Copyright © FirEUrisk Consortium. All rights reserved.

## Executive Summary

This deliverable describes the FirEURisk's numerical modelling systems, which were developed in the scope of Task 2.3 - Improve response to reduce risk of high-impact fires, and it is based on activities A2.3.1 (Extreme fire behavior modelling) and A2.3.2 (Smoke modelling and health impact). These systems aim at simulating extreme fire behavior and smoke emission and dispersion considering the most recent scientific/technical advances on fire spread, smoke emission and dispersion models as well as mathematical functions to estimate human exposure and health effects (on population and firefighters).

Available fire progression, fire emissions and smoke dispersion models were reviewed to identify modelling approaches adequate to be part of FirEURisk. The selected models and approaches were applied to FirEURisk Demonstration and Pilot Sites to better characterise their characteristics and performance. The successful application of modelling tools to FirEURisk case studies, such as Ukraine (DS5), Portugal (PS3) and Greece (PS5) allowed identifying their main potentialities and adapting them to be integrated into the FirEURisk smoke modelling system.

Two integrated modelling systems, IMFIRE-DISPERFIRE and DISPERFIRE-CHIMERE, have been developed to simulate fire spread and smoke at local and regional scales, respectively. IMFIRE-DISPERFIRE is useful for simulating fire behavior during small fires, while DISPERFIRE-CHIMERE is composed of a local scale dispersion model and a regional scale chemical transport model designed to simulate smoke as a multi-scale process.

With these modelling developments, FirEURisk is contributing to state-of-the-art modelling tools able to simulate and forecast fire progression, emissions and smoke dispersion on a spatial and temporal scale adequate to national, regional and local stakeholders needs.

Copyright © FirEURisk Consortium. All rights reserved. 

### *Disclaimer*

The content of the publication herein is the sole responsibility of the publishers and it does not necessarily represent the views expressed by the European Commission or its services.

While the information contained in the documents is believed to be accurate, the authors(s) or any other participant in the FirEUrisk consortium make no warranty of any kind with regard to this material including, but not limited to the implied warranties of merchantability and fitness for a particular purpose.

Neither the FirEurisk Consortium nor any of its members, their officers, employees or agents shall be responsible or liable in negligence or otherwise howsoever in respect of any inaccuracy or omission herein.

Without derogating from the generality of the foregoing neither the FirEurisk Consortium nor any of its members, their officers, employees or agents shall be liable for any direct or indirect or consequential loss or damage caused by or arising from any information advice or inaccuracy or omission herein.

### *Copyright message*

© FirEUrisk Consortium, 2021-2025. This deliverable contains original unpublished work except where clearly indicated otherwise. Acknowledgement of previously published material and of the work of others has been made through appropriate citation, quotation or both. Reproduction is authorised provided the source is acknowledged.

# Table of Contents

1 Introduction ..... 12
1.1 Purpose of the document ..... 12
1.2 Structure of the document ..... 12
2 State-of-the-art in fire behavior modelling ..... 14
2.1 Fire spread ..... 14
2.2 Smoke emission and dispersion ..... 16
2.3 Smoke impacts on health ..... 20
3 FirEUrisk fire behaviour modelling ..... 22
3.1 Fire spread ..... 22
3.2 Smoke emissions ..... 24
3.2.1 Bottom-up ..... 24
3.2.2 Top-down ..... 26
3.3 Smoke dispersion ..... 30
3.3.1 Local scale - DISPERFIRE ..... 30
3.3.2 Regional scale - CHIMERE ..... 31
3.4 Health impact ..... 34
4 Case studies ..... 36
4.1 Chornobyl Exclusion Zone (DA15) ..... 36
4.1.1 Fire progression ..... 37
4.1.2 Emissions and dispersion ..... 38
4.2 Mediterranean Portugal / Central Region of Portugal (PS3) ..... 42
4.2.1 Emissions ..... 42
4.2.1.1 Top-down ..... 42
4.2.1.2 Bottom-up ..... 46
4.2.2 Smoke dispersion ..... 50
4.2.2.1 Modelling setup ..... 50
4.2.2.2 Results ..... 52
4.3 Mediterranean Greece / Attica Region (PS5) ..... 56
4.3.1 Modelling setup ..... 57
4.3.2 Results ..... 59

Copyright © FirEUrisk Consortium. All rights reserved. 

5 Integration of existing systems ..... 64
5.1 IMFIRE-DISPERFIRE ..... 64
5.2 DISPERFIRE-CHIMERE ..... 68
6 Conclusions and final comments ..... 73
References ..... 74

Copyright © FirEUrisk Consortium. All rights reserved. 

# List of figures

**Figure 1.** General structure of the health impact assessment scheme (Silveira et al., 2024). ..... 21
**Figure 2.** Example data of matchup fires used to develop smoke emissions coefficients. (a) VIIRS RGB image of three landscape fire smoke plumes, (b) the corresponding image of Sentinel-5P derived total column CO. ..... 27
**Figure 3.** Carbon monoxide smoke emission coefficients (in $g.MJ^{-1}$) derived from matchup fires burning across four fire-affected biomes of Africa. ..... 28
**Figure 4.** Example of a single matchup fire, with the AOD product and the excess total particulate matter in the plume. ..... 30
**Figure 5.** Scheme of the WRF-CHIMERE modelling system. ..... 32
**Figure 6.** Scheme of the CHIMERE wildfire emissions model, the APIFLAME (Turquety et al., 2020). ..... 33
**Figure 7.** The Chornobyl Exclusion zone demonstration area (DA15). ..... 36
**Figure 8.** Landscape spatial distribution before wildfire in 2016. ..... 37
**Figure 9.** Simulated wildfire progression lines (start time – 15 July 2016, 4 pm) ..... 38
**Figure 10.** Spatial distribution of Sr-90 and Pu-238-240 radionucleides emissions ($kBq/m^2$) to the air. ..... 40
**Figure 11**. Spatial distribution of Sr-90 concentration levels ($mBq/m^3$) at two heights and two time periods after the fire began. ..... 41
**Figure 12.** Left Panel: Serra da Estrela land cover types over fire-affected areas. Right Panel: Simulated PM10 maximum concentration daily values (6 to 15 of August 2022). ..... 43
**Figure 13**. a) Daily fire radiative energy emitted (6 to 11 of August 2022); b) Estimated TPM daily mass values emitted considering FERM TPM emission coefficients; c) As in b) but considering FEER TPM emission coefficients, respectively. ..... 44
**Figure 14**. Daily evolution of maximum observed PM10 values (CAMS reanalysis), and TPM estimated mass emitted (from 6 to 15 of August 2022) considering the FERM coefficients. ..... 45
**Figure 15.** Left panel: Scatter plot of TPM mass emitted (from 6 to 15 of August 2022) considering FEER and FERM coefficients and maximum observed PM10 values (CAMS reanalysis); Right panel: As in left panel but for maximum observed in-situ PM10 values. ..... 45
**Figure 16.** Spatial distribution (500 × 500 $m^2$) of atmospheric emissions for PM2.5 and CO (kt) from 15 to 16 October 2017 (Fernandes et al., 2022) ..... 48
**Figure 17.** Hourly total atmospheric emissions of PM10, PM2.5, NOx, CO, $SO_2$, $NH_3$, $CO_2$ and $CH_4$ (in kt), from 15$^{th}$ to 16$^{th}$ October 2017. ..... 49
**Figure 18**. PM10 and PM2.5 emissions (in kt) from EWE in October 2017, with SEVIRI, this study and MODIS approaches (spatial resolution 10×10 $km^2$). ..... 50
**Figure 19**. Spatial domains used in this study. ..... 51
**Figure 20.** Air quality monitoring stations for daily validation of WRF-CHIMERE simulations (6-20 October 2017). ..... 52
**Figure 21**. PM10, CO and $O_3$ hourly simulated concentrations considering the most relevant atmospheric emissions sources, for 01 and 16 UTC on 15 October and 00 UTC on 17 October 2017. ..... 53

Copyright © FirEURisk Consortium. All rights reserved. 

**Figure 22**. PM10 simulated concentrations due to forest fires, for 00 UTC on 14 October and 06 UTC on 15 October, 2017. ..... 54
**Figure 23.** Observed (light blue) and simulated (dark blue) daily PM10 concentrations in selected air quality stations, October 2017. ..... 55
**Figure 24**. Observed (light blue) and simulated (dark blue) daily $O_3$ concentrations in selected air quality stations, October 2017. ..... 55
**Figure 25**. WRF-CHIMERE nested domains over an elevation. D01 - 25 $km^2$ resolution; D02 - 5 $km^2$ resolution; D03 - 1 $km^2$ resolution. ..... 58
**Figure 26.** Spatial distribution of simulated PM10, CO and $O_3$ concentrations values (3 to 9 August 2021) (Osswald et al., 2023). ..... 60
**Figure 27**. Print screen of a wildfire simulation in the IMFire online platform, with three types of ignitions: point, line and polygon. ..... 66
**Figure 28.** Print screen of REN's infrastructure management platform with IMFire's API integrated (predicted fire spread and time and point of fire impact in the gas and power transport infrastructure). ..... 67
**Figure 29**. Diagram of the Disperfire-Chimere integration. (Green boxes: data. Blue boxes: programs.) . 69
**Figure 30**. DISPERFIRE-CHIMERE PM10 concentrations during a controlled burn in Portugal. ..... 72

Copyright © FirEUrisk Consortium. All rights reserved. 

# List of tables

**Table 1**. List of Acronyms ..... 10
**Table 2.** Proportion by combustion phase (Prichard et al., 2020). ..... 25
**Table 3.** Averaged emission factors (g.kg$^{-1}$ fuel burned, dry basis) per pollutant and vegetation type. ..... 25
**Table 4.** Burning efficiencies for fire emission estimation (EEA, 2019). ..... 26
**Table 5.** Combustible biomass and radioecological parameters for 2016 Fire. ..... 39
**Table 6.** Time series of RNs emissions (GBq) during the Chornobyl wildfire. ..... 40
**Table 7.** Information about the burned area, ignition time, and wildfire duration for the seven EWE between 15$^{th}$ and 16$^{th}$ October 2017 (ADAI 2019). ..... 46
**Table 8.** Fire activity information. ..... 56
**Table 9.** Performance metrics of model results against monitoring station observations (Osswald et al., 2023). ..... 62

Copyright © FirEUrisk Consortium. All rights reserved. 

# List of Acronyms

*Table 1. List of Acronyms*

| List of Acronyms | |
|---|---|
| A | Burned area |
| AOD | Aerosol Optical Depth |
| APA | Portuguese Environment Agency |
| AQ | Air Quality |
| B | Fuel load |
| BenMAP-CE | Environmental Benefits Mapping and Analysis Program – Community Edition |
| CAMS | Copernicus Atmosphere Monitoring Service |
| CCDR | Commission for Coordination and Regional Development |
| CHA | Chamusca |
| CRF | Concentration–Response Functions |
| COS | "Carta de Uso e Ocupação do Solo" |
| CTM | Chemical Transport Models |
| DRN | Douro Norte |
| E | Emission of a pollutant |
| ECMWF | European Centre for Medium-Range Weather Forecasts |
| EF | Emission Factors |
| EFFIS | European Forest Fire Information System |
| ERV | Ervedeira |
| EWE | Extreme Wildfire Event |
| F | Flaming |
| FC | Fuel Consumption |
| FCCS | Fuel Characteristic Classification System |
| FEER | Fire Energetic and Emissions Research |
| FEPS | Fire Emission Production Simulator |
| FlamMap | Fire mapping and analysis system |
| FOFEM | First Order Fire Effects Model |
| FRE | Rate of release of Fire Radiative Energy |
| FREM | Fire Radiative Energy Emission |
| FRP | Fire Radiative Power |
| KFSDP | Korean Forest fire smoke dispersion prediction |

Copyright © FirEUrisk Consortium. All rights reserved.

| | |
|---|---|
| GIS | Geographic information system |
| IOA | Index of agreement |
| MFB | Mean fractional bias |
| MODIS | Moderate-Resolution Imaging Spectroradiometer |
| MOV | Montemor o Velho |
| NCAR | Fire Inventory from National Center for Atmospheric Research |
| NMB | Normalized mean bias |
| NOAA | National Oceanic and Atmospheric Administration |
| R | Pearson's correlation coefficient |
| RMSE | Root mean square error |
| ROS | Rate Of Spread |
| RR | Relative Risk |
| RS | Long term residual smouldering |
| S | Smouldering |
| SEVIRI | Spinning Enhanced Visible and InfraRed Imager |
| SIS | Smoke Impact Spreadsheet |
| VIIRS | Visible Infrared Imaging Radiometer Suite |
| WRF | Weather Research and Forecasting |
| WHO | World Health Organization |
| WUI | Wildland Urban Interface |
| β | Burning efficiency |

Copyright © FirEUrisk Consortium. All rights reserved.

# 1 Introduction

## 1.1 Purpose of the document

Wildfires are among the most dangerous natural hazards, and their impact has been increasing significantly in recent years (San-Miguel-Ayanz *et al*., 2019). They can affect ecosystems by destroying natural habitats, resources, and wildlife. Furthermore, they cause significant damage to society, being responsible for numerous fatalities, accidents, injuries, health problems, and the destruction of human infrastructures. The latest edition of the Commission's Joint Research Centre Annual Report on Forest Fires in Europe, the Middle East and North Africa in 2021 (San-Miguel-Ayanz, 2022), documents 5500 $km^2$ of land burnt in 2021 with over 1000 $km^2$ burnt within protected Natura 2000 areas, the European Union's reservoir of biodiversity.

Previous fire events and research have also highlighted the vulnerabilities of firefighters in facing extreme fires and those in the Wildland Urban Interface (WUI), noticeably due to the lack of specific knowledge, inadequate modelling tools and the inappropriate application of fighting techniques intended for high-impact fires. Moreover, population, health and environmental entities lack sufficient awareness regarding the potential health impacts of smoke. Additionally, existing modelling tools fail to adequately address the effects of smoke on air quality and human health with the appropriate temporal and spatial scales.

Task 2.3 is about the improvement of response to reduce the risk of high-impact fires, and it is aimed at upgrading fire behaviour modelling tools to better address extreme fire behaviour as well as smoke emission and dispersion. It is based on knowledge produced in WP1 - Fire risk assessment to improve prevention, is providing information to WP4 - Multi-level integration, and being tested in WP5 - Pilot Sites and Demonstration Areas.

This deliverable aims to describe the development of numerical tools for estimating fire behaviour, including smoke production and dispersion.

## 1.2 Structure of the document

The document is organized into six chapters, starting with this introductory one. Chapter 2 provides a state-of-the-art overview of current fire behaviour models. It includes information on fire spread modelling, smoke emissions and dispersion modelling, and the modelling of smoke impacts on health.

Chapter 3 provides a comprehensive overview of FirEUrisk modelling tools, which were developed based on the most recent scientific and technical advances in fire spread, smoke emission, and dispersion models, as well as mathematical functions to estimate human exposure and health effects.

The application of these FirEUrisk models is reported in Chapter 4, where the modelling of the fire spread and smoke emissions and dispersion by a wildfire near the Chornobyl Exclusion Zone is described, as well as the simulation of the impact of smoke emissions in the air quality of the 2017 Central Region of Portugal wildfires and the 2021 Greece/Attica Region wildfires.

Copyright © FirEUrisk Consortium. All rights reserved.

Two integrated modelling systems – IMFIRE-DISPERFIRE and DISPERFIRE-CHIMERE –, which include fire spread and smoke at the local scale and mesoscale, respectively, are presented in Chapter 5.

Finally, Chapter 6 summarises the main achievements of FirEUrisk in fire behaviour modelling and outlines future research activities aimed at enhancing our operational modelling capabilities. These efforts are intended to better serve and engage important stakeholders

Copyright © FirEUrisk Consortium. All rights reserved.

# 2 State-of-the-art in fire behavior modelling

## 2.1 Fire spread

Wildfires damages bear a significant economic impact, not only due to the fire damage but also the large investments in prevention, preparedness, fire suppression and recovery efforts. It is essential to direct efforts towards understanding the behaviour of wildfires and improving their management. In this sense, knowledge of how wildfires propagate is critical, allowing the prediction of a fire's path and taking the appropriate measures to mitigate its impact.

The spread of forest fires is a complex process that is not fully understood despite the variety of approaches that have been used in research in recent decades, from purely empirical to fully theoretical approaches that aim to model and predict fire behaviour. Pastor *et al.* (2003) and Sullivan (2009) provide an overview of the state of the art in fire behaviour research and provide a variety of references that illustrate the complexity of the problem and the difficulty in finding a general and complete solution. Currently, it is only possible to predict fire behaviour under very limited conditions (Thomas *et al.,* 2017), and some of the cases that could be of greater practical importance, such as very intense or fast-moving fires, which are of great concern to fire managers and put people's lives at risk (Bowman *et al.,* 2017) are not yet considered.

Forest fire propagation is often analysed as a static process that depends on several factors - wind speed, slope gradient and fuel - which, according to some formulations, should be sufficient to determine a well-defined value for the Rate Of Spread (ROS) of a fire front (Rothermel, 1972, 1983). This concept is due to the little attention that was paid to the role of convection induced by the presence of fire and its interaction with the surrounding flow (Viegas, 2002, 2004; Finney *et al.,* 2015).

A fundamental step in fire modelling is to understand how fire behaviour changes their properties over time due to the dynamic interaction between the fire and its environment. In 1959, Berlad and Yang questioned the conditions for the existence of a steady state in flame propagation based on the law of conservation of energy (Berlad and Yang, 1959). In an earlier work developed by Viegas (2004), it was stated that fire behaviour in general is a dynamic process in the sense that even if the boundary conditions are permanent, the characteristics of fire behaviour depend explicitly on time or distance. In Viegas (2002), it was shown that transverse convection along the fire line changes the ROS of the fire and causes its rotational movement. In Viegas and Pita (2004), research on the dynamic behaviour of fires was extended to fires in canyons. In Viegas (2005, 2006) it was shown that the convection caused by the fire causes an acceleration of the fire, called an eruption, which is often observed in canyons or on steep slopes. According to the proposed mathematical model, the ROS increases after a relatively short period of time, depending on the fuel bed properties, and reaches very high values tending towards infinity, although it was realised that this is not possible under real conditions. In the model, the residence time of the combustion in the fuel bed plays an important role (Viegas, 2005), and it is used to characterise the dynamic response of the fuel to changes in environmental conditions (namely wind or slope changes) caused either by external conditions or by the fire itself. In Viegas (2005), the concept of the *"square fire*

Copyright © FirEUrisk Consortium. All rights reserved. 

*factors"* was introduced, which proposes "time" as an explicit factor for fire spread characteristics to account for the dynamic nature of combustion. Dold *et al.* (2006) also addressed this problem.

When analysing the junction of two linear fires (Viegas *et al.,* 2012; Viegas *et al.,* 2013; Raposo *et al.,* 2014, 2018; Xiaodong *et al.,* 2014; Raposo, 2016; Ribeiro *et al.,* 2023), a non-monotonic evolution of the ROS of the head fire was observed, with a very rapid increase in ROS followed by a decrease. In Raposo *et al.* (2018), this fact was interpreted as the effect of an opposing flow caused by the very fast spreading fire, which is consistent with the statement of Byram (1959), showing that this flow could limit the growth of the fire and provide a solution to the problem of an infinite ROS predicted by the mathematical model. Thomas *et al.* (2017) also studied this problem. In Ribeiro *et al.* (2023), the interaction of two non-symmetric fire fronts was analysed and they found that the ROS for a small rotation of the Junction Fire depends on the slope angle and the initial angle between the fire fronts. It was also reported that in the interaction of non-symmetrical fire fronts, the convection mechanism is dominant and changes the fire behaviour when the slope angle is high. However, for lower slope angles the radiation becomes more important and influences the fire behaviour.

Albini (1982) studied the variability of wind-assisted fires and found that ROS fires in natural fuels are very sensitive to wind speed, but in many cases, the ROS can also vary considerably with time, even though the fuels and meteorological conditions remain essentially constant. Based on the spectral density of wind fluctuations at frequencies below 0.1 Hz, Albini predicted that the fire's response would be oscillatory, with a spectral response that depends on the type of fuel and the average value of the wind speed. According to this model, there is a dominant oscillatory amplitude of the ROS for a frequency between 0.01 and 0.02 Hz, but the average value of the ROS does not seem to change. Although this study captured some of the characteristics of dynamic fire behaviour, it did not consider the natural fluctuations that occur even when there is no wind and the large amplitude fluctuations of the ROS. Finney *et al.* (2015, 2019) and Silvani *et al.* (2018) also addressed the problem of variations in fire properties due to turbulence in fire-induced convection.

Silvani *et al.* (2012) analysed the effect of slope on fire spread in laboratory experiments using video images and heat measurements. Using spectral analysis of gas temperature and total heat flux density, they found an increase in the frequency of fluctuations when the slope was increased from 0° to 30°.

Several authors have studied the spread of a point or linear fire in a slope, namely Mendes-Lopes *et al.* (2003), Dupuy *et al.* (2011) and Silvani *et al.* (2018). Although they acknowledge the variability of fire spread, they assume that the fire spreads in a steady state and essentially give average values for the fire spread characteristics.

Theoretical, empirical and semiempirical models have been developed to predict the wildfire behaviour (Pastor *et al*., 2003). The semiempirical Rothermel model (Rothermel, 1972) is the most widely used model for wildfire spread prediction (Pastor *et al*., 2003), particularly in Mediterranean European countries (Sullivan, 2009), being the core of some of the most cited fire simulators such as FARSITE (Finney, 1998) and FIRESTATION (Lopes *et al*., 2002).

Copyright © FirEUrisk Consortium. All rights reserved. 

## 2.2 Smoke emission and dispersion

Wildfires can produce substantial emissions of carbon dioxide ($CO_2$), carbon monoxide (CO), nitrogen oxides (NOx), volatile organic compounds (VOC), and particulate matter (Andreae and Merlet, 2001; Crutzen *et al*., 1979; Miranda *et al*., 2005, 1994; Reddington *et al*., 2016). These emissions affect the global atmospheric chemistry (Jaffe *et al*., 2008; Monks *et al*., 2012; Spracklen *et al*., 2007), impact the radiative transfer in the atmosphere (Clinton *et al*., 2006) and reduce visibility (Valente *et al*., 2007; Wade and Ward, 1973). Moreover, they strongly impair the quality of the air (Bytnerowicz *et al*., 2010; Carvalho *et al*., 2011; Keywood *et al*., 2015; Martins *et al*., 2012; Miranda *et al*., 2009; Turquety *et al*., 2014; Valente *et al*., 2007), with important effects on human health (Akagi *et al*., 2014; Apte *et al*., 2018; Dennekamp *et al*., 2015; Johnston *et al*., 2012; Knorr *et al*., 2012; Martins *et al*., 2012; Miranda *et al*., 2012, 2010; Reid *et al*., 2016).

To protect the health of populations, it is important to provide information about the areas covered by the smoke from wildfires and the concentration of atmospheric pollutants. In recent decades, scientific developments regarding smoke dispersion and its impacts were achieved using modelling systems, and nowadays some numerical models allow the simulation of fire emissions to the atmosphere, their dispersion and their impact on air quality. In Europe, for instance, the European Forest Fire Information System (EFFIS) provides a fire database with fire danger and fire detection forecasts based on satellite imagery. EFFIS is currently providing fire emissions based on the emission plots derived from the Copernicus Atmosphere Monitoring Service (CAMS). CAMS, which is implemented by the European Centre for Medium-Range Weather Forecasts (ECMWF) on behalf of the European Union, provides daily estimates of global fire emissions through its Global Fire Assimilation System that combines observations of fire radiative power from sensors on satellites with numerical models. These two initiatives are mainly addressing the European region and cannot answer country and/or more localised needs.

Over North America, the systems BlueSky (https://www.airfire.org/data/bluesky) and FireWork (https://weather.gc.ca/firework/index_e.html) provide near-real-time forecast data regarding wildfires' spread and smoke dispersion. BlueSky is a smoke modeling framework that links fire activity information, various fuel models, consumption and emissions models, and dispersion and trajectory models into one system for predicting the cumulative impacts of smoke from fires.

### 2.2.1 Emissions

Most of the forest fire emission studies rely on the model proposed by Seiler and Crutzen (1980) and Ward and Hardy (1991), which is based on information about the burned area extent, the amount and type of vegetation burned (fuel types, fuel loads), and the conditions under which fires take place (combustion efficiencies). Emission factors are also used to estimate the amount of emissions of each species (gases and particles). More recently, global satellite-derived burned area information has become available. Thus, the scientific community has put a considerable effort in quantifying the impact of wildland fires by remote-sensing approaches to improve these estimates (Giglio *et al*., 2006; Mouillot *et al*., 2006;

Copyright © FirEURisk Consortium. All rights reserved. 

Reid *et al*., 2009; Mieville *et al*., 2010; Wiedinmyer *et al*., 2011; Kaiser *et al*., 2012; Monteiro *et al*., 2013; Ichoku and Ellison, 2014; Darmenov and da Silva, 2015; Chuvieco *et al*., 2016; van der Werf *et al*., 2017). Furthermore, the instantaneous fire radiative power (FRP) is currently used as a measure of the rate of radiant energy emission from the fire, to derive directly the amount of fuel burned (Freeborn *et al*., 2008), to facilitate real-time applications (Kaiser *et al*., 2012; Sofiev *et al*., 2009).

For instance, the Fire Inventory from the National Center for Atmospheric Research (NCAR) version 2.5 (FINNv2.5) is a fire emissions inventory that provides publicly available emissions of trace gases and aerosols for various applications, including use in global and regional atmospheric chemistry modelling (Wiedinmyer *et al*., 2023). Global observations from sensors on board satellites are used to detect fire activity. Active fire detections from the Visible Infrared Imaging Radiometer Suite (VIIRS) at 375 m spatial resolution are used, which allows smaller fires to be included in the emissions processing.

Although much progress has been made over the last couple of decades in improving the quality of vegetation fire emission datasets (e.g. Pereira et al. 2009; Van Der Werf et al. 2010, 2017; Sofiev et al. 2013; Rémy et al. 2017; Prichard et al. 2020), uncertainties are still relevant but still poorly estimated and considered in modelling, mainly at regional and local levels (e.g. Liousse et al. 2010; Kaiser et al. 2012; Petrenko et al. 2012; Bond et al. 2013; Zhang et al. 2014; Ichoku et al. 2016; Pereira et al. 2016; Reddington et al. 2016; Pan et al. 2020). They are mainly associated with fire characteristics (vegetation burned and fuel load consumed) and emission factors (EF) (Miranda et al. 2008; Ottmar et al. 2008; Langmann et al. 2009). Regarding EF, most of the information is available for the United States of America (USA) forest (Urbanski, 2013), and it would not be a suitable proxy for wildfires in Europe, namely due to vegetation cover and the differences in combustion characteristics (e.g., flaming and smouldering phases). Efforts to narrow the uncertainties in the emission factors are ongoing in the form of numerous field campaigns and laboratory studies (e.g. Alves et al. 2011; Vicente et al. 2012, 2017; Van Der Werf et al. 2017).

The accuracy and high resolution of fire emission inventories are particularly important for air quality modelling studies at regional and local scales (Miranda *et al.,* 2005; Valente *et al.,* 2007; Akagi *et al.,* 2011; Martins *et al.,* 2012; Van Marle *et al.,* 2017; Mota and Wooster, 2018). Emission models can strongly contribute to emission inventories and provide data for air quality assessment. The Fire Emission Production Simulator (FEPS), for example, is a user-friendly computer program that manages data concerning consumption, emissions, and heat release characteristics of prescribed burns and wildland fire events. It can be used for most forest, shrub and grassland types in North America and may be applied to other regions of the world (Anderson *et al*., 2004). FEPS incorporates a flexible user interface that allows users to customize a burning event. Users may adjust fuel loadings, fuel moistures, fuel consumption algorithms, fuelbed proportions and fire growth rates to fit specific events, and can specify diurnal changes in meteorological conditions that will modify plume rise.

Consume (https://www.fs.usda.gov/research/pnw/projects/consumesoftware) and FOFEM - First Order Fire Effects Model (https://www.firelab.org/project/fofem-fire-effects-model) are other examples of emission models. Consume calculates fuel consumption and emissions by combustion phase. It is designed to import data directly from the Fuel Characteristic Classification System (FCCS) and can be used for most forest, shrub, and grassland areas in North America. FOFEM is a computer program for predicting

Copyright © FirEUrisk Consortium. All rights reserved. 

tree mortality, fuel consumption, smoke production, and soil heating caused by prescribed fire or wildfire. SpatialFOFEM is a spatial implementation of the point-scale FOFEM model. The last version of the fire mapping and analysis system (FlamMap) software can estimate emissions through FOFEM.

### 2.2.2 Dispersion

Smoke dispersion models are used to predict the behavior and movement of smoke in the atmosphere. By accurately predicting smoke dispersion, these models help to minimize the impact of smoke on public health by allowing the adoption of population exposure mitigation measures and the environment, making it an asset to government agencies, fire management teams and other organizations that manage wildfires and other smoke-producing events.

Smoke dispersion can be simulated with different types of models with different scales of analysis and including, or not, chemical reactions. The simplest ones are gaussian-based models and simulate smoke emissions as passive pollutants based on a gaussian dispersion approach. They're used to be applied, as screening models, to estimate the impact of smoke from prescribed fires. One example is the two simple screening models (VSmoke and VSmoke-GIS) that have been developed by the USDA Forest Service to determine what impact particulate matter emissions may have on highway visibility and people's health in flat to rolling terrain. Both VSmoke and VSmoke-GIS (https://webcam.srs.fs.usda.gov/tools/vsmoke/index.shtml) are classified as Gaussian plume atmospheric dispersion models.

The Smoke Impact Spreadsheet (SIS) model is another simple-to-use, screening-level modelling system for calculating PM2.5 emissions and airborne concentrations downwind of natural or managed wildland fires. It contains an emissions module that calculates emissions for broadcast and wildfire burns using the First Order Fire Effects Model, version 5 (FOFEM5), and from pile burns using the CONSUME 2.1 pile wizard and it is based on a dispersion module that uses the CALPUFF dispersion model (version 5.5).

The Korean Forest fire smoke dispersion prediction (KFSDP) system integrates modules from different models, including a Korean forest fire growth prediction model, grid-based geographic information system (GIS) fuel loading and consumption maps generated by national forest fuel inventory data, and the Korean Weather Research and Forecasting Model, into a Gaussian plume model to simulate local- and regional-scale smoke dispersion (Lee *et al*., 2019). The forecast system is operated using grid-based fires and simulates a cumulative smoke dispersion of carbon monoxide (CO) and PM2.5 and PM10 ground-level concentration contours at 30-min intervals during the fire in concert with weather forecasts.

Another simple way to simulate smoke dispersion is to use lagrangean models that can calculate the trajectory of passive pollutants. For instance, the lagrangean particle dispersion model (FLEXPART) was used to simulate the impact of a wildfire event that affected the urban area of Barcelona during a short period of time in July 2012 (van Drooge *et al*., 2016). Forward simulations of the fire pollution plumes were made with FLEXPART (Stohl *et al*., 1998), driven by ECMWF (European Centre for Medium-Range Weather Forecasts) operational analysis data with 0.18° × 0.18° latitude/longitude resolution, 91 vertical model levels and 3 h time resolution. Simulations were made both for a passive carbon monoxide (CO) tracer and a PM2.5 aerosol tracer.

Copyright © FirEUrisk Consortium. All rights reserved. 

The DISPERFIRE system is a real time system that was developed to simulate the dispersion in the atmosphere of the pollutants emitted during a forest fire. It is based on a diagnostic wind model and on a lagrangean dispersion model. It was applied and successfully validated by Valente *et al*. (2007) during a field experimental fire.

The HYSPLIT model (Draxler and Hess, 1998), which is a comprehensive dispersion and transport modelling system for computing trajectories, complex transport, dispersion, chemical transformation, and deposition simulations, has evolved over more than 30 years. Li *et al*. (2020) conducted an ensemble forecast to predict surface PM2.5 during the 2018 California Camp Fire event using the National Oceanic and Atmospheric Administration (NOAA) HYSPLIT dispersion model at 0.1° horizontal resolution. Different combinations of four satellite-based fire emission data sets (FEER, FLAMBE, GBBEPx, and GFAS), two plume rise schemes (Briggs and Sofiev), various meteorology inputs, and model setup options were used to create the forecast ensemble, for a total of 112 experiments. Results confirmed the large uncertainty associated to the different variables that are part of the modelling system.

Chemical Transport Models (CTM) are more complex, because they integrate chemical transformations of pollutants in the air. They are usually applied at mesoscale and can simulate smoke transport and chemistry. AIRFIRE, for instance, is a numerical system that was developed to estimate the effects of forest fires on air quality, integrating several modules, such as a mesoscale meteorological model, a photochemical model and the Rothermel fire spread model (Miranda, 2004).

The meso-scale CHIMERE model is another example of a CTM that was used, together with ground based and satellite aerosol optical measurements, to assess the dispersion of fire emissions and to quantify the associated radiative effects during the intense fire season that occurred in summer 2003 (Hodzic *et al*., 2007) and in summer 2016 in Portugal (Turquety *et a*l., 2020). Péré *et al*. (2014) simulated an event near Moscow in 2010 using the Weather Research and Forecasting (WRF) meteorology model coupled with the CHIMERE CTM fed with emissions derived from the Global Fire Assimilation System.

Nuryanto (2015) applied the WRF-CHEM modelling system to simulate the forest fires smoke event of 7 March 2014 in Sumatera-Indonesia. The Weather Research Forecasting (WRF) model coupled with Chemistry (WRF-Chem) is a weather regional model that makes use of chemical compounds in its calculation and allows for coupled simulations of atmospheric chemistry and meteorology. The coupled fire-atmosphere model (WRF-SFIRE; Mandel *et al*., 2011) was integrated with a chemical model (WRF-SFIRE-CHEM; Kochanski *et al*., 2016) to simultaneously simulate fire spread, fire plume rise, smoke dispersion, and plume chemistry. Kochanski *et al*. (2019) tested the WRF-SFIRE-CHEM framework by applying it to a case study where significant wildfire smoke was observed.

The review paper by Liu *et al*. (2019) presents simulations and experiments of hypothetical prescribed burns with a suite of selected fire behaviour and smoke models and identifies major issues for model improvement and the most critical observational needs. According to these authors, the next-generation smoke forecasting systems should have more coupling of fire, smoke and atmospheric processes.

Copyright © FirEUrisk Consortium. All rights reserved.

## 2.3 Smoke impacts on health

The World Health Organization (WHO), aware of the health effects of smoke from wildfires, provided air quality guidelines for vegetation fire events to protect the population (WHO, 1999), particularly in the Wildland-Urban Interface (WUI) due to the high risk of human exposure (Ager et al., 2019; A.I. Miranda et al., 2008). Exposure to high levels of air pollution during wildfire events can lead to a wide range of adverse health outcomes, including increases in respiratory morbidity (Black *et al*., 2017; Cascio, 2018; Elliott *et al*., 2013; Haikerwal *et al*., 2016; Reid *et al*., 2016) and negative cardiovascular effects (Haikerwal *et al.*, 2015; Wettstein *et al*., 2018; Yao *et al*., 2016). The populations most vulnerable to smoke exposure are the common risk groups (e.g., children and older adults) (Rappold *et al*., 2017) and personnel involved in firefighting operations (Miranda *et al*., 2012, 2010; Sebastião *et al*., 2019). The short-term exposure to very high air pollution levels during a fire event can lead to acute health problems, which can be instantaneous rashes on eyes, irritations in nose and throat, and shortness of breath. These symptoms often evolve into headaches, dizziness and nausea, lasting up to several hours.

Health impacts are often expressed through morbidity and mortality indicators derived from epidemiological studies, being mostly related to respiratory and cardiovascular diseases (Costa *et al*., 2014; Héroux *et al*., 2015; Rückerl *et al*., 2011; Seethaler *et al*., 2003; WHO, 2013a). Epidemiological studies combine meta-analyses recorded during air pollution episodes to provide statistical associations by relating ambient concentration changes and different types of health outcomes (Costa *et al*., 2014; WHO, 2013b). The resulting concentration-response functions (CRF) could then be included in linear or nonlinear relative risk (RR) models, which may or not contain threshold exposure values, and are used to translate unit concentration changes in health impacts. Normally, greater health risks related to ambient air pollution are attributed to linear RR models and certain vulnerable age groups, such as elderly people or children (Pervin *et al*., 2008; Silveira *et al*., 2016; WHO, 2013c). Silveira et al. (2024) show a general structure of the health impact assessment methodology (see Figure 1) and provide a detailed description of this methodology.

Copyright © FirEURisk Consortium. All rights reserved.

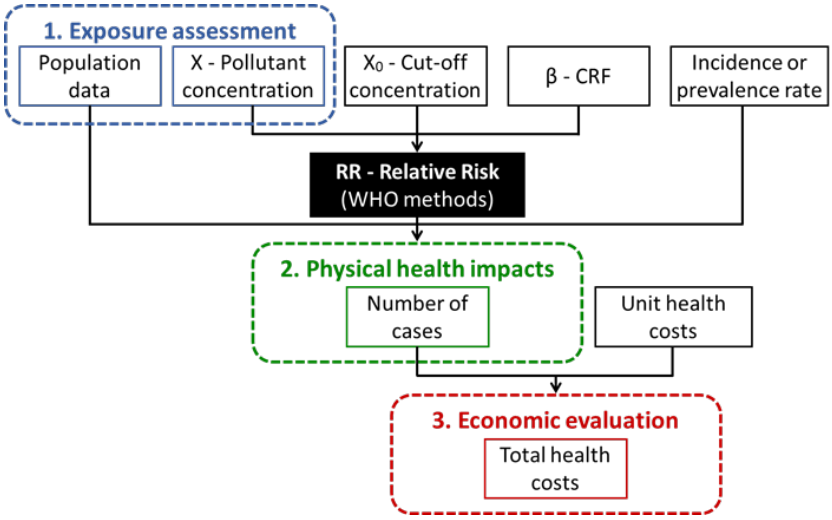



***Figure 1.*** *General structure of the health impact assessment scheme* (Silveira *et al*., 2024).

To quantify the magnitude of health effects, many tools and methodologies have been developed and applied to different spatiotemporal scales. Among them, AirQ+ is a valid and reliable software that was designed by the WHO Regional Office for Europe (WHO, n.d.), and has been extensively used to estimate health impacts from air pollutants in a wide range of population densities and time periods *(*Arregocés *et al.,* 2023; Asgari *et al.,* 2021; Brito *et al.,* 2022; De Marco *et al.,* 2022; Egerstrom *et al.,* 2023; Hopke *et al.,* 2018; Jariwala and Kapadia*,* 2022; Kliengchuay *et al.,* 2022; Rovira *et al.,* 2020; Zhu *et al*., 2022). All AirQ+ calculations are based on methodologies and CRF from systematic reviews and well-established meta-analyses of epidemiological studies *(*Ansari and Ehrampoush, 2019; Arregocés *et al*., 2023; Oliveri Conti *et al*., 2017; Zhu *et al*., 2022). Another tool commonly used to calculate health impacts from air pollution is the Environmental Benefits Mapping and Analysis Program – Community Edition (BenMAP-CE) (Bayat *et al*., 2019; Parvez and Wagstrom, 2020). In general, these health risk modelling approaches have been mainly employed considering linear RR models for regulatory and decision-making purposes.

Copyright © FirEURisk Consortium. All rights reserved.

# 3 FirEUrisk fire behaviour modelling

## 3.1 Fire spread

In FirEUrisk the approach of fire behaviour modelling using the classical formulation proposed by Rothermel (1972) was only partially adopted; it considers fire spread as a static process that is dependent on the local properties of topography (usually only slope), fuel cover (described by fuel model parameters) and meteorology (mainly wind velocity), without considering the interaction between the fire and the atmosphere and the convective flow induced by the fire that modifies strongly fire behaviour in adjacent sections and of the fire as a whole.

This approach is used in several fire behaviour models that were used in the project, like the FireStation, the Farsite and the Flamap, as despite their limitations, they provide plausible results on the fire spread, that can be used to extract conclusions on the relative effect of some of the parameters that are used in the calculation of fire spread, to assess the effectiveness of measures to reduce the risk, like for example the modification of the vegetation cover. Nevertheless, this approach is not adequate to predict fire spread in the general case for operational purposes, especially for the sake of fire safety. For this reason, in the project, we performed research along an innovative approach that considers the dynamic character of the fire and its implication on the prediction of fire behaviour. Due to its relevance, our research deals mostly with surface fire spread. Although some work was performed on the spread of crown fires and spot fires, due to time limitations these were not analysed extensively. For the same reason, phenomena such as fire whirls and peat fires were not studied extensively during the project.

### 3.1.1 Dynamic fire behaviour modelling

Our research on dynamic fire behavior followed the pioneer work performed in earlier EU projects, like INFLAME (ref. ENV4-98-0700) and SPREAD (ref EVG1-CT-2001-00043), on the concept of dynamic fire behavior, eruptive fires in canyons and the junction fires, that were mentioned above, and produced some innovative concepts and research topics that are being followed internationally.

Our attention was focused on the prediction of the head fire ROS during the evolution of large fires, as it is a driver of the entire fire and therefore a very important parameter to be evaluated to assess the behavior of the fire. Our research showed that the evolution of the ROS in the course of time is not a monotonic function, but it exhibits oscillations with amplitude and frequency that depend on the overall properties of the fire, namely its size or dimension, and of the ROS value itself. This oscillatory behavior was found to occur at all scales of fires, from laboratory tests to field experiments to very large fires. A conceptual physical model was proposed to justify the oscillatory behavior of the fire. The fact that the amplitude of the oscillations of the ROS increased with the average value of the ROS meant that in the case of very fast spreading fires the instantaneous value of the ROS could vary in a range of one to five or more times its average value, rendering the estimation of the average value of the ROS – that is used in most simulations – void of significance, particularly in the scope of fire safety concerns. This fact implied

Copyright © FirEUrisk Consortium. All rights reserved. 

the need to have better predictors of the varying value of the ROS. The results of this preliminary research were published in Viegas *et al.* (2021, 2022).

A corollary of the oscillatory behavior was what we designated the "intermittent fire behavior" consisting of a sequence of a fire acceleration followed by a deceleration that was observed in many situations including in real fires. Current fire behavior models do not account for the convective processes and cannot explain this behavior, particularly the rapid deceleration process. We had come across this behavior in the analysis of eruptive fires and of junction fires and this enabled us to interpret and explain the behavior of the large and deadly fire that occurred in Pedrogão Grande in 17 June 2017 in Central Portugal. Based on extensive field work complemented by very detailed atmospheric scrutiny using radar tools and an original experimental simulation, we were able to provide a scientifically based explanation of the Pedrogão Grande fire that was published in Pinto *et al.* (2022) and Viegas *et al.* (2023).

The analysis of the process of acceleration and deceleration of the head fire ROS is ongoing. A semi-empirical mathematical model based on the one that was proposed for the eruptive fires in canyons (Viegas, 2005), is being developed and tested to predict these processes at various scales. We do not have a general model that can be applied to predict head fire behaviour in arbitrary boundary conditions. This will require the gathering of a large amount of data on the spread of large fires, which is being attempted with the Project.

The lack of accurate data and the novelty of these concepts make it difficult to produce practical models that can be used to predict the behaviour of a large fire in general conditions. We expect to advance further in the duration of the project, but it should be recognized that this is a new field of research in which there are yet not many teams working around the World.

It must be said that the original approach addressed in the Project brought many changes to the interpretation of fire behavior and it is already contributing to increase the safety of fire fighters that are trained following the concepts of dynamic fire behavior and are introduced to the process of eruptive fires that are associated to many fatal accidents. These materials are in fact included in Deliverable D2.6 that contains guidelines to train fire fighters that must face extreme and dangerous fires.

### 3.1.2 Fire perimeter growth

One of the limitations of current fire simulators that are based on the Rothermel (1972, 1983) model is the assumption of an elliptical growth of the fire, to estimate the evolution of the fire perimeter from one-time step to the next one. The transition from an initial circular shape to the elliptical shape is not justified in previous work and it is observed that in the general case the shape of the fire perimeter does not conform to an ellipse or even to a double ellipse. As said above, this approach is adopted by most fire simulators, including those mentioned above and used in the Project.

To overcome this limitation, we are proposing a novel methodology to predict the evolution of the fire perimeter. In this approach, we consider elements of the fire perimeter and their evolution over time, accounting for the convective effects near the fire front. Because of these heat transfer process, the fire line element undergoes a translation, a rotation and an extension, that must be estimated in each time step assuming that the ROS at given points of the fire perimeter are known or can be determined

Copyright © FirEURisk Consortium. All rights reserved. 

from models. These concepts were developed in previous EU projects, namely INFLAME (ref. ENV4-98-0700) and SPREAD (ref EVG1-CT-2001-00043), and published in Viegas and Rossa (2009).

In FirEUrisk project we are developing this methodology that requires the analysis of a large number of cases of experimental and real fires. At present a model to predict the evolution of a point ignition fire on a slope at laboratory and field scale was developed with good results (cf. Viegas *et al.,* 2024). Its extension to the general case of wind and slope effects and to large-scale fires is under way.

## 3.2 Smoke emissions

Wildfire's emissions are highly variable in time and space, and their calculation requires a numerical tool capable of estimating gas and particle emission flows with an adequate spatiotemporal resolution. In FirEUrisk, two types of approaches were selected to estimate/model fire emissions, one based on surface data (bottom-up) and the other based on satellite data (top-down).

### 3.2.1 Bottom-up

The atmospheric emissions estimation from wildfires using a bottom-up approach is based on the following well-known equations:

$$E_{p,f,i} = FC_i \times A_i \times EF_{p,f,i} \quad \text{Equation 1}$$

$$\mathrm{FC} = B_i \times \beta_i \quad \text{Equation 2}$$

where, $E_{i,f,p}$ represents the emission (g) of compound p during the combustion phase f caused by the burning of fuel i, FC is the fuel consumption ($kg.m^{-2}$) of fuel i, A is the burned area ($m^2$) of fuel i, $EF_{p,f,i}$ is the emission factor ($g.kg^{-1}$) of the pollutant p during the combustion phase f caused by the burning of fuel i, B is the fuel load ($kg.m^{-2}$) of fuel i, and β the burning efficiency (unitless) of fuel i.

The emissions released into the atmosphere depend on the type of fuel, available fuel load, combustion phase, and burned area. Fuel characteristics (i.e., fuel type, and fuel load) and burnt areas were obtained from the datasets developed under the FirEUrisk project (Chuvieco et al., 2023). For the combustion phases, two approaches were considered: one based on the fuel category and the other on burn intensity ($kW.m^{-2}$). In the first approach, as assumed by the CONSUME model, a generic proportion for each fuel category (e.g., herbs, shrubs, 1-h wood, 1000-h wood, litter or duff) is used for the partition of consumption values into flaming, smouldering, and residual consumption (**Table 2**) (Prichard *et al*., 2020). In the second approach, the burn intensity is provided from the FirEUrisk datasets, considering a threshold of > 15 $kW.m^{-2}$ for flaming combustion and < 15 $kW.m^{-2}$ for smouldering combustion (Prichard *et al*., 2019). It should be noted that both approaches can be applied depending on the emission estimation objective and the available datasets.

Copyright © FirEUrisk Consortium. All rights reserved.

*Table 2. Proportion by combustion phase* (Prichard *et al*., 2020).

| Fuel category | Proportion by combustion phase | | |
|---|---|---|---|
| | Flaming | Smouldering | RS* |
| **Herb** | 1 | 0 | 0 |
| **Shrub** | 1 | 0 | 0 |
| **1 h** | 0.95 | 0.05 | 0 |
| **10 h** | 0.90 | 0.10 | 0 |
| **100 h** | 0.85 | 0.10 | 0.05 |
| **Sound 1000 h** | 0.60 | 0.30 | 0.10 |
| **Rotten 1000 h** | 0.60 | 0.30 | 0.10 |
| **Litter** | 0.90 | 0.10 | 0.00 |
| **Duff** | 0.10 | 0.70 | 0.20 |

*RS – concerns long-term residual smouldering, which is generally associated with marginally combustible fuels such as coarse wood and duff that generally have incomplete combustion and smoulder for extended periods

A literature review was performed to obtain the most suitable emission factors by fuel type and combustion phase for the European Region. The compiled dataset was adapted to fit the FirEUrisk fuel classification. **Table 3** includes the averaged emission factors (in $g.kg^{-1}$ fuel burned, dry basis) for relevant air pollutants.

*Table 3. Averaged emission factors ($g.kg^{-1}$ fuel burned, dry basis) per pollutant and vegetation type.*

| Species | Eucalyptus[c, d, e] | Other resinous[b] | Oak, Chestnut, Cork Oak[b] | Acacia[c, d, e] | Other hardwoods[a] | Pinus pinaster[c, d, e] | Stone pine[b] | Shrub[b] |
|---|---|---|---|---|---|---|---|---|
| **PM10** | 21 | 10 | 13 | 11 | 8.3 | 13 | 10 | 20 |
| **PM2.5** | 19 | 9 | 11 | 10 | 6.3 | 11 | 9 | |
| **NOx** | 5 | 3 | 3 | 5 | 3.11 | 3 | 5 | |
| **CO** | 170 | 100 | 128 | 232 | 102 | 204 | 91 | 82 |
| **$SO_2$** | 0.8 | 0.8 | 0.8 | 0.8 | 0.4 | 0.8 | 0.8 | |
| **$NH_3$** | 0.6 | 0.6 | 0.6 | 0.6 | 2.17 | 0.6 | 0.6 | |
| **$CO_2$** | 1408 | 1497 | 1393 | 1561 | 1585 | 1398 | 1487 | |
| **$CH_4$** | 6 | 6 | 6 | 4.7 | 5.82 | 6 | 5 | 4 |

[a] Van Der Werf *et al.* (2017), [b] Miranda (2004), [c] Vicente *et al.* (2012), [d] Vicente *et al.* (2017), [e] Alves *et al.* (2011)

Regarding burning efficiency, which is related to fuel consumption or the fraction burned related to the total available biomass, and considering the difficulty in accurately estimating it, two approaches are proposed based on the available dataset: i) burning efficiency from the European emission inventory guidebook (EEA, 2019), for shrubs and forest species (Table 4); ii) fuel consumption based on an empirical model developed by Prichard *et al*. (2017).

Copyright © FirEUrisk Consortium. All rights reserved.

***Table 4.*** *Burning efficiencies for fire emission estimation* (EEA, 2019).

| Biome | Burning efficiency |
|---|---|
| **Boreal forest** | 0.2 |
| **Temperate forest** | 0.2 |
| **Mediterranean forest** | 0.25 |
| **Scrubland** | 0.5 |
| **Grassland (steppe)** | 0.5 |

Besides the methodology presented, the wildfire atmospheric emissions can also be estimated over time considering the rate of spread (Equation 3).

$$ER_{f,p} = (EF_{f,p}) \times w_f \times R \qquad \text{Equation 3}$$

where, $ER_{yn}$ is the source strength of emission n ($g.m^{-1}.s^{-1}$); p represents the emitted pollutant (e.g, CO, $CH_4$, or NOx); $EF_{yn}$ is the emission factor ($g.kg^{-1}$); $w_y$ is the mass of available fuel per unit of area ($kg.m^{-2}$); R is the rate of fire spread ($m.s^{-1}$); and f (if data is available) equals the phase of combustion (i.e., flaming or smoldering). However, if data is not available the average emission factor should be used.

While emissions estimations involve uncertainties at each step of the process, the greatest errors stem from fuel characteristics and fuel consumption. Despite advancements in fuel characterization and consumption modelling over the past 30 years, the uncertainty in emissions estimation remains high, necessitating further studies, particularly considering climate change.

### 3.2.2 Top-down

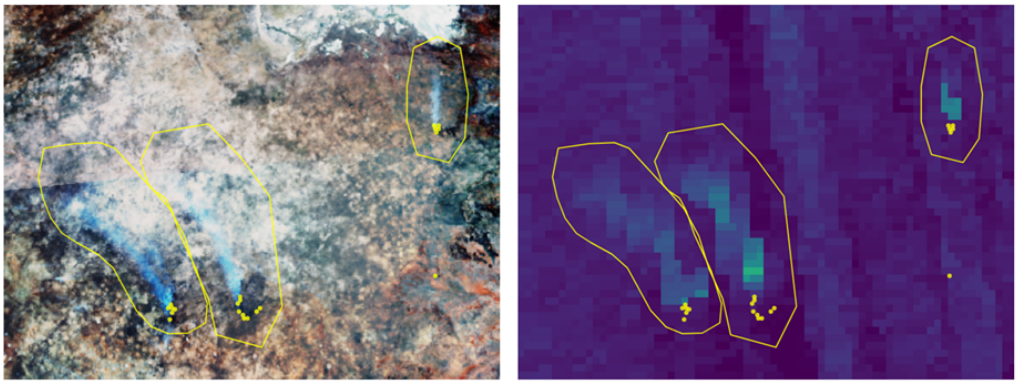
Certain 'top-down' procedures to estimate fire emissions are based on active fire observations. These more direct approaches to emissions estimation attempt to remove some of the assumptions required in bottom-up calculations that turn the burned area into fire emissions, and since they are based on observations made when the fires are still burning, they can be applied in almost real-time – potentially aiding smoke and air quality forecasting. Such approaches include the Fire Energetics and Emissions Research (FEER) approach of Ichoku and Ellison (2014) and the Fire Radiative Energy Emissions (FREM) method of Mota and Wooster (2018), Nguyen and Wooster (2020) and Nguyen *et al*. (2023). Both FEER and FREM approaches derive landscape fire emissions estimates directly from satellite-derived active fire data, specifically from fire radiative power (FRP) data that is now commonly derived from active fire observations (e.g., Terra and Aqua MODIS, Sentinel-3 SLSTR, NPP and NOAA 20 VIIRS and Meteosat over Europe; see Wooster *et al*., 2021). The approaches remove the fuel consumption estimation step required in the bottom-up methods, and thus also the uncertainties inherent in that calculation.

*In the FEER and FREM methods, a scalar (a so-called "smoke emission coefficient"; in $g.MJ^{-1}$) is generated for each fire-affected biome of interest, since these coefficients may vary between biome just as fire emissions factors do. The coefficients aim at capturing the relationship between the rate of release of fire radiative energy (FRE) (i.e., the fire radiative power –FRP- of the causal fire) and the associated*

Copyright © FirEUrisk Consortium. All rights reserved. 

*emission rate of a particular trace gas or aerosol species. Importantly, because values of these coefficients derived from laboratory fire measurements (e.g., as per Freeborn et al., 2008) may not be fully representative of all the effects relevant to satellite data of real landscape fires (see Freeborn et al., 2008; Mota and Wooster, 2018), the FEER and FREM approaches instead rely on emissions coefficients generated only from satellite data itself. The approaches specifically use a set of individual fire matchups for each biome of interest where the active fires and smoke plume are observed, with the active fires providing an FRP and/or FRE estimate and the smoke plume providing a total particulate matter mass or CO mass estimate.* (yellow points are the AF pixel detections taken from the Meteosat FRP-PIXEL product superimposed along with the bounding polygons used to delineate the fire plumes)

**Figure 2** shows an example from the FREM methodology aimed at generating CO emissions coefficients, in this case for African Savannah; satellites data are from 11:24 and 11:30 UTC respectively, on September 9th over an area in northern Botswana.



(yellow points are the AF pixel detections taken from the Meteosat FRP-PIXEL product superimposed along with the bounding polygons used to delineate the fire plumes)

***Figure 2.*** *Example data of matchup fires used to develop smoke emissions coefficients. (a) VIIRS RGB image of three landscape fire smoke plumes, (b) the corresponding image of Sentinel-5P derived total column CO.*

Smoke plume observations of aerosol optical depth (AOD) have been used to generate emissions coefficients relevant to total particulate matter (Ichoku and Ellison, 2014; Mota and Wooster, 2018; Nguyen and Wooster, 2020), whilst those of smoke plume carbon monoxide made from Sentinel-5P TROPOMI as in Figure 2 above have been used to generate CO emissions coefficients (Nguyen et al., 2023).

Figure 3, illustrating the FREM approach for estimating carbon monoxide emissions, showcases an example of the emissions coefficients generated for four different African biomes. Each coefficient is derived from the slope of an ordinary least squares (OLS) regression between the fire-emitted CO calculated from Sentinel-5P total column CO (TCCO) observations and the fire's matching FRE. The shaded grey area indicates the error of each slope. Error bars represent the uncertainty in both the FRE and total plume CO calculated from the uncertainty measures of the FRP-PIXEL product and the S5P TCCO product

Copyright © FirEUrisk Consortium. All rights reserved. 

respectively. As can be seen in this figure some of the biomes actually have emissions coefficients linking FRE to total CO mass emitted that are very similar to those of other biomes.

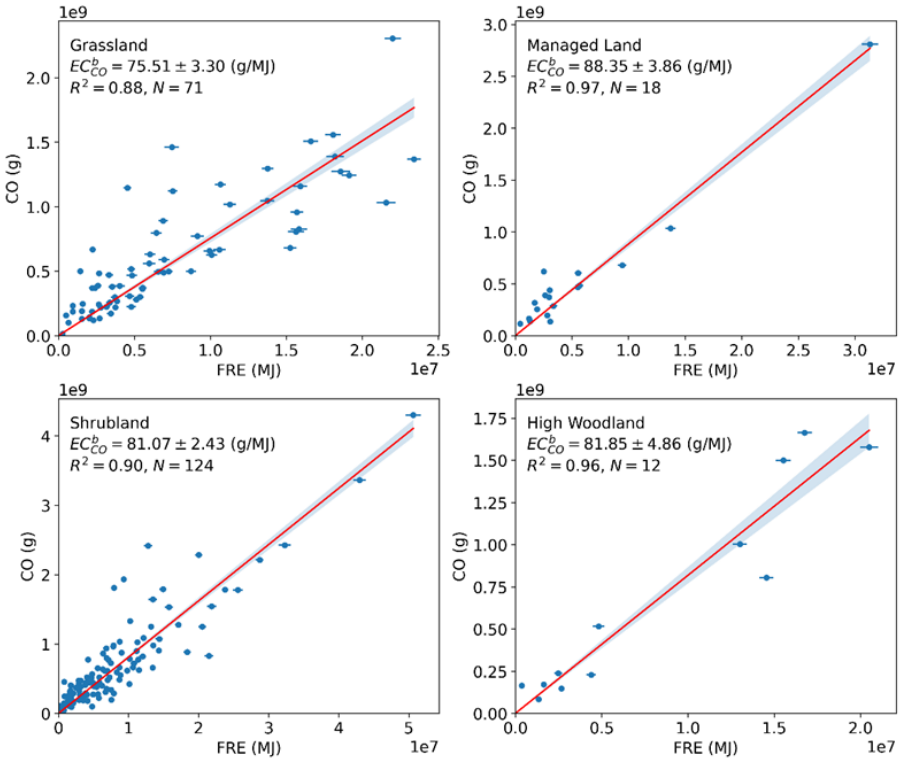



**Figure 3.** *Carbon monoxide smoke emission coefficients (in g.MJ$^{-1}$) derived from matchup fires burning across four fire-affected biomes of Africa.*

A key difference between the FEER and FREM approaches is that whilst in the FREM approach the emissions coefficients are generated from per-fire matchups in different biomes, in the FEER approach per pixel coefficients are generated from fire match ups within grid cells. This requires that the FEER approach have a much longer time-series of historical data to generate the coefficients with, as there needs to be sufficient fires in every grid cell to do so. Another difference is that the FEER approach is based on MODIS, and so provides a few observations of rates of emission of Total Particulate Matter (TPM) each day at present, whereas the FREM approach is based on far more frequent geostationary FRP observations. These are typically available every 10 or 15 minutes across the day, fully capturing the fire diurnal cycle. Such high temporal resolution smoke emission information has been shown useful for maximising the accuracy of smoke transport modelling (Baldassarre *et al*., 2015; Garcia-Menendez *et al*., 2014), and at present, the FREM approach has been developed using Meteosat data of Africa available every 15 minutes (Nguyen and Wooster, 2020). One limitation of these geostationary FRP data is that they cannot detect fires having as low an FRP as polar-orbiting systems such as MODIS can, due to their larger pixel sizes. However, Metosat Third Generation (MTG) is currently undergoing testing and once operational this will be able to

Copyright © FirEUrisk Consortium. All rights reserved. 

detect fires in southern Europe roughly as small and low FRP as those of MODIS. Once representative emissions coefficients are obtained using the matchup fires, these coefficients can be applied to the FRP data of any fire to derive the emission rate of the relevant particulate or trace gas species. This can be done from near real-time satellite data feeds if necessary, and it is planned to generate a real-time fire emissions product for Europe from the MTG data feed. This will cover total particulate matter and CO using the emissions coefficients generated from AOD and CO observations of the plumes as shown in Nguyen and Wooster (2020) and Nguyen *et al*. (2023) respectively, but will also cover other trace gas species by simply multiplying these emissions from a fire by the ratio of the emissions factor of the species of interest to that of the original TMP or CO emissions factor (see Nguyen *et al*., 2020). In this way it is planned to generate fire smoke emission rates for multiple species at a relatively high spatial resolution (e.g., 10 km grid) at 1 hr or 30 minutes intervals, in almost real-time to support smoke forecasting applications – including those related to air quality and health.

Within FireEURisk, we plan to expand on the work of Nguyen and Wooster (2020) and Nguyen *et al.* (2023) to generate smoke emissions coefficients for European fires, for both CO and TPM and via the emissions factor ratio approach for other species as well. A version of the ESA CCI land-cover map at 300 m pixel resolution used by Nguyen and Wooster (2020) and now adapted for use globally within the Copernicus Atmospheric Monitoring Service will be used to classify each of a series of matchup fires (see example in **Figure 4**) into different biomes across Europe and the biome-specific CO and TMP emissions coefficients estimated from a series of such matchup fires. In Figure 4, the conversion between AOD and TPM uses the simple linear relationship and the smoke mass extinction coefficient reported in Nguyen et al. (2023); the AOD product from VIIRS is outlined to first select the AOD of the fires smoke plume, and ultimately the excess total particulate matter in the plume as assessed against the non-smoke plume background.

Copyright © FirEURisk Consortium. All rights reserved.

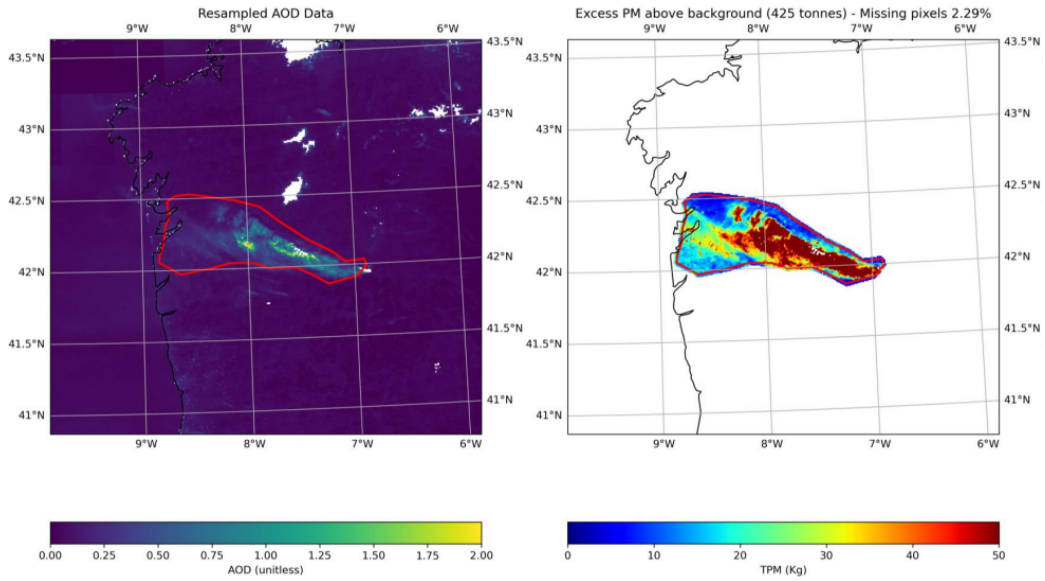



***Figure 4.*** *Example of a single matchup fire, with the AOD product and the excess total particulate matter in the plume.*

## 3.3 Smoke dispersion

Based on the review of available smoke dispersion systems and on the need to develop an operational forecasting system able to predict smoke dispersion and its impacts on the air quality and human health, two models were selected. They cover the local scale – DISPERFIRE – and the regional scale – CHIMERE.

### 3.3.1 Local scale - DISPERFIRE

DISPERFIRE (Valente *et al.*, 2007) is a simple modelling system comprised of a wind estimation module and a lagrangean dispersion module. The lagrangean approach for dispersion assumes that many marker particles statistically reproduce the turbulent transport. The displacement of each particle can be described as the sum of three components: the deterministic contribution from the average wind field, known from the meteorological module; the random 3D displacement; and the component linked with gravity effects, considering the difference in density between the gaseous particle and its environment. The turbulent 3D displacement is a function of local conditions. This component is modelled as a random displacement of mean zero and variance proportional to the effective components. Once the particle trajectories are determined, a given mass of pollutant is associated with each marker particle. Then, the mean concentration at a point is determined by counting the number of particles present in an appropriate control volume around that point.

Copyright © FirEURisk Consortium. All rights reserved.

At each iteration each particle is moved according to the following 3D equation:

$$\vec{x}_{i+1} = \vec{x}_i + \vec{r} + \vec{s} \quad \text{Equation 4}$$

where $x_{i+1}$ is the new position of the particle, $x_i$ its old position, r the displacement due to the mean wind (assuming that the particle will follow it) and s a displacement caused by turbulent diffusion. Turbulent diffusion is modelled as a random number taken from a zero-mean gaussian distribution with a standard deviation calculated by equation Equation 5:

$$\sigma = \sqrt{2 \cdot \Delta t \cdot \nu_t} \quad \text{Equation 5}$$

where Δt is the time-step and $\upsilon_t$ the eddy diffusivity. The physical basis for this simplification of turbulent diffusion is first described in Gifford (1982). In DISPERFIRE, eddy diffusivity is divided into horizontal and vertical diffusivity, where both are a function of the vertical coordinate η.

After the displacement of all particles in the domain, new particles are generated at cells with fire activity during the present time-step. The number of particles is proportional to the emitted mass. New particles are immediately displaced in the vertical direction according to a plume rise parameterization that is a function of heat released, as shown in Equation 6:

$$H = c1 \cdot Q^{c2} \cdot U^{c3} \quad \text{Equation 6}$$

where H is the plume rise height, Q the heat released (which can be calculated by a fire spread model) and U the magnitude of the wind-speed near the ground. $c_1$ to $c_3$ are constants that depend on atmospheric stability.

The results of DISPERFIRE are 3D concentration fields of emitted pollutants during the fire duration.

### 3.3.2 Regional scale - CHIMERE

CHIMERE is an open-source multi-scale Eulerian chemical transport model, which includes detailed gas-, aerosol- and cloud-phase chemistry. The chosen MELCHIOR2 chemistry mechanism takes 49 species and 120 reactions into account. Additionally, seven aerosol species are subdivided into 10-size bins, whose chemistry is also considered. CHIMERE can run over a range of spatial scales from the hemispheric to the urban scale (up to 1 km × 1 km). It has been widely used for air quality studies in Europe, which has allowed extensive testing and model evaluation over this study region (e.g., Monteiro *et al.*, 2007; Kukkonen *et al.*, 2012; Bessagnet *et al.*, 2016; Colette *et al.,* 2017). The model works with a structured hexahedral mesh that can be divided into subdomains of different resolutions so that a simulation with e.g., 25 km resolution can feed data to a 5 km resolution domain. This allows for a faster computation without losing the detail required for an accurate result. WRF, the meteorological model, is run on the same grid in parallel and feeds CHIMERE with data on meteorological variables such as wind speed, temperature and humidity. **Figure 5** presents a scheme of the WRF-CHIMERE modelling system.

Copyright © FirEUrisk Consortium. All rights reserved.

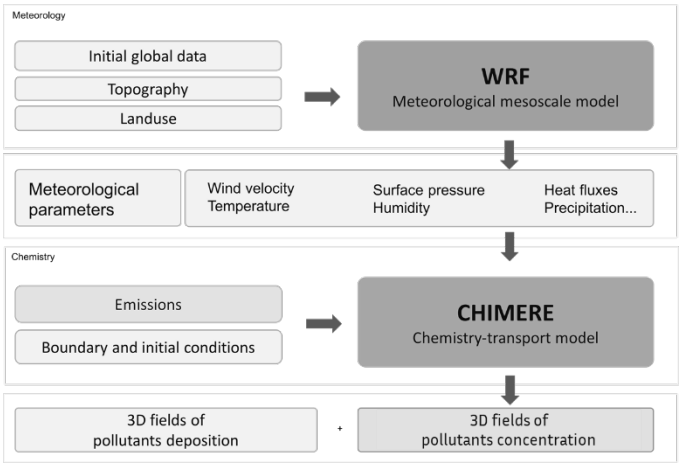



***Figure 5.*** *Scheme of the WRF-CHIMERE modelling system.*

The meteorological input variables are taken from the European Centre for Medium range Weather Forecast (ECMWF): 3D fields of horizontal wind, temperature, specific humidity, cloud liquid water content, and 2D fields of surface pressure, heat fluxes, 2 m temperature and cloud cover, with different resolutions according to the domain of simulation. They are linearly interpolated to the CHIMERE grid, and linear time interpolation is also applied to obtain hourly values. Besides the meteorological input, the CHIMERE model needs boundary and initial conditions, emission data, and the land use and topography characterization.

Lateral and top boundaries for the large-scale run are obtained by the MOZART second-generation model monthly climatology as described in Monteiro *et al*. (2005). As regards emissions, CHIMERE considers anthropogenic, mineral dust, biogenic and sea salt emissions. Anthropogenic emissions from EMEP/Centre on Emission Inventories and Projections database are processed to obtain hourly fluxes for the different model species and the specific simulation grids. Available time profiles for specific countries are used, as well as spatial proxies such as land use, population density and road network density. Desert dust, marine aerosols and biogenic emissions are estimated by the model during the simulations, taking static datasets and meteorological data into account. The hourly emissions fluxes of all sources are linearly interpolated in time at each time-step and injected into the corresponding cells of CHIMERE.

CHIMERE can be applied with a particular model able to estimate emissions from wildfires – the APIFLAME model (Turquety *et al.,* 2020). **Figure 6** depicts a scheme of the APIFLAME.

Copyright © FirEUrisk Consortium. All rights reserved.

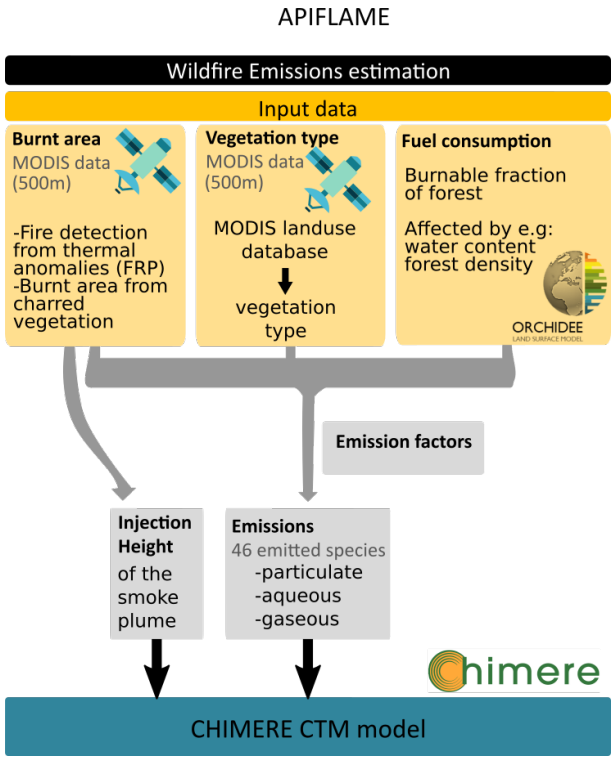



***Figure 6.*** *Scheme of the CHIMERE wildfire emissions model, the APIFLAME (Turquety et al., 2020).*

The burned area processing method provided with the code is based on the Moderate-Resolution Imaging Spectroradiometer (MODIS) fire observations of burned scars (Giglio *et al*., 2018) and active fires (Giglio *et al*., 2006). APIFLAME can merge both products to use the daily variability from the active fires (FRP dependent) and/or include small fires that may not have been detected in the burned scar product. Hourly variability based on geostationary observations (SEVIRI for Europe) is also included. In the last version of APIFLAME (v2.0), emission factors have been updated according to published data, and the possibility of using tabulated fuel consumption from the literature has been added.

The injection-height of the wildfire-plume in CHIMERE is calculated according to the parameterisation of Sofiev *et al.* (2012) with a correction of the FRP in the case of large fires as suggested by Veira *et al.* (2015). Menut *et al.* (2018) tested another profile and concluded that no clear differences in performance could be found. The empirical correlation developed by Sofiev *et al.* (2012) assumed that the wildfire-plume rises due to the heating generated up to a height at which all the energy from the fire has been dissipated. Thus, it depends only on the state of the atmosphere and the heat transfer to the air:

$$H_p = \alpha\, H_{abl} + \beta \left(\frac{FRP}{P_{f0}}\right)^{\gamma} \exp(-\delta\, N_{FT}^2 / N_0^2) \qquad \text{Equation 7}$$

where $H_p$ is the plume rise height, $H_{abl}$ the atmospheric boundary layer height, FRP the fire radiative power and NFT the Brunt-Väisälä frequency of the free troposphere (calculated as the average value of grid-cells

Copyright © FirEUrisk Consortium. All rights reserved. 

between $H_{abl}$ and 300 hPa). The other parameters were adjusted to satellite observations for the optimal performance of the model and are set to:

$$\alpha = 0.24;\ \beta = 170\ m;\ \gamma = 0.35;\ \delta = 0.6 \quad \text{Equation 8}$$

$$P_{f0} = 10^6\ W;\ N_0^2 = 2.5E-4\ s^{-2} \quad \text{Equation 9}$$

Values are hourly adjusted based on hourly atmospheric values calculated by WRF-CHIMERE, such as boundary layer height.

In CHIMERE, for cases where $H_p$ > 1500 m, the correction of Veira *et al.* (2015) is applied such that:

$$FRP^* = FRP\left(\frac{H_p}{1500}\right)^{0.5} \quad \text{Equation 10}$$

as Veira *et al.* (2015) considered that MODIS observations tended to underestimate FRP in the cases of high-intensity wildfires due to the opacity of the smoke to satellites. Another correction is applied in all cases whenever the considered period is between 18:00 and 06:00. During this night-time period, where the boundary layer height tends to be lower, only half of the FRP is considered in the calculation of the plume-rise. The next step of the algorithm consists in comparing the obtained value to other estimates. In cases where the atmospheric boundary layer height is larger than the estimated, the former is used instead. Finally, a lower threshold of 1 km is applied.

APIFLAME data is fed to the chemical transport model CHIMERE, with the chemical species injected into the CHIMERE grid as sources.

Recently, Turquety *et al.* (2020) used the WRF-CHIMERE system coupled with APIFLAME for the 2016 fire season in Portugal. Osswald *et al.* (2023) also applied WRF-CHIMERE-APIFLAME to simulate the 2021 summer Greek fires (please, see 4.2 for more details).

## 3.4 Health impact

Health impacts are calculated based on an exposure assessment approach considering the smoke exposure duration, as well as the concentration of the different pollutants along the exposure period and the toxicity of the different compounds. Short-term physical impacts of exposure to smoke are expressed as morbidity and mortality indicators, mostly related to respiratory and cardiovascular diseases. The latest version of the AirQ+ software (v1.3 released by the World Health Organization in 2018), using methodologies and concentration-response functions well established by epidemiological studies, is the basis for the estimation.

Both, linear and non-linear, WHO methodologies use the same base formulation (Equation 11), differing only in the calculation of the adjusted relative risk (RR). The linear RR function assumes a positive linearity between concentration and risk (Equation 12), whereas the non-linear method uses a RR function in which health risks tend to increase slower with increasing concentrations (Equation 13).

$$HI_{(p,i)} = ( pop_{(p,i)} \times Inc_{(i)} ) \times RR_{(p,i)} \quad \text{Equation 11}$$

Copyright © FirEURisk Consortium. All rights reserved.

where:

$HI_{(p,i)}$ represents the number of unfavourable implications (cases of disease, deaths) associated with the health indicator i, due to pollutant p´s short term exposure;

$pop_{(p,i)}$ is the population at risk (all ages or certain age groups) associated with the RR meta-analysis;

$Inc_{(i)}$ corresponds to the baseline incidence/prevalence rate of a specific health indicator i (expressed as the number of new cases per 100000 individuals per year);

$RR_{(p,i)}$ correlates a pollutant p´s concentration variation with the probability of experiencing or avoiding a specific health indicator i.

To calculate the adjusted RR for a given health indicator, the linear function assumes a positive linearity between concentration and risk (Equation 12, hereinafter referred to as linear RR), whereas the nonlinear method uses a logarithmic RR function in which health risks tend to increase slower with increasing concentrations (Equation 13, hereinafter referred as nonlinear RR) (Ostro, 2004).

$$RR_{(p,i)} = \exp [ \beta_{(p,i)} (X - X_0) ] \quad \text{Equation 12}$$

$$RR_{(p,i)} = \exp [ \beta_{(p,i)} (\ln (X + 1) - \ln (X_0 + 1)) \quad \text{Equation 13}$$

where:

$\beta$ coefficient denotes the change in the RR for unit change in concentration X (expressed as the natural logarithm of RR);

X is the pollutant p´s concentration ($\mu g.m^{-3}$). Daily or hourly values are used to calculate the short-term exposure risk;

$X_0$ indicates the pollutant p´s cut-off or counterfactual concentration value ($\mu g.m^{-3}$) above which health impacts are calculated.

Standard CRF values (i.e., β coefficients) are often presented with a 95 % confidence interval (CI) and result from a systematic review based on published epidemiological studies and their meta-analyses, hence they are highly recommended rather than single local studies (WHO, 2013a, 2013b). Regarding the cut-off concentration values, the WHO air quality guidelines are suggested, as these provide overall guidance on thresholds and limits for key air pollutants harmful to human health (WHO, 2021).

Short-term exposure studies are usually focused on exploring the high variability of acute health effects using hourly/daily time-series of pollutant concentrations, as estimated by dispersion models. Thus, hourly spatial distributions of modelled air pollutants concentrations are crossed with time activity patterns of populations (or firefighters) affected by the smoke resulting in population exposure estimations. The main output is an hourly spatial distribution of population's exposure to air pollutants during the smoke event, and the changes in mortality morbidity indicators due to this exposure.

Copyright © FirEURisk Consortium. All rights reserved.

# 4 Case studies

The case studies presented here were conducted to test and refine various FirEUrisk modeling tools, aiming for enhanced integration within the FirEUrisk modeling system. They cover one demonstration area (Chornobyl exclusion zone - DA15) and two pilot sites (PS3 – Mediterranean Portugal / Central Region of Portugal and PS5 – Mediterranean Greece / Attica Region). Chornobyl's case is about modelling fire progression and fire smoke dispersion for a fire event in 2016, the first "big" wildfire within the near fallout zone of the radioactive track. Both Mediterranean pilot sites are about smoke emissions and chemical transport from large fire events.

## 4.1 Chornobyl Exclusion Zone (DA15)

The demonstration area DA15 covers the Chornobyl Exclusion Zone (CEZ) in Ukraine and neighbouring regions of Belarus contaminated after the Chornobyl accident at the CNPP (**Figure 7**). The current extent of the DA15 (70 km × 110 km) has been defined to consider the effects of transboundary fires spreading towards the CEZ.

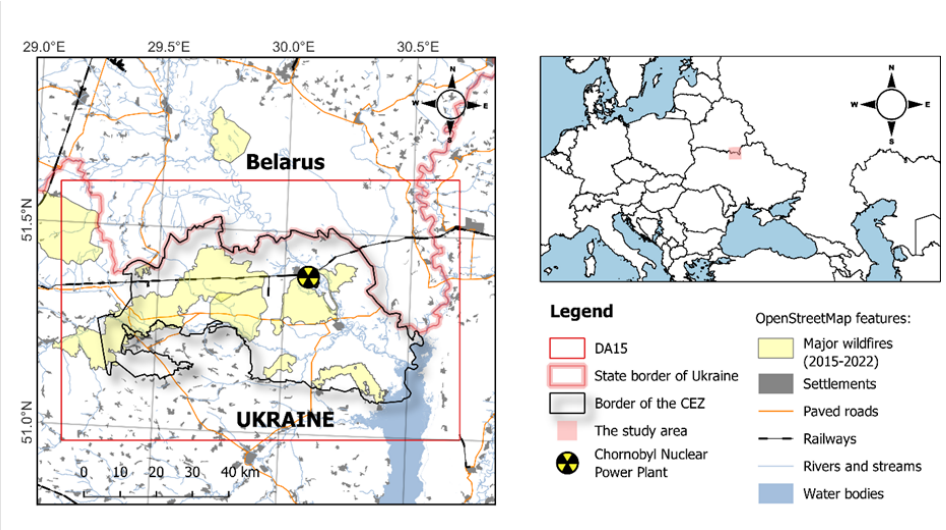



***Figure 7.*** *The Chornobyl Exclusion zone demonstration area (DA15).*

More than half of the area is covered by forests, dominated by Scots pine (*Pinus sylvestris L.*) and mixed broadleaf stands of silver birch (*Betula pendula L.*), black alder (*Alnus glutinosa (L.) Gaertn.*), aspen (*Populus tremula L.*) and oak (*Querqus robur L.*). The forests have remained largely unmanaged since the 1986 accident, with limited logging associated with the construction of nuclear waste disposal facilities, salvage logging and fuel breaks. In contrast to the CEZ, where agricultural land has been abandoned and

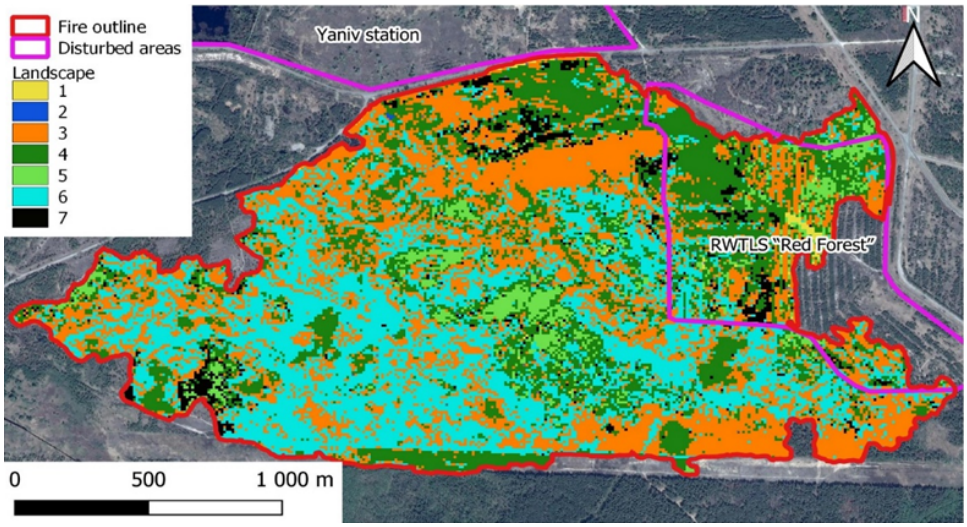
Copyright © FirEUrisk Consortium. All rights reserved. 

transformed into natural meadows or mixed forests (Matsala *et al.,* 2021) agricultural land outside the CEZ is still used by farmers and the local population for crop production. The practice of burning grass and crop residues in areas surrounding the CEZ has resulted in large wildfires in this area.

The first "big" wildfire within the near fallout zone of the west radioactive track began on July 15, 2016, at about 4:25 p.m. and lasted until the morning of July 18. The boundary of the 2016 Fire was determined in September 2016 by a regular walking tour using a GPS tracker. This area is contaminated by radionuclides (RN) due to the Chornobyl NPP accident in 1986.

### 4.1.1 Fire progression

Ecosystems classification was performed using Sentinel-2 satellite images: before (2016-06-17) and after (2017-08-01) the fire. The following biomes were identified as important for the assessment of radioecological parameters and biomass: sparse grass, pine stands, swamps, meadow, birch/deciduous stands and dead forest. The number of sampling points for identification landscapes was more than 2000 pcs within Chornobyl Exclusion Zone and XGBoost was applied as a classification algorithm (in Scikit-learn API). The total accuracy of landscape classification was more than 85%, and for forests (pine+deciduous) was more than 90%. **Figure 8** depicts the spatial distribution of vegetation in the Red Forest burnt area, before the fire.




1 – sparse grass, 2 – water basins, 3 – pine stands, 4 – swamp, 5 – meadow, 6 – birch/deciduous stand, 7 – dead forest

***Figure 8.*** *Landscape spatial distribution before wildfire in 2016.*

The 2016 fire started in a forest stand further south of the "Pripyat-Chystogalivka" road near Yaniv station RWTLS (radioactive waste temporary localization site). The fire growth was simulated using the FARSITE fire behaviour modelling approach incorporated into the FlamMap v.6.2 software (Finney 1998, 2004). This utilized information on surface and crown fuels distribution to compute wildfire spread with

Copyright © FirEUrisk Consortium. All rights reserved. 

sequences of weather conditions. A set of raster layers of 100-m spatial resolutions to characterize topography (elevation, slope, aspect), surface fuels (fuels models by Scott and Burgan, 2005), and canopy fuels (canopy cover, canopy height, canopy base height, canopy bulk density) were used. The simulation was performed within the delineated final fire outline. The historical weather records required for the modelling were extracted using 6-h intervals. The fuel content moisture of the fuel models was adjusted to obtain precise correspondence between the arrival time of the final fire contour with actual fire duration and its outline. Given the information about the location and time when the wildfire started and its total duration, perimeters were generated using 6-h time lag. **Figure 9** shows the fire progression along time.

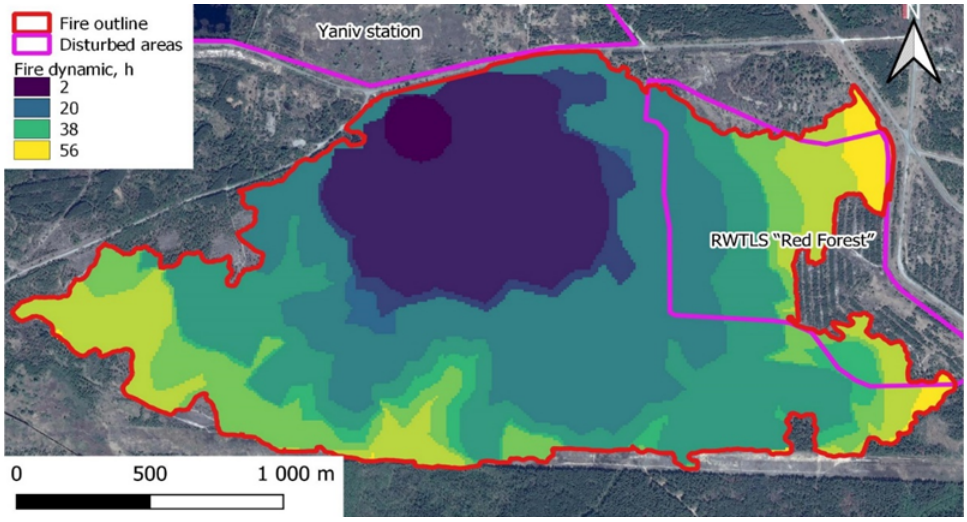



***Figure 9.*** *Simulated wildfire progression lines (start time – 15 July 2016, 4 pm)*

### 4.1.2 Emissions and dispersion

It is not common to model the smoke impact from wildfires in areas contaminated with radionuclides, but it is crucial to be prepared to acquire maps of radionuclide concentration levels in the air. In this scope, the DISPERFIRE modelling system was adapted and applied to the wildfire that took place in 2016 in the Red Forest close to the Chernobyl Nuclear Power Plant. The region is contaminated with radionuclides, due to the nuclear accident of 1986, that were scattered and dispersed in the air alongside with the wildfire smoke.

For the estimation of radionuclides emissions to the air due to the wildfire, the following information was used: maps of main Chornobyl RNs (isotopes Sr-90, Cs-137, plutonium isotopes (Pu-238-240) and Am-241) density contamination of soil (top layer to up a depth of 20 cm) as of 2020; field data on fuel load of forest stands; radionuclides content and transfer factors from the soil into biomass components; landscape classification implemented based on satellites remote sensing.

Copyright © FirEUrisk Consortium. All rights reserved.

RNs activity in the soil and biomass components was based on radioecological methods, namely aggregated transfer factors for biological mobile RNs (Sr-90 and Cs-137) from soil to individual vegetation organs (which are a source of combustible materials: foliage, bark and so on). For Red Forest RWTLS, the determination of RNs and biomass inventory have been used empirical data from two forest sites in 2015. For herbaceous landscapes, we took radioecological indicators from scientific publications where the material collections were obtained within Chornobyl Exclusion Zone. The main input data parameters for the calculation of RN activity are presented in Table 5 (Beresford *et al*., 2018; IAEA, 2010; Kashparov *et al*., 2020; Holiaka *et al*., 2020a,b).

***Table 5.*** *Combustible biomass and radioecological parameters for 2016 Fire.*

| Landscape | Combustible biomass, kg/m$^2$ (Paskevich, 2005; Borsuk, 2020) | Aggregated transfer factor ($Tf_{ag}(i)$), (Bq/kg)/(kBq/m$^2$) (outside "Red Forest" RWTSP) | | Activity concentration in combustible biomass, Bq/kg (within"Red Forest" RWTSP) | |
|---|---|---|---|---|---|
| | | Sr-90 | Cs-137 | Sr-90 | Cs-137 |
| Sparse grass | 0.01 | 14 | 2.3 | 22±18** | 0.6±0.6 |
| Pine forest | 1.43 (+2.2)* | 100±74 | 23.8 | 855±450 | 43±24 |
| Swamp | 0.74 | 7.4±4.9 | 1.7±0.9 | 22±18 | 0.6±0.6 |
| Meadow | 0.27 | 14 | 2.3 | 22±18 | 0.6±0.6 |
| Birch/Deciduous forest | 0.35 (+1.7)* | 100±74 | 16 | 1950±960 | 95±66 |
| Dead forest | 3.6 | 100±74 | 23.8 | 855±450 | 43±24 |

*Note*: * is if crown fire needs to add this weight; ** is standard deviation

RNs (*i*) activity concentration of fire material ($A(i)_{fm}$, Bq kg$^{-1}$) was calculated as:

$$A(i)_{fm}=Tf_{ag}(i)\cdot A_{soil}(i) \qquad \text{Equation 14}$$

where: $A_{soil}(i)$ is soil density of contamination with i-radionucledes, kBq m$^{-2}$; $Tf_{ag}(i)$ is aggregated transfer factor is the ratio of the dry mass activity concentration ($A(i)_{fm}$, Bq kg$^{-1}$) in fire material to the unit soil density of contamination ($A_{soil}(i)$, kBq m$^{-2}$).

Transuranic elements (TUE: plutonium isotopes and Am-241) are not accumulated in plants. Therefore, the emission of these RNs into the air during fires was calculated dependent on the density of their contamination of the soil and the probable values of stocks of combustible materials. According to the results of experimental studies, the Pu-238-240 "rise" share into the air is only 8E-07 for grass fires and 24E-07 for forest fires from density contamination of soils. Am-241 has 5 times more value for this parameter. Sr-90 and Cs-137 emissions in the air are 1% and 2% of their activity in combustible materials respectively.

Moreover, the RNs contamination density of soils (unit in kBq m$^{-2}$) along time was calculated considering the classical radioactive decay law. Thus, reduction of RNs activity was calculated based on the RNs half-life equation:

Copyright © FirEUrisk Consortium. All rights reserved.

$$N = N_0 \cdot 2^{-\frac{\Delta t}{T_{1/2}}}$$ Equation 15

where: $N$ – final contamination (activity/density/dose rate), $N_0$ – initial contamination (activity/density/dose rate); $\Delta t$ – time period, which is a difference between the final and the initial measurement of time, $T_{1/2}$ – the half-life of the radionuclide.

RNs half-lives ($T_{1/2}$) have obtained from IAEA web-application "Livechart - Table of Nuclides - Nuclear structure and decay data" (https://www-nds.iaea.org/relnsd/vcharthtml/VChartHTML.html#dcy1).

Figure 10 shows the spatial distribution of Sr-90 and Pu-238-240 total radionuclides emissions to the air due to the 2016 wildfire event.

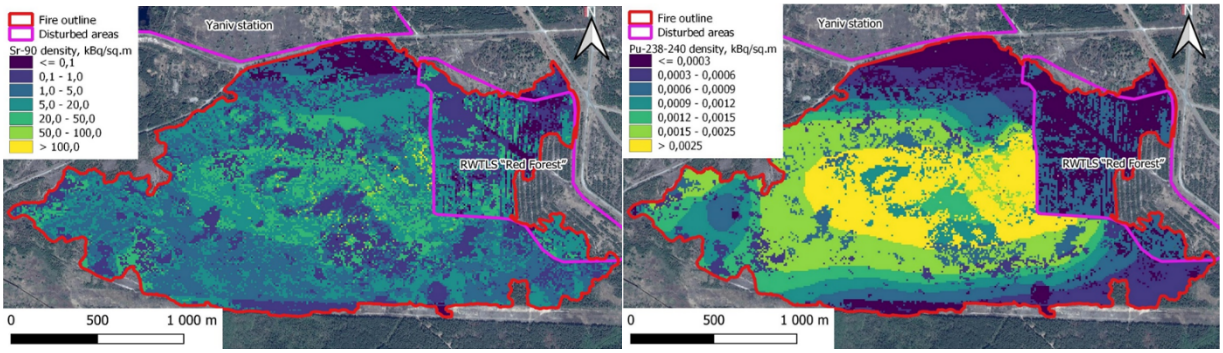



***Figure 10.*** *Spatial distribution of Sr-90 and Pu-238-240 radionucleides emissions (kBq/m$^2$) to the air.*

These emissions were distributed along time taking into consideration their temporal profile along the fire (see Table 6).

***Table 6.*** *Time series of RNs emissions (GBq) during the Chornobyl wildfire.*

| Day/Time | Fire time, h | Cs-137 activity, GBq | Sr-90 activity, GBq | Pu-238-240 activity, GBq | Am-241 activity, GBq |
|---|---|---|---|---|---|
| 15 / 18:00 | 2 | 0.27 | 0.19 | 0.00003 | 0.00014 |
| 16 / 0:00 | 8 | 8.34 | 7.50 | 0.00112 | 0.00559 |
| 16 / 6:00 | 14 | 1.42 | 1.25 | 0.00027 | 0.00137 |
| 16 / 12:00 | 20 | 0.26 | 0.29 | 0.00007 | 0.00036 |
| 16 / 18:00 | 26 | 9.18 | 9.64 | 0.00192 | 0.00962 |
| 17 / 0:00 | 32 | 4.21 | 4.87 | 0.00082 | 0.00412 |
| 17 / 6:00 | 38 | 0.65 | 0.93 | 0.00015 | 0.00073 |
| 17 / 12:00 | 44 | 1.93 | 2.55 | 0.00033 | 0.00163 |
| 17 / 18:00 | 50 | 1.55 | 2.09 | 0.00026 | 0.00129 |
| 18 / 0:00 | 56 | 0.10 | 0.28 | 0.00003 | 0.00015 |
| **TOTAL** | | 27.9 | 29.6 | 0.0050 | 0.0250 |

Copyright © FirEUrisk Consortium. All rights reserved.

It was estimated that during the wildfire a total of 27.9 GBq of Cs-137, 29.6 GBq Sr-90, 5MBq Pu isotopes and 25MBq Am-241 were emitted. During the simulation period a total of 9,64 GBq of Sr-90 were emitted.

Finally, the produced data on emissions of the five isotopes (Cs-137, Sr-90, Pu-238, Pu-240 and Am-241) with a detailed spatial and temporal distribution were used as input data for the dispersion simulation with DISPERFIRE.

The concentrations of each radionuclide, throughout the event, were estimated with the DISPERFIRE smoke modelling system at a horizontal resolution of 10 m in a 3.5 km × 1.6 km domain. The heat released by the flames was used to estimate the smoke plume rise while the emissions at each cell and at each time-step obtained from the FlamMap wildfire dynamics simulations provided the amount of each radionuclide to be emitted. The dispersion was calculated using the lagrangean formulation, where each particle represents a given amount of the emitted radionuclides. Particles are advected by the joint effect of the mean wind and a random motion. **Figure 11** shows the spatial distribution of Sr-90 at two heights and two time periods after the beginning of the simulation.

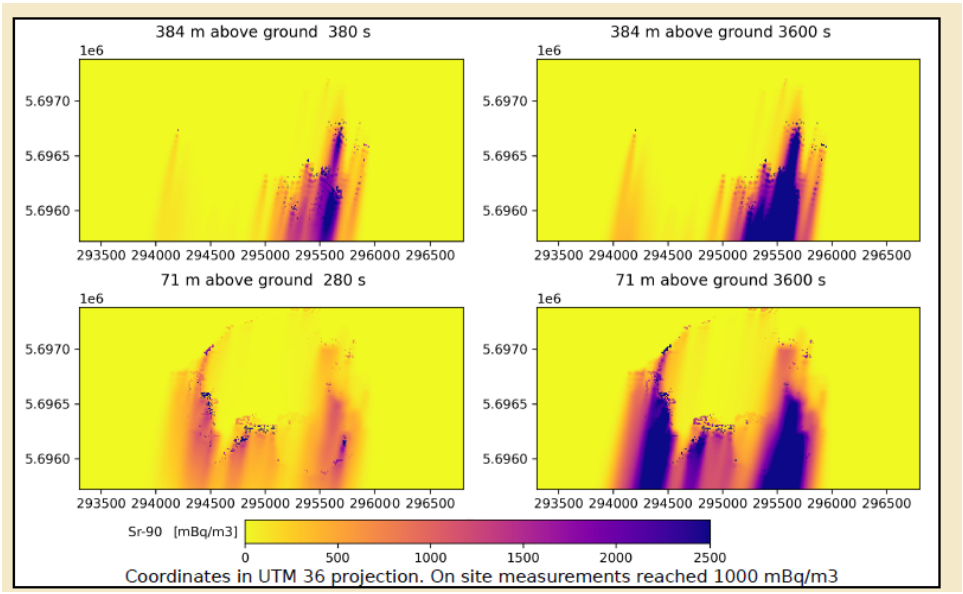



***Figure 11**. Spatial distribution of Sr-90 concentration levels (mBq/m$^3$) at two heights and two time periods after the fire began.*

The local levels of radionuclides reached dangerous levels for human health near the wildfire location. The developed methodology will allow for better preparedness and response to wildfires in forests contaminated with radionuclides.

Copyright © FirEUrisk Consortium. All rights reserved.

## 4.2 Mediterranean Portugal / Central Region of Portugal (PS3)

The Portuguese pilot site (PS3) included emissions estimation by top-down (2022 August fire event) and bottom-up (2017 October fire event) approaches, as well as the simulation with a CTM of the smoke levels during the extreme fire events in October 2017.

### 4.2.1 Emissions

#### 4.2.1.1 Top-down

The fire event over Serra da Estrela, in central Portugal, that occurred during August 2022 was analysed. According to national authorities, Serra da Estrela (SE) fire broke out on 6 August 2022, affecting 27,340 hectares in several local municipalities in the districts of Castelo Branco and Guarda, located in the Centre Region of mainland Portugal (between latitudes 40º 17' 58''N and 40º 37' 21''N and longitudes 07º 09' 06''W and 07º 40' 40''W). The SE fire was reported extinguished on 2 September and lasted 28 days.

In this case study, the rationale was to use a top-down approach to estimate smoke emissions from fires, based on Fire Radiative Power (FRP) data, as smoke production is directly linked to the intensity of a wildfire, which can be assessed based on released energy, obtained through FRP data (Wooster, 2015). Since the FRP is proportional to the amount of burned biomass, higher FRP values are linked to more severe fires, with high levels of smoke production and, consequently, high emissions of particulate matter and other smoke pollutants. In this work, the goal was to explore FRP ability to be used as an indicator of fire smoke pollution, taking advantage of the very high temporal resolution of data retrieved from geostationary satellites (15 minutes for Meteosat Second Generation, MSG). For that, the estimation of TPM emissions during the recent 2022 August wildfires in Portugal was done to assess the link between air pollution levels and fire intensity over the Portuguese affected areas. The computation of the emitted TPM mass considers the spatial and temporal characteristics of each fire event.

The daily FRE values emitted by SE fire were calculated from the temporal integration of FRP data (SEVIRI/MSG disseminated by LSA-SAF), based on the formula by Pinto *et al.* (2018), during the fire lifetime. The hourly energy emitted by the SE fire at a specific pixel was computed by integrating the radiative power measured by SEVIRI in that pixel over the considered hour. Since the data are collected every 15 minutes, the hourly energy, FRE (in gigajoules, GJ), for each pixel *p* and hour *h* was estimated by the equation 16:

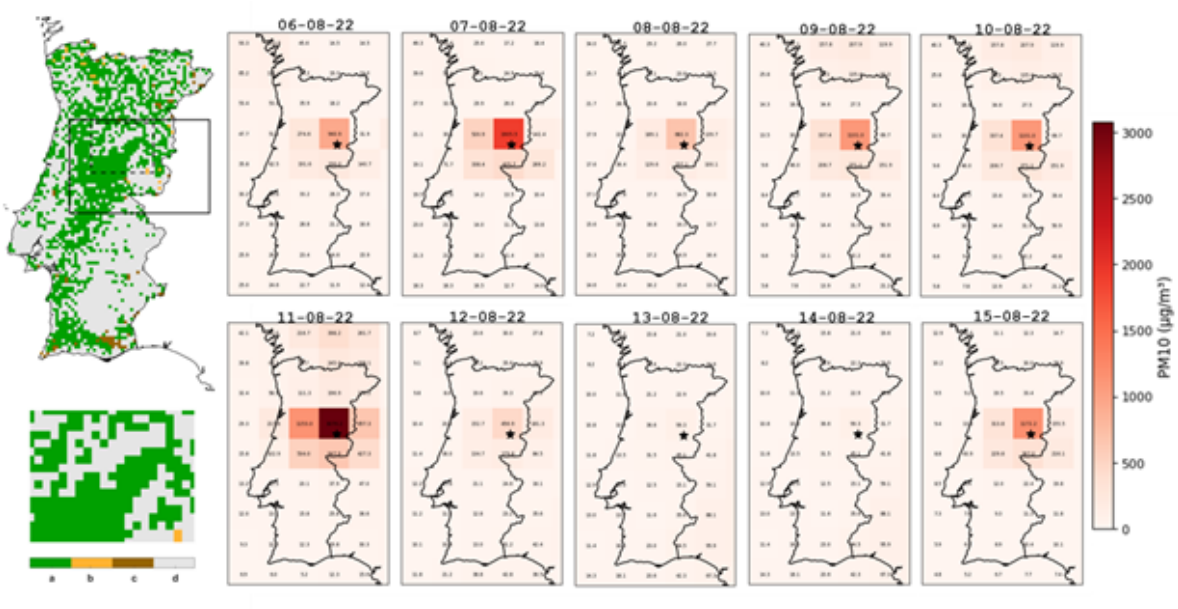
$$FRE_{ph} = 0.9 * \left(\sum_{k=1}^{4} FRP_p\right)_h \qquad \text{Equation 16}$$

where the index *k* indicates the sequence of 15 minutes of each hour, $FRP_p$ is the fire radiative power (in MW) in pixel *p,* and 0.9 is a factor that converts the result into GJ.

Copyright © FirEURisk Consortium. All rights reserved.

The daily $FRE_{pd}$ is the accumulated hourly $FRE_{ph}$, over the 24 hours *h*, for each pixel *p*. Moreover, the daily FRE for the fire event corresponds to the daily accumulated FRE, of all pixels present over the study area.

Apart from the methodological difference between FEER and FREM approaches (see section 3.2.2), the estimated daily mass of total particulate matter (TPM in kg or g) emitted by Serra da Estrela fire was computed by multiplying the daily FRE values by the specific TPM coefficient values for European regions. In the case of the FEER approach (Ichoku and Ellison, 2014), a single value was considered (24 $g.MJ^{-1}$). Conversely, the FERM approach (Nguyen and Wooster 2020), considered the TPM coefficients for each European Temperate biome type (broadleaved (21.9 $g.MJ^{-1}$), evergreen-broadleaved (24.4 $g.MJ^{-1}$), deciduous (23.6 $g.MJ^{-1}$); grassland (20.6 $g.MJ^{-1}$); shrubs (12.8 $g.MJ^{-1}$) and sparse vegetation (9.6 $g.MJ^{-1}$) for each land cover type over SE-affected areas, following the classification provided by the European Space Agency Climate Change Initiative (CCI) land cover map (2020). Thus, the considered TPM coefficient values for the SE local land cover classes (see Figure 12) result from a coefficient average of the given three Forest classes (broadleaved, evergreen-broadleaved, deciduous); (23.3 $g.MJ^{-1}$); a single value for the grassland class (20.6 $g.MJ^{-1}$); and a coefficient average of the given two shrubs and sparse vegetation classes (11.2 $gMJ^{-1}$), respectively.




a – forest, b – grassland, c – shrub land and sparse vegetation; ★Fundão air quality monitoring station

***Figure 12.*** *Left Panel: Serra da Estrela land cover types over fire-affected areas. Right Panel: Simulated PM10 maximum concentration daily values (6 to 15 of August 2022).*

The concentrations levels of PM10 over the Serra de Estrela (SE) region were also evaluated through the CAMS model reanalysis and forecast data, as well as from in-situ data, provided by the local

Copyright © FirEUrisk Consortium. All rights reserved. 

air quality monitoring station, Fundão station, (40.2331ºN; -7.29959ºW) to check if TPM space and time emissions estimation patterns were captured by the national monitoring station network and by CAMS products, as well. Maps of maximum and mean daily PM10 concentrations based on the fire lifetime were produced for Portugal mainland, during the SE fire lifetime. Figure 12 (right panel) illustrates the maximum daily PM10 concentrations over the first 8 days of fire; where the 7$^{th}$ and the 10$^{th}$ of August are the fire days with the highest daily PM10 concentrations observed. These patterns are also following FRE emitted by the fire during these days derived from FRP data, as can be seen in section a) of Figure 13. The estimated TPM emissions based on FEER and FERM coefficients presented in sections b) and c) of Figure 13 reveal similar space-time behaviour, following FRE patterns, as expected.

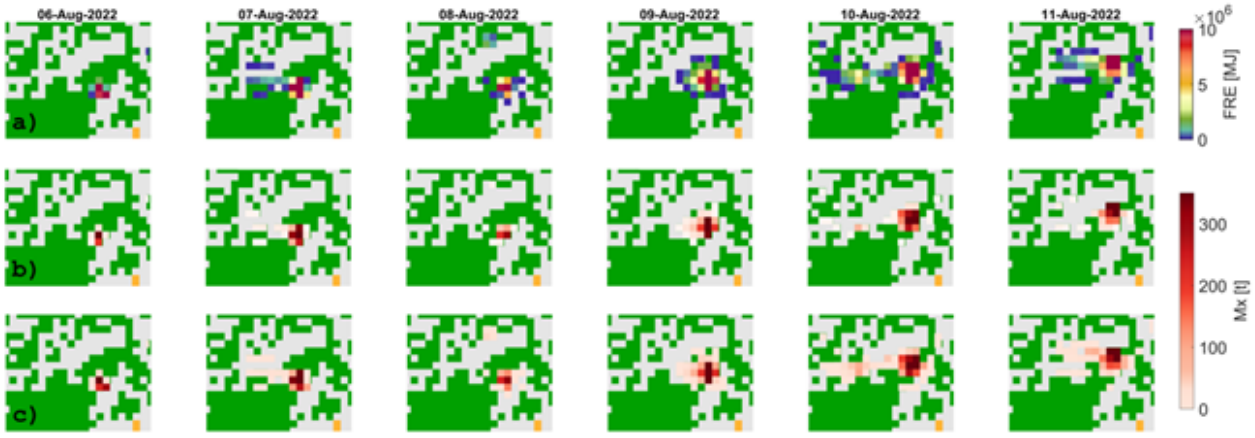



***Figure 13**. a) Daily fire radiative energy emitted (6 to 11 of August 2022); b) Estimated TPM daily mass values emitted considering FERM TPM emission coefficients; c) As in b) but considering FEER TPM emission coefficients, respectively.*

The temporal evolution of the estimated TPM emissions is well captured by the daily PM10 concentrations provided by CAMS products, and that are simply represented in Figure 14, where TPM emissions and maximum daily PM10 concentrations observed are in good agreement.

Copyright © FirEUrisk Consortium. All rights reserved.

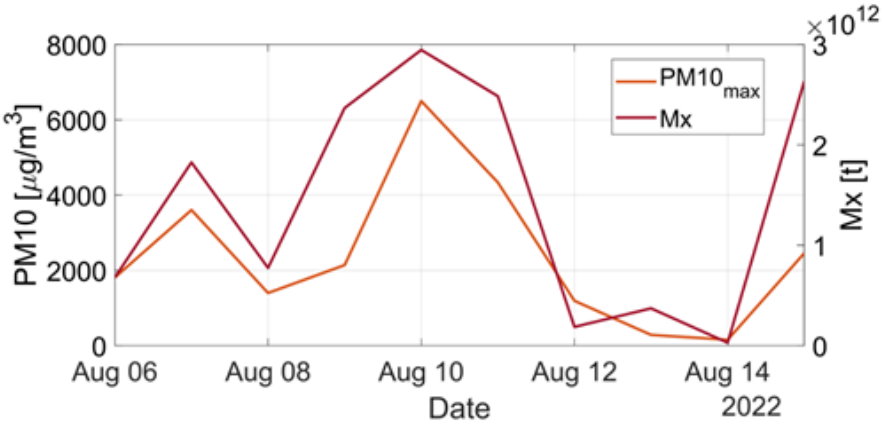
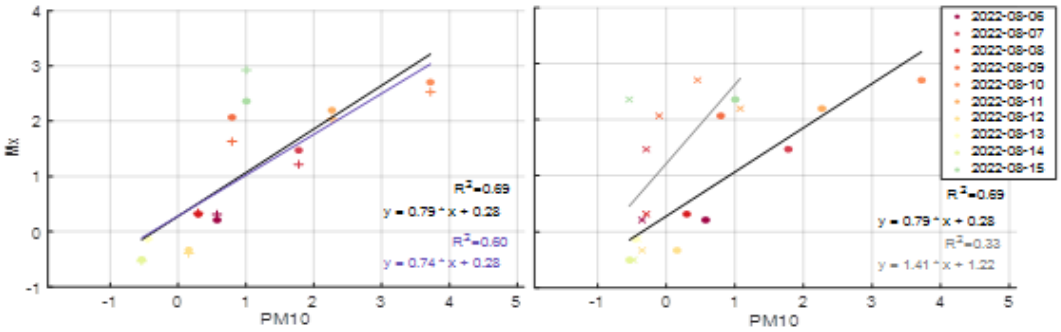



***Figure 14**. Daily evolution of maximum observed PM10 values (CAMS reanalysis), and TPM estimated mass emitted (from 6 to 15 of August 2022) considering the FERM coefficients.*

To assess the relation between air pollution levels observed and fire intensity over the SE fires affected areas, a correlation analysis between maximum daily PM10 concentrations, TPM coefficients (FEER and FERM), and in-situ observations was performed (where all the variables normalized by all August daily data values), as shown in Figure 15.




+ FEER, o FERM, x maximum observed values at Fundão

***Figure 15.** Left panel: Scatter plot of TPM mass emitted (from 6 to 15 of August 2022) considering FEER and FERM coefficients and maximum observed PM10 values (CAMS reanalysis); Right panel: As in left panel but for maximum observed in-situ PM10 values.*

Again, a significant agreement between TPM emissions and maximum daily PM10 concentrations is observed, with FERM coefficients revealing a better result, with a correlation of ~70% (and ~60% for FEER); revealing also a weak agreement with the in-situ monitoring data, with a correlation coefficient of 30%, as expected, due to the localization characteristics of this monitoring station. The fire intensity, based on the emitted FRE values, aligns with the known severity of this event, consistent with the observed

Copyright © FirEURisk Consortium. All rights reserved. 

concentrations of air pollutants, being demonstrated that the FRP can be associated with smoke production, particularly TPM emissions during SE fire.

In general, the presented results are quite good, showing that the proposed methodology has the potential to use FRP data as an indicator of air pollution and smoke dispersion over fire-affected regions. However, further detailed comparisons and validations, between other fire-based pollutants must be accomplished, considering also other recent fire events.

#### 4.2.1.2 Bottom-up

On the morning of 15th October 2017, at 6 a.m., in the central region of Portugal, a serious wildfire situation started and developed into seven extreme wildfire events (EWE) that lasted until 8 a.m. on the 16th of October. Fire data, such as ignition location and time, and burned area, for each EWE, were reported by the "Associação para o Desenvolvimento da Aerodinâmica Industrial" (ADAI, 2019), based on fire data collected in the field, namely on many interviews with operational and affected people, among others who experienced the fire firsthand. Besides, several photographs and videos of the fire progression were considered. This detailed information allowed to inventory the different ignition points, how fires spread and affected the territories, and therefore to estimate the burned area with a high spatial and temporal resolution. Table 7 shows a summary of the information about the burned area, ignition time and wildfire duration for each EWE.

***Table 7.*** *Information about the burned area, ignition time, and wildfire duration for the seven EWE between 15th and 16th October 2017 (ADAI 2019).*

| Extreme Wildfire Events (EWE) | Burned area (ha) | Start Time (Day – hh:mm) | Finish Time (Day – hh:mm) | Duration (hh:mm) |
|---|---|---|---|---|
| Leiria | 20,014 | 15 – 14:10 | 16 – 01:00 | 10:50 |
| Lousã | 54,407 | 15 – 10:15 | 16 – 03:00 | 17:45 |
| Oliveira do Hospital | 51,429 | 15 – 11:00 | 16 – 05:00 | 18:00 |
| Quiaios | 23,844 | 15 – 11:50 | 16 – 00:00 | 12:10 |
| Seia | 17,003 | 15 – 06:00 | 16 – 08:00 | 26:00 |
| Sertã | 30,977 | 15 – 12:10 | 16 – 01:00 | 13:10 |
| Vouzela | 15,959 | 15 – 17:30 | 16 – 03:00 | 09:30 |

The first forest fire warning was issued in Seia, where 17,003 ha of forest and shrubland were burned. Four hours later, a second occurrence was registered in Lousã, in which 54,407 ha were burned. The fire in Oliveira do Hospital started at 10:26 a.m. and resulted in the destruction of several houses and industrial facilities as well as a vast burned area (51,429 ha). In Sertã the fire started around midday on October 15th (30,977 ha burned). In the coastal zone of Portugal, the first forest fire ignition occurred around 2 p.m. in Leiria and Quiaios with a burned area of 20,014 and 23,844 ha, respectively. The last forest fire alert was registered at 5:21 p.m. in Vouzela with the smallest burned area (15,959 ha).

Copyright © FirEUrisk Consortium. All rights reserved.

Bottom-up emissions were estimated using the information collected by ADAI (ADAI, 2019) that resulted in hourly fire progression (burned area) data. Fuel load was obtained from the sixth Portuguese Forest Inventory (ICNF 2019), which is based on data collection from aerial images and vegetation measurements on the ground (~12 000 measurement sites) across the Portuguese mainland in 2015. This inventory provides surface fuel load by land-use type (trees, under vegetable cover, standing trees, fallen trees, stump and foliage) and forest species (acacia, carob, chestnut, cork oak, eucalyptus, holm oak, oaks, other hardwoods, other resinous, Pinus pinaster and stone pine) for the Portuguese Nomenclature of Territorial Units for Statistical Purposes (NUTS) III. To improve the spatial distribution of the fuel load data over the study areas, values were spatially disaggregated using the Portuguese land use data ("Carta de Uso e Ocupação do Solo" - COS) (DGT 2018) and applying an area weighting technique. The COS dataset was produced based on visual interpretation of orthorectified aerial images with a spatial resolution of 0.5 m. Other sources of information, including satellite images, were also used during the production process as well as in the quality control. In addition, measurement datasets (7964 sites across the Portuguese mainland) provided by the Portuguese Institute for Nature Conservation and Forests were also used to improve the accuracy of the estimated fuel load as well as the identification of the forest species in the study area. This join compilation of data allowed reducing the uncertainty of the considered fuel load, as well as producing fuel load maps per forest species with a high spatial resolution.

For shrubs, the burning efficiency value of 0.8 suggested by the National Program for Climate Changes (PNAC 2002), was selected, because it represents Portuguese conditions for understory vegetation, as well as fine fuel from other vegetation species. Regarding forest, a value of 0.25 burning efficiency was taken from the EEA (2019) guidance document as representing the southern European forest species, namely communities of eucalyptus, resinous and deciduous trees.

Emission factors for the conditions of these EWE were applied and emissions of PM10, PM2.5, NOx, CO, $SO_2$, $NH_3$, $CO_2$ and $CH_4$ estimated (Fernandes et al., 2022). Figure 16 shows the spatial distribution (500×500 $m^2$) of PM2.5 and CO emissions (in kt) during the EWE.

Copyright © FirEUrisk Consortium. All rights reserved.

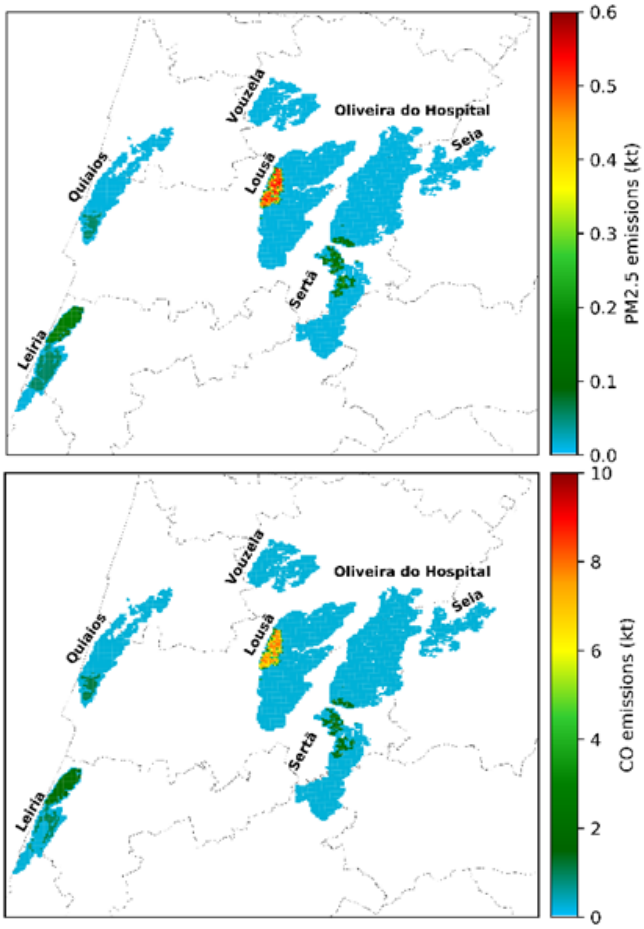



***Figure 16.*** *Spatial distribution (500 × 500 $m^2$) of atmospheric emissions for PM2.5 and CO (kt) from 15 to 16 October 2017 (Fernandes et al., 2022)*

The emissions in Lousã were 43.4–45.8% higher than the sum of emissions from all the other case studies. This EWE was responsible for the largest burned area (54,407 ha – **Table 7**) and had the highest available fuel load (15,188.8 kt). The lowest emissions were calculated for the Seia EWE (17,003 ha – **Table 7**) and Vouzela EWE (15,959 ha – **Table 7**), which are the regions with the smallest burned area, representing 0.19–0.32% and 0.61–0.63%, respectively, of the total emissions in the study region.

To understand the temporal distribution of PM10, PM2.5, NOx, CO, $SO_2$, $NH_3$, $CO_2$ and $CH_4$ atmospheric emissions from each EWE, Figure 17 presents hourly emissions (in kt) during the study period.

Copyright © FirEURisk Consortium. All rights reserved.

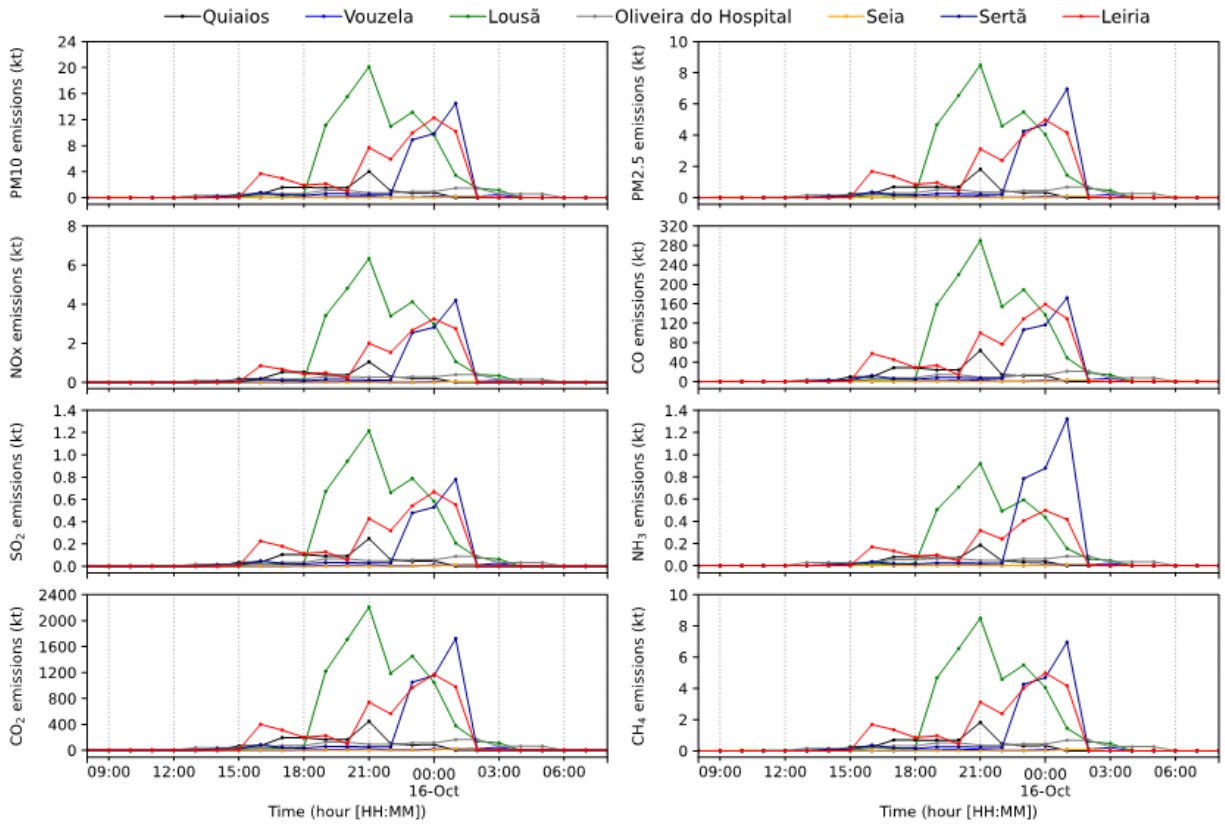



***Figure 17.*** *Hourly total atmospheric emissions of PM10, PM2.5, NOx, CO, $SO_2$, $NH_3$, $CO_2$ and $CH_4$ (in kt), from 15th to 16th October 2017.*

Figure 17 shows that the Lousã, Leiria and Sertã EWEs were the largest contributors, with emissions from the Lousã EWE predominating. The period with the highest total emission values lasted for 12 h, between 15:00 hours on 15 October and 02:00 hours on 16 October. The time with the highest emission values was at 21:00 hours on 15 October, with the biggest contribution from the Lousã EWE (61.38%) and Leiria EWE (21.58%). Furthermore, the temporal distribution profiles of the pollutants were similar, but with different absolute values, because for each pollutant, the burned area, burning efficiency and fuel load values considered varied the same way.

To compare the obtained results with data from other approaches, Figure 18 shows the PM10 and PM2.5 emissions from the wildfires events between 15th and 16th October 2017 (~24 hours) quantified using Moderate Resolution Imaging Spectroradiometer (MODIS) and Spinning Enhanced Visible and InfraRed Imager (SEVIRI) sensors. To facilitate the comparison between the results obtained by the different approaches (SEVIRI vs Bottom-up vs MODIS), Figure 18 presents the PM10 and PM2.5 emission values with a horizontal spatial resolution of 10×10 $km^2$ for the study period.

Copyright © FirEURisk Consortium. All rights reserved.

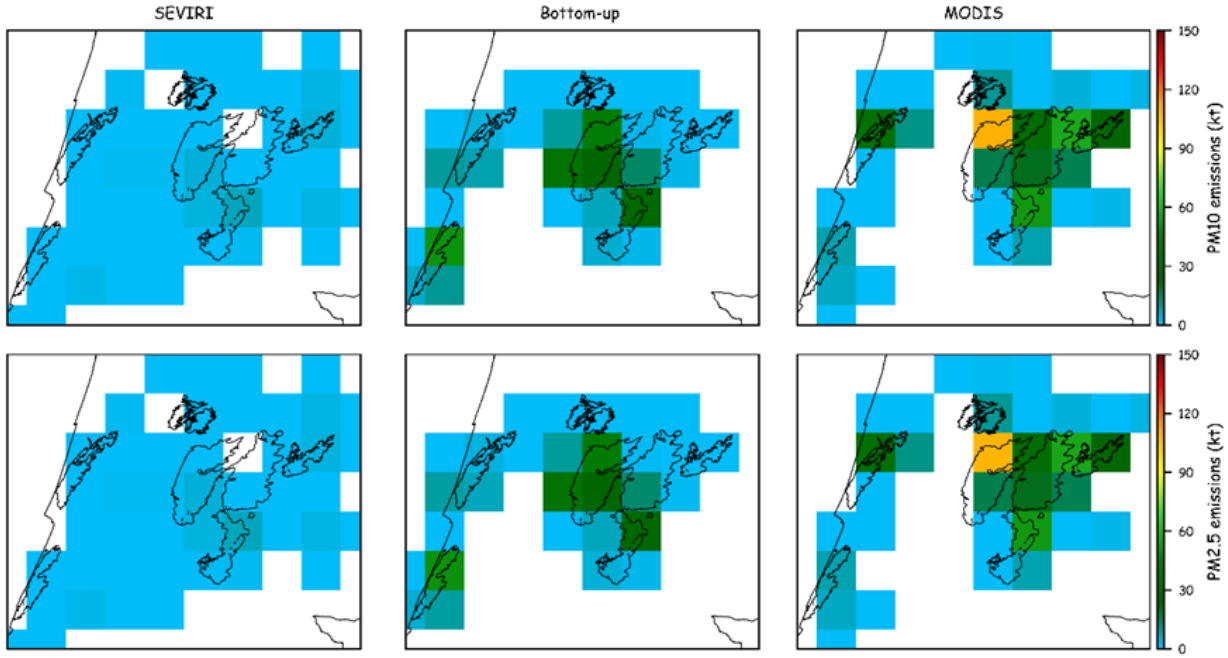



*Figure 18. PM10 and PM2.5 emissions (in kt) from EWE in October 2017, with SEVIRI, this study and MODIS approaches (spatial resolution 10×10 km$^2$).*

The ratios between the PM2.5 and PM10 emissions were on average 0.99 (SEVIRI), 0.94 (Bottom-up) and 0.99 (MODIS). In this bottom-up study, the spatial distribution of PM10 and PM2.5 emissions covered the seven EWE, while for the MODIS and SEVIRI approaches some burned areas did not present atmospheric emissions. These results are probably due to the coarse spatial (3×3 km$^2$) and temporal (2-4 overpasses per day) resolutions of the SEVIRI and MODIS sensors, respectively.

More details about the bottom-up emissions estimation for the October 2017 EWE can be found in Fernandes et al. (2022).

### 4.2.2 Smoke dispersion

During the EWE of October 2017, the hurricane Ophelia promoted strong winds and fires generated smoke plumes along with a Saharan dust event led to a considerable deterioration of the air-quality in Portugal. The transport, dispersion and chemistry of the smoke emitted by the October 2017 EWE was simulated by the regional modelling system CHIMERE-APIFLAME.

#### 4.2.2.1 Modelling setup

Simulations with CHIMERE-APIFLAME were done by forcing meteorological conditions by the WRF model. Regarding pollutant emissions, two different scenarios were considered: (i) simulations with anthropogenic emissions (e.g., traffic, industry, energy production, etc.), biogenic, desert dust, and sea

Copyright © FirEUrisk Consortium. All rights reserved. 

salt emissions; and (ii) simulations with all emissions from the previous scenario, plus emissions associated with fires. These two scenarios allowed to distinguish between the dispersion of smoke and the presence of desert dust, which coexisted during the event, and to assess the contribution of the forest fire emissions to atmospheric pollution, considering the range of the most relevant atmospheric emission sources.

The CHIMERE model was run for two nested domains (D01 and D02), as shown in **Figure 19**. In the first domain, D01, the model has a horizontal resolution of 25 km, and in the second domain has a resolution of 5 km. The simulation period was done from 1 to 24 October 2017, with 24 vertical levels (from surface to 200 hPa).

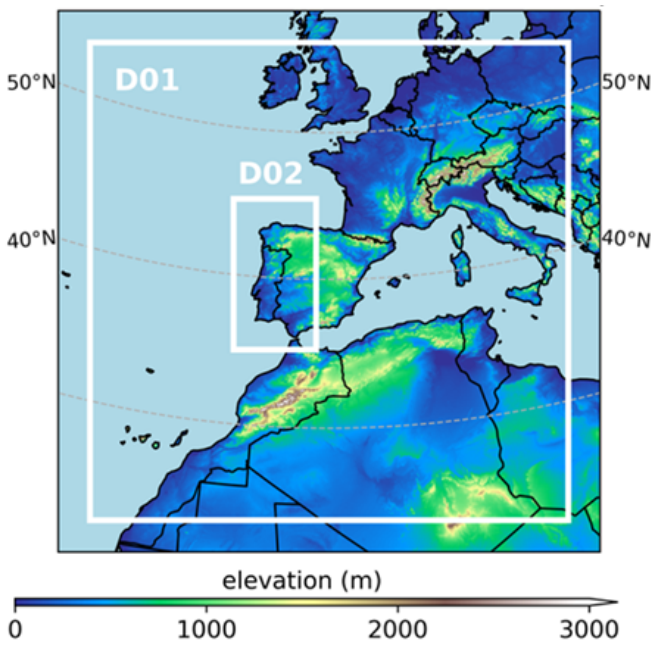



***Figure 19**. Spatial domains used in this study.*

Aiming at assessing model performance regarding the extent of the smoke plume and the concentrations of pollutants in the air, modelling results were compared with available measured data, such as hourly values of particulate matter (PM10) and ozone ($O_3$) concentrations retrieved from surface air quality monitoring stations, from October 6 to 20, 2017. Four background air quality stations (Chamusca (CHA), Ervedeira (ERV), Montemor o Velho (MOV), and Douro Norte (DRN)), geolocated in the North and Central region of mainland Portugal, identified with red dots in **Figure 20**, were used for the validation of modelling results.

Copyright © FirEUrisk Consortium. All rights reserved.

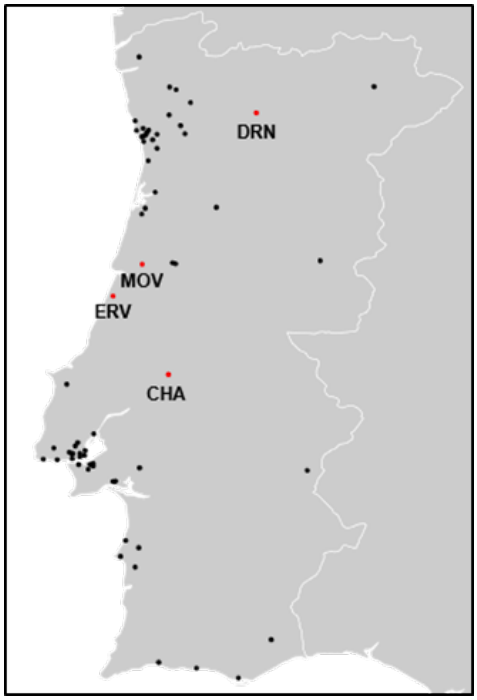



***Figure 20.*** *Air quality monitoring stations for daily validation of WRF-CHIMERE simulations (6-20 October 2017).*

These stations are the responsibility of the Portuguese Environment Agency (APA) in coordination with the corresponding Commission for Coordination and Regional Development (CCDR). The data measured continuously at the various stations are reported, in near real time, and made available to the public through the QUALAR online database (https://qualar.apambiente.pt/indices). The comparison between modelled values and observations has been based on daily averages for PM10 and daily maximum of eight-hour averages for $O_3$ concentrations, as these are the averaging periods of the Air Quality Standards defined for the protection of human health, for these two pollutants.

#### 4.2.2.2 Results

The impact of EWE emissions on air quality can be seen in Figure 21 and Figure 22. Figure 21 shows the spatial distribution of simulated concentrations of PM10, CO and $O_3$, for several hours of the simulation period, considering the whole range of the most relevant atmospheric emissions sources. **Figure 21** depicts the PM10 levels on 14 October 2017 at 00 UTC and on 15 October at 06 UTC, considering only the pollution due to the forest fires emissions.

Copyright © FirEUrisk Consortium. All rights reserved.

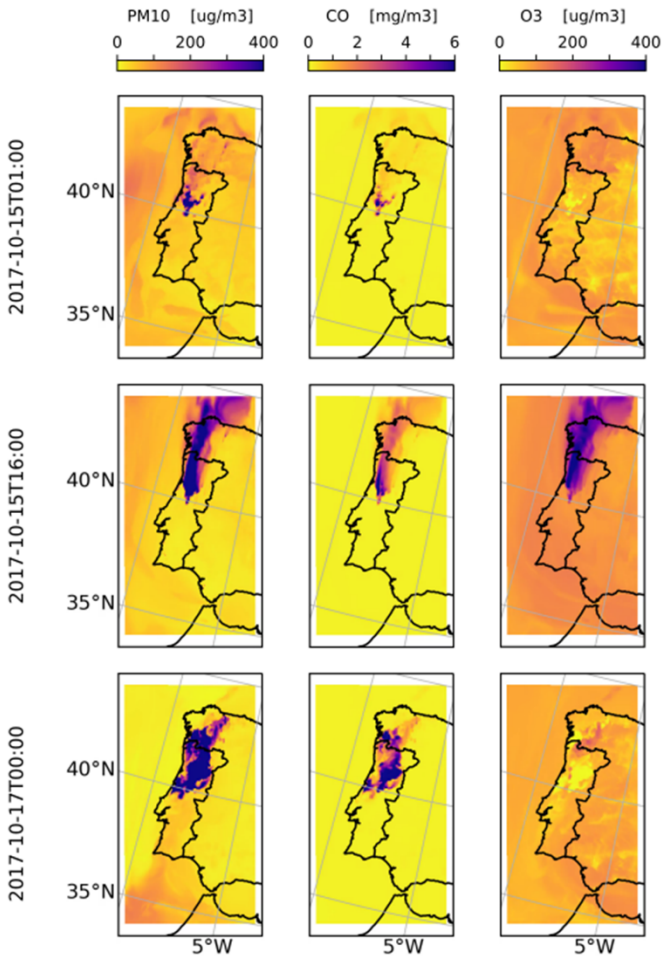



***Figure 21**. PM10, CO and $O_3$ hourly simulated concentrations considering the most relevant atmospheric emissions sources, for 01 and 16 UTC on 15 October and 00 UTC on 17 October 2017.*

The pollutants' levels are very high and exceed the standard values for the protection of human health. Ozone has a particular behaviour due to its secondary production characteristics, which include ozone titration close to the fire events.

Copyright © FirEURisk Consortium. All rights reserved.

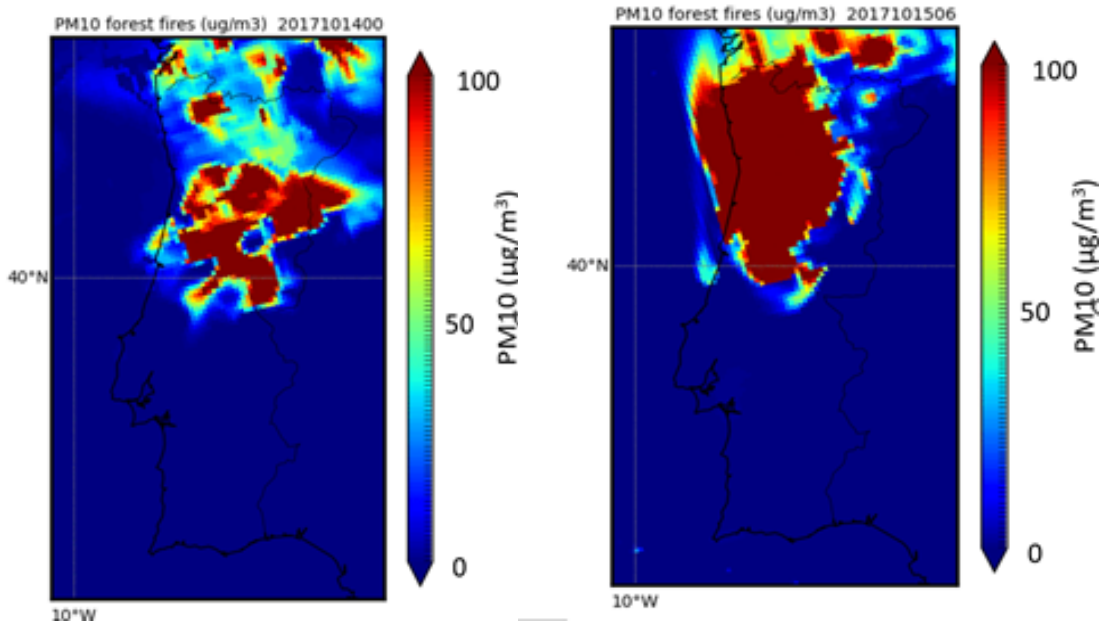



***Figure 22**. PM10 simulated concentrations due to forest fires, for 00 UTC on 14 October and 06 UTC on 15 October, 2017.*

CHIMERE-APIFLAME results indicate a large impact of the EWE on the air quality and chemical composition of the troposphere in the northern half of mainland Portugal, with very high PM10 concentrations (> 100 µg/m$^3$) in the Center and North of Portugal.

The comparison of the daily values of the output of the CHIMERE model simulations and the observed values in the stations of Chamusca (CHA), Douro Norte (DRN), Ervedeira (ERV) and Montemor-o-Velho (MOV) is shown in **Figure 23** and **Figure 24**, for PM10 and $O_3$, respectively. The location of these sites is available in **Figure 20**.

Copyright © FirEUrisk Consortium. All rights reserved.

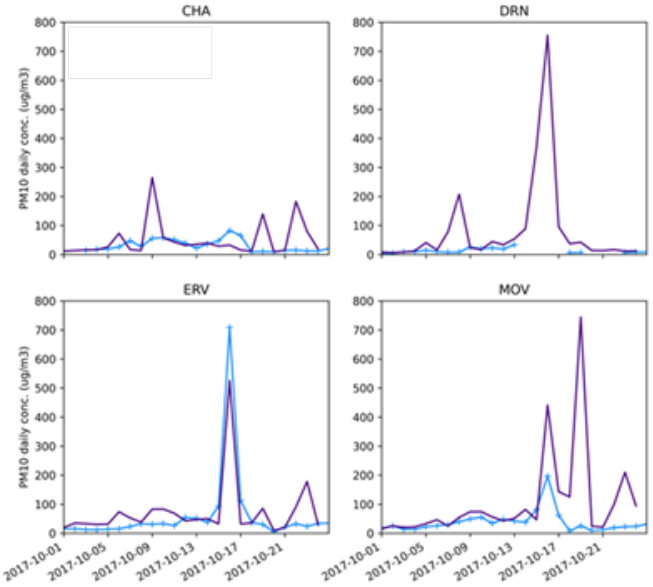



***Figure 23.*** *Observed (light blue) and simulated (dark blue) daily PM10 concentrations in selected air quality stations, October 2017.*

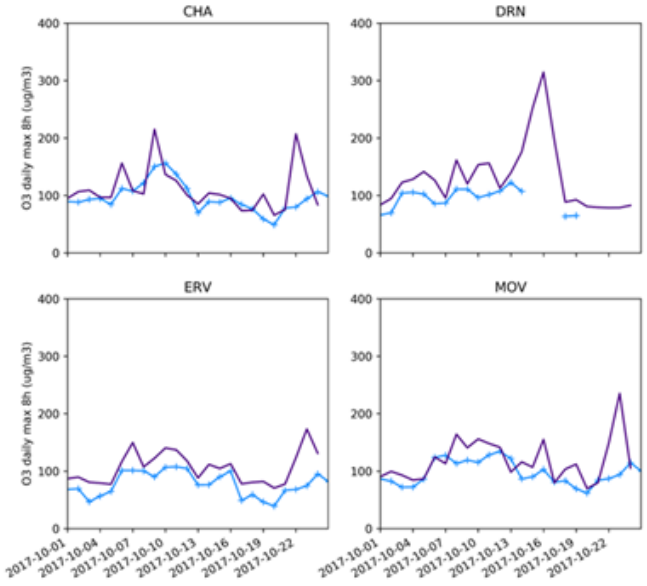



***Figure 24****. Observed (light blue) and simulated (dark blue) daily $O_3$ concentrations in selected air quality stations, October 2017.*

Copyright © FirEURisk Consortium. All rights reserved.

**Figure 23** and **Figure 24** suggest that the model can simulate the background pollution levels in the atmosphere and the impact of forest fires on air quality, both for PM10 and $O_3$ (a secondary pollutant). However, the model overestimates peaks of particle concentration ($PM_{10}$) - except at the ERV station, of surface ozone ($O_3$) during wildfires. The Douro Norte station has no records of values during the fire period, from the 14th to the 17th of October, probably due to excessive levels of pollution. The hourly validation of simulations highlights the importance of model validation, and the need to improve the temporal allocation of fire emissions in the model APIFLAME, namely by increasing the frequency of input data, from daily to hourly. Overall, this study suggests that the CHIMERE-APIFLAME modelling system is suitable for addressing the impact of forest fires on a regional scale.

## 4.3 Mediterranean Greece / Attica Region (PS5)

In the beginning of August 2021 several wildfires broke out in the Greek regions of Attica, Euboea, Ilia, Messinia, and Lakonia and kept burning for several days. Surface weather conditions have been marked by a heat wave peaking to 40–45 °C by the end of July, that contributed to suppressing relative humidity levels to below 20% in all fire-affected regions (Giannaros *et al.* 2022). Five wildfires collectively burnt nearly 94000 ha, a surface that accounts for more than 70% of the 2021 total burnt area. Table 8. Fire activity information. includes fire activity information for these five largest wildfires. This information is based on data provided by the Hellenic Fire Service, on data published by Giannaros *et al.* (2022) and on information from Xanthopoulos *et al.* (2022).

***Table 8.*** *Fire activity information.*

| Region | Ignition date, time | Ignition location (°N, °E) | Burnt area (ha) | Comments |
|---|---|---|---|---|
| Attica (near Athens) | 3 August, 13:22 | 38.1317, 23.8044 | 8400 | It started 18 km north of the center of Athens, near a settlement called Varympompi, which is one of the wildland-urban interface areas that exist around the city. |
| Euboae (Evia Island) | 3 August, 17:11 | 38.7940, 23.3242 | 51200 | Included areas recognized as landscapes of high quality and biotopes characterized by Natura and Corine |
| Lakonia | 3 August, 10:30 | 36.8472, 22.3885 | 10100 | Peloponnese Peninsula; forest and agricultural lands |
| Ilia | 4 August, 10:03 | 37.7016, 21.5747 | 18400 | |
| Messinia | 4 August, 16:51 | 37.3251, 21.9410 | 5100 | |

According to the Hellenic Fire Service (Hellenic Fire Service, 2021) a wildfire started 100 km to the North of the city in Evia Island at 17:11 on the 3rd of August and continued to burn until the 17th of August. This resulted in about 51200 ha of burned area (40% of the total during that fire season in Greece) as estimated by the European Forest Fire Information System Burnt Area satellite product (EFFIS, 2022).

Copyright © FirEUrisk Consortium. All rights reserved.

Another wildfire started directly to the Northeast of Athens on the 3rd of August at 13:22 ending on the 12th of August with a rekindling on the 5th resulting in 8400 ha of burned area (Hellenic Fire Service, 2021).

Almost simultaneously, three other aggressive fires had started in Peloponnese, the most threatening being the one in the prefecture of Ilia. According to Xantopoulos *et al.* (2022), they became very large: the fire in Ilia-Gortynia reached 15000 hectares; the fire in Messinia 5100 hectares; and the fire in Lakonia (Mani) 10100 hectares, devastating both forest and agricultural lands.

Other significant fires were detected through their FRP signatures in western Greece and in neighboring countries during that period (Giglio *et al.,* 2021). Residents reported a strong deposition of ashes inside the city and authorities advised the population to stay indoors or use respiratory masks otherwise (Smith, 2021).

The numerical modelling system WRF-APIFLAME-CHIMERE, which comprises a meteorological model, a smoke emissions model and a chemical transport model, was employed in estimating the hourly three-dimensional distribution of PM, CO and $O_3$ concentrations during the wildfires. The performance of the modelling system was evaluated by comparing modelled results with air quality observations and atmospheric optical depth measurements. Osswald *et al.* (2023) describe in detail this Greek case study.

### 4.3.1 Modelling setup

The APIFLAME model (version 2.0) was used for estimating biomass burning emissions, while other emissions, meteorology and chemical transport phenomena were handled by the WRF-CHIMERE model and its pre-processors.

APIFLAMEv2 estimates were based on pre-processed satellite imagery in the form of the MODIS burned scars product (MCD64A1) which uses thermal anomalies from active fires and changes in reflectance due to the charring of the vegetation to detect burned regions. This product has a 500 m resolution and is released monthly indicating the estimated day of burning for each detection. For each fire and associated vegetation type, the consumed fuel was calculated, and the corresponding emissions of trace gases and aerosols were derived using a list of emission factors. Biomass burning emissions were distributed throughout the day using a typical wildfire temporal profile. The module also uses the fire radiative power (FRP) from the MOD14 satellite product, which processes four daily observations at 1 km resolution. Out of these the daily maximum is used by CHIMERE to calculate the injection height.

The impact of the emissions of wildfires on AQ was therefore quantified using the CHIMERE model, driven by meteorological conditions provided by the WRF model. The WRF-CHIMERE system was run between 27-07-2021 and 10-08-2021 providing a seven-day spin-up period to stabilize all simulation variables that may be affected by inaccuracies in the initial conditions before the first fires in the vicinity of Athens started. A fine simulation domain of Athens was nested inside a medium one containing most of Greece which in turn was nested in a continental domain resulting in three computational domains with resolutions of 25 $km^2$, 5 $km^2$ and 1 $km^2$ (see **Figure 25**).

Copyright © FirEUrisk Consortium. All rights reserved.

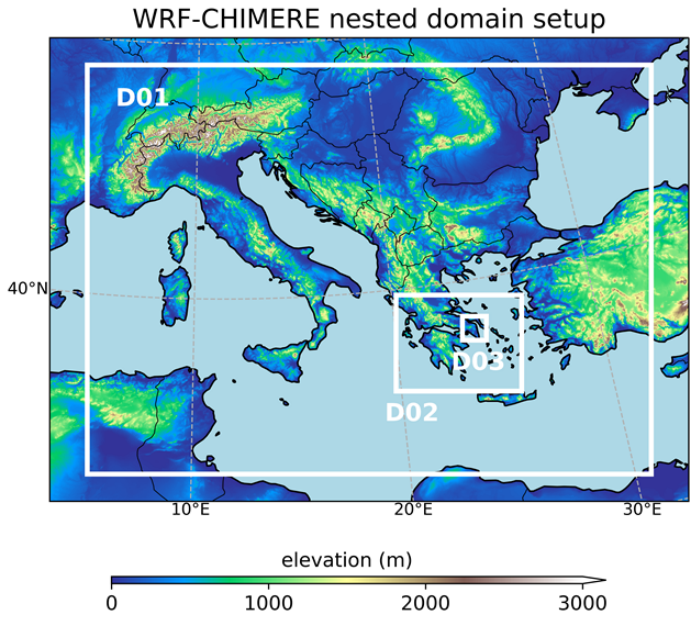



***Figure 25**. WRF-CHIMERE nested domains over an elevation. D01 - 25 km² resolution; D02 - 5 km² resolution; D03 - 1 km² resolution.*

The coarser mesh captured phenomena at the level of the Mediterranean Basin with 95 x 69 cells, the intermediate one was positioned around Greece with 106 × 81 cells and the smallest one was composed of 100 × 100 cells over Athens thus providing a detailed picture of the AQ over the city. The structured hexahedral mesh was created over a Lambert conformal map of the computational domain with 24 cells between the surface and 200 hPa.

Wildfire emissions coming from APIFLAME were re-distributed in the vertical direction according to a plume rise profile that assigns 20% of the emissions below the injection-height and the remainder around that same height. The assumption was that the strong mixing in the boundary layer quickly disperses the initial shape of the plume so that its effect would only be relevant at a local scale. The injection-height of the wildfire-plume in CHIMERE was calculated according to the parameterisation of Sofiev *et al.* (2012) with a correction of the FRP in the case of large fires as suggested by Veira *et al.* (2015).

In addition to biomass burning, the AQ simulations considered anthropogenic, mineral dust, biogenic and sea salt emissions. Anthropogenic emissions from EMEP (EMEP, 2021) were processed to obtain hourly fluxes for the different model species (associated to the selected chemical mechanism) and the specific simulation grids. Available time profiles for specific countries were used, as well as spatial proxies such as land-use, population density, and road networks density. Desert dust, marine aerosols and biogenic emissions were estimated by the model during the simulations, taking static datasets and meteorological data into account.

For the AQ simulations the boundary conditions for the WRF meteorology were obtained from the ERA-5 reanalysis dataset (ECMWF, 2022). Variables were taken with a horizontal resolution of 30 km and

Copyright © FirEURisk Consortium. All rights reserved. 

37 pressure levels between 1000 hPa and 1 hPa, at six-hour intervals. Once these calculations were performed the higher resolution data was passed on directly to CHIMERE.

More details about this modelling application can be found in Osswald *et al.* (2023).

### 4.3.2 Results

Concentrations of CO, PM10 and $O_3$ at the surface were analysed through time-series of maps from the simulations of the 5 km and 1 km resolution domains. Concentration snapshots at critical hours from 4 to 9 of August 2021 are shown in **Figure 26**.

Copyright © FirEUrisk Consortium. All rights reserved.

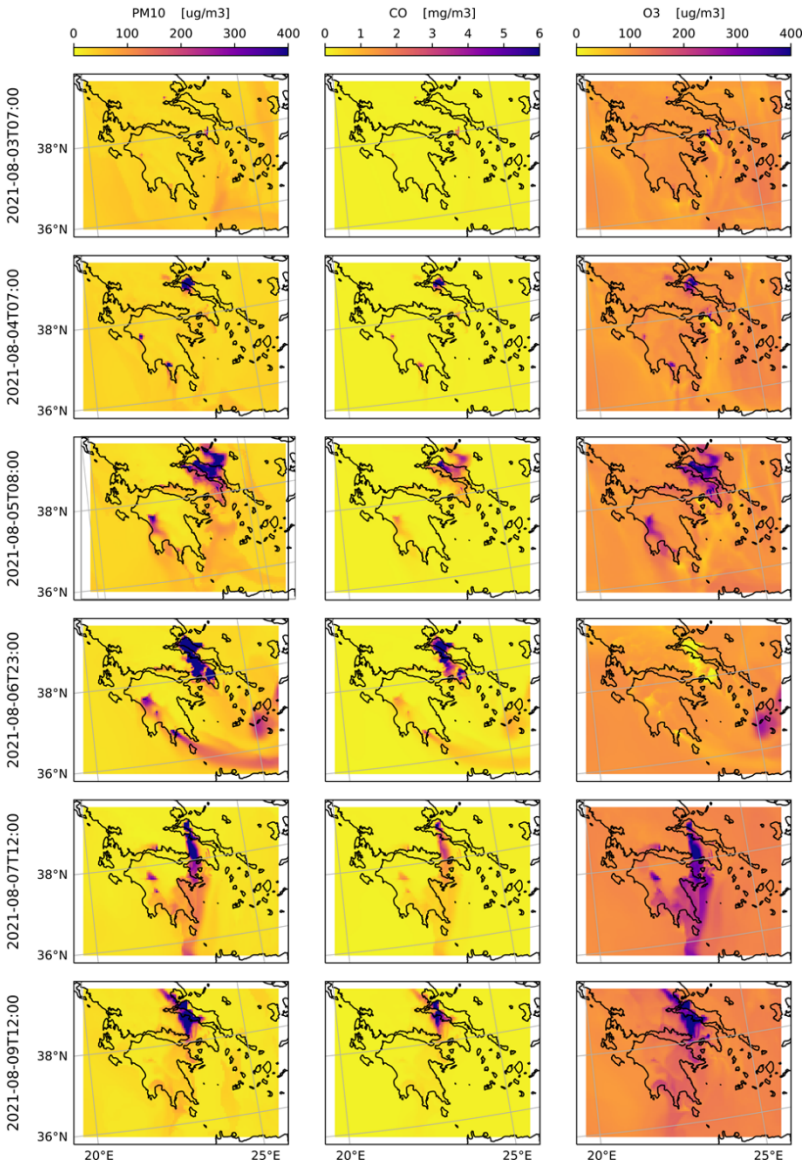



***Figure 26.*** *Spatial distribution of simulated PM10, CO and $O_3$ concentrations values (3 to 9 August 2021) (Osswald et al., 2023).*

The simulations reveal that on the 3rd of August, a wildfire in the northern urban area of Athens was actively producing a smoke cloud as seen in Figure 26. During that day simulated values at locations south of Thrakomakedones and north of Koropi exceeded the daily limit value established by the European Commission for the protection of the human health for PM10 (50 $\mu g.m^{-3}$). At Lykovrisi, closest to the wildfire, the results indicate an exceedance of twice the daily LV.

The Athens wildfire mostly dies out during the 4th of August, while emissions from the fire in Evia begin at 1 am according to the model. The smoke is mostly contained over the island until the end of the

Copyright © FirEURisk Consortium. All rights reserved. 

day. Nonetheless the locations of Nea Smirni and Peristeri, both urban areas, register exceedances of the PM10 daily LV.

On the 5th of August the Athens fire is reactivated and produces, together with the Evia wildfire a smoke cloud over the peninsula. All locations exceed the daily LV of PM10, in particular, Peristeri exceeds twice this value.

Both fires continue to burn throughout the 6th of August, however, a strong westerly wind during the morning pushes the smoke cloud away from the city. In the afternoon the wind veers to the north and smoke from both fires accumulates over the peninsula leading to exceedances in the daily LV of PM10 in all locations except for Nea Smirni and Koropi, which are further away from the fires. The simulated values at Lykovrisi reach extreme hourly values of 1152 $\mu g.m^{-3}$. Since the high concentrations of smoke are experienced after sunset, $O_3$ levels are not as high as during the previous day. In the absence of photolysis, the destruction of this secondary pollutant exceeds its production within the smoke cloud, leading to a local concentration minimum.

The wildfire in Evia emitted a considerable smoke cloud that reached the city of Athens. During midday of the 7th of August model results showed transport by a northerly wind. When the wind was blowing from other directions or with less intensity it led to periods of less smoke over the city, such as on the midday of the 9th of August. Both simulated values and observations show lower concentrations following the peak of the 7th of August, except for modelled CO values at Nea-Smirni which exhibit abnormally high values in the simulation. Before the 8th of August, the performance of CO at Nea-Smirni is clearly better. Throughout the simulated period the CO concentrations in Nea Smirni never exceed the daily 8-hour mean LV.

For the validation of the modelling results, air quality observations were extracted from the AQ database of the European Environmental Agency (EEA 2021), for the air quality monitoring stations located within D02 and D03, and for the selected pollutants PM10, PM2.5, CO, and $O_3$. The selected monitoring stations include only “background” stations, which are more representative of a larger area around them, as opposed to “traffic” or “industrial” stations which are greatly affected by local phenomena, i.e., sub-grid phenomena for the mesoscale model. Five performance metrics were calculated for all the stations of interest using the predictions of both the D02 and the D03 domains. The normalized mean bias (NMB), mean fractional bias (MFB), root mean square error (RMSE), Pearson’s correlation coefficient (R) and the index of agreement (IOA). The results can be seen in Table 9.

Copyright © FirEURisk Consortium. All rights reserved.

***Table 9.*** Performance metrics of model results against monitoring station observations (Osswald *et al.*, 2023).

| | | NMB | RMSE | MFB | IOA | R | Ō | NMB | RMSE | MFB | IOA | R | Ō |
|---|---|---|---|---|---|---|---|---|---|---|---|---|---|
| | | PM10 | | | | | | PM2.5 | | | | | |
| D02 vs stations | agia_paraskevi | 0.53 | 101 | 0.11 | .17 | .15 | 44 | 1.12 | 76 | 0.44 | .20 | .22 | 24 |
| | aliartos* | 0.64 | 174 | **0.06** | .25 | **.27** | 63 | 0.63 | 131 | 0.17 | **.36** | **.31** | 48 |
| | koropi | 0.40 | 89 | -0.06 | .22 | .24 | 40 | | | | | | |
| | lykovrisi | 0.65 | 124 | 0.27 | .37 | .27 | 59 | | | | | | |
| | nea_smirni | 0.16 | 57 | 0.14 | **.38** | .17 | 54 | | | | | | |
| | peristeri | 0.17 | 65 | 0.06 | .34 | .10 | 61 | | | | | | |
| | thrakomakedones | **-0.11** | **56** | -0.24 | .31 | .02 | 58 | **0.18** | **37** | **0.04** | .32 | .08 | 31 |
| | | CO | | | | | | O3 | | | | | |
| | agia_paraskevi | | | | | | | -0.06 | 66 | -0.34 | .67 | .70 | 112 |
| | aliartos* | | | | | | | 0.65 | 109 | 0.41 | .54 | .68 | 95 |
| | koropi | | | | | | | **0.02** | **53** | -0.12 | .63 | .62 | 106 |
| | lykovrisi | | | | | | | 0.21 | 59 | 0.09 | **.78** | .67 | 91 |
| | nea_smirni | 0.34 | 0.83 | 0.21 | 0.37 | 0.19 | 0.58 | 0.11 | 57 | -0.43 | .78 | **.74** | 82 |
| | peristeri | | | | | | | 0.20 | 64 | -0.14 | .75 | .72 | 87 |
| | thrakomakedones | | | | | | | 0.07 | 68 | **0.07** | .62 | .35 | 145 |
| | | PM10 | | | | | | PM2.5 | | | | | |
| D03 vs stations | agia_paraskevi | 0.43 | 112 | **0.03** | .17 | .18 | 44 | 0.96 | 82 | 0.35 | .23 | .29 | 24 |
| | aliartos* | | | | | | | | | | | | |
| | koropi | **-0.06** | **33** | -0.17 | **.57** | **.40** | 40 | | | | | | |
| | lykovrisi | 0.23 | 117 | 0.10 | .27 | .14 | 59 | | | | | | |
| | nea_smirni | 0.09 | 52 | 0.07 | .51 | .27 | 54 | | | | | | |
| | peristeri | 0.38 | 73 | 0.22 | .34 | .10 | 61 | | | | | | |
| | thrakomakedones | -0.19 | 48 | -0.32 | .46 | .22 | 58 | **0.07** | **32** | **-0.06** | **.51** | **.28** | 31 |
| | | CO | | | | | | O3 | | | | | |
| | agia_paraskevi | | | | | | | **0.04** | 54 | -0.12 | .73 | .71 | 112 |
| | aliartos* | | | | | | | 0.71 | 117 | 0.40 | .57 | **.79** | 95 |
| | koropi | | | | | | | 0.04 | **48** | **-0.04** | .63 | .57 | 106 |
| | lykovrisi | | | | | | | 0.26 | 60 | 0.16 | .79 | .71 | 91 |
| | nea_smirni | 0.48 | 0.98 | 0.10 | 0.52 | 0.37 | 0.58 | 0.17 | 64 | -0.39 | .74 | .70 | 82 |
| | peristeri | | | | | | | 0.04 | 54 | -0.37 | **.80** | .75 | 87 |
| | thrakomakedones | | | | | | | 0.13 | 74 | 0.10 | .65 | .45 | 145 |

*The Aliartos station is outside the D03 domain

(values of stations with highest performance are highlighted)

Where O and M are the hourly observations and model results respectively, with the overbar denoting averaging. The average value of the observations is also provided.

The D03 domain is tendentially better, though for some cases D02 has a better performance. This suggests that there is no clear reason to disregard the D02 results altogether. To evaluate the performance of D02 outside of Athens only the Aliartos station can be used as all other stations in the EEA AQ database were not recording during the period of interest. Its performance metrics are close to those for the remaining stations. An exception to this is the RMSE of PM10 that exhibits the highest value, or the metrics of O3 that are tendentially worse than in other stations available within the D03 domain. Differences can be explained not only by its distance to other stations but also by the fact that it is the only rural station analyzed. Moreover, since $O_3$ is a photochemical pollutant, it depends among other variables on temperature and solar radiation. On the other hand, temperature and solar radiation are meteorological variables that are affected by the direct feedback of aerosols emitted during wildfires (Péré *et al.* 2014).

Copyright © FirEURisk Consortium. All rights reserved.

However, our simulations do not consider the feedback between atmospheric composition and meteorology, which may contribute to a poorer model performance in simulating $O_3$ concentrations.

Despite the identified limitations in the simulation of the chemical processes of $O_3$, the index of agreement shows that this pollutant was better simulated than the others, with IOA values varying between 0.54 and 0.80. There was only one monitoring station with CO available data for the evaluation, with a calculated IOA of 0.37 and 0.52 for D02 and D03, respectively. Except for the Agia-Paraskevi monitoring station location, where a simulated peak value was not observed, the hourly performance metrics for particulate matter, for both PM10 and PM2.5, were quite acceptable and it is well known that particulate matter is a difficult pollutant to model when compared to other gases. It can have primary or secondary origin, and a wide range of sources. In the case of forest fires, in addition to the difficulty of representing primary PM emission from biomass burning, the inaccuracy of secondary organic aerosol formation may play an important role in model performance. In summary, the calculated performance metrics indicate a reasonable performance of the modelling system supporting its usefulness to predict smoke transport and chemistry and delivering information to prevent human exposure to smoke.

Copyright © FirEUrisk Consortium. All rights reserved.

# 5 Integration of existing systems

In the scope of FirEUrisk two integrated modelling systems were developed based on several available models. These systems aim at simulating fire progression and smoke dispersion at the local scale (IMFIRE-DISPERFIRE) and smoke behaviour at both local and regional scales (DISPERFIRE-CHIMERE). The final goal is to include these systems in the FirEUrisk platform in a close link to WP4.

## 5.1 IMFIRE-DISPERFIRE

IMFire is an online platform for the management of wildfires, whose development was initiated by ADAI and other key partners within the national project IMFire – Intelligent Management of Wildfires. The highlights of this platform include:

- Advanced fire spread models;
- Advanced 3D wind map calculation models capable of depicting the two-way coupling between fire and atmosphere;
- Machine learning (ML) methods for dynamic and near real-time input parameter correction, towards more accurate predictions;
- User-friendly GIS-based interface, suited for any users without wildfire expertise;
- API for the integration of the simulator with already existing platforms;
- Automatic real-time data fetching tools, regarding fire and weather from multiple online sources.

The basic fire spread model adopted is the Rothermel model (Rothermel, 1972), a semi-empirical fire spread model whose output is the fire rate of spread $R$, which corresponds to the linear velocity (m/s) of propagation of the fire front. However, in a real wildfire situation, it is important to obtain information about the shape and size of the wildfire in a two-dimensional way. Thus, the Rothermel model is coupled with models which provide the mathematical description of the fire shape. One of these models defines the fire shape as a double ellipse (Anderson, 1983) and the other defines the fire shape as a single ellipse (Alexander, 1985). Typically, the single ellipse model is used when the wind speed at midflame height is inferior to 0.2 m/s, while the double ellipse model is employed for higher values of wind speed.

The fire growth simulation is performed using a raster approximation. The terrain is divided into cells (25 m × 25 m) over which all properties are assumed to be constant. Based on this premise, fire growth can be considered a process of contagion between burning and non-burning cells (cell-automata scheme). The time required for the fire to propagate from one burning cell to neighbour cells is computed considering the rate of spread and shape of the fire. Then, each neighbour cell is assigned a number that represents the minimal computed time at which ignition would occur in that cell. Finally, the neighbour cell with the lowest assigned time becomes a burning cell, and the process is carried on for the remaining cells.

Copyright © FirEUrisk Consortium. All rights reserved. 

Fuel and topography maps are retrieved from online databases and soil occupation maps. New tools for automatically producing high-resolution fuel maps from satellite data are being developed, leveraging machine learning classifiers.

The NUATMOS model (Ross *et al.,* 1988) is used to build the wind map for the whole domain, from online available discrete weather data acquired automatically from the closest weather stations. The NUATMOS wind model do not consider the non-linear fire-atmosphere interactions, which are not significant in the case of small-scale prescribed burns. However, for large fires, the 3D Canyon wind model, a more advanced wind model than the NUATMOS, which uses Navier-Stokes solvers to consider the non-linear fire/atmosphere interactions, can be used. This wind model uses the outputs of the fire simulation every certain time step to update the wind map in the domain.

Currently, ADAI's team is working towards the implementation of more fire spread models to depict spot fires, crown fires and extreme fire behaviour. However, and despite the inclusion of more models to predict fire and weather, the challenge remains to obtain accurate predictions of such complex and dynamic events. As stated in Cruz and Alexander (2013), "the only certainty about wildland fire behaviour predictions is that it is extremely unlikely that a prediction will exactly match the observed fire behaviour". One of the main reasons for this is the unreliability of the input data that is fed into the fire simulator/model (Benali *et al.,* 2016). Rothermel's model input parameters include topography, fuel, weather and fire data. While some parameters can be obtained with sufficient accuracy, for example, terrain elevation and slope, which are retrieved from high-resolution satellite data and remain constant throughout time, other input parameters, such as fuel cover and its characteristics, vary over time and at multiple temporal scales. Despite the efforts to produce accurate and updated fuel maps, identifying and applying the correct fuel models and characteristics (e.g., fuel load and moisture content), it is still a challenge and the cause of simulation uncertainties. Other input parameters, such as wind speed and direction, have even more variability, making it even harder to obtain precise values that represent the real wind behaviour during the prediction of wildfire propagation. IMFire uses a two-stage process calibration: (i) the calibration of the fire spread model's input parameters and (ii) the wildfire spread prediction using the calibrated input parameters. These stages are iteratively repeated over time. By exploiting available real-time wildfire data, the calibration is performed by differential evolution (DE) metaheuristics algorithms (Storn and Price, 1997). The calibrated inputs are the surface-area-to-volume ratio, fuel bed depth, live fuel moisture and dead fuel moisture. The rest of the fuel input parameters are set to default values according to the respective fuel model. The choice for calibrating these four parameters is justified as follows: fuel parameter values ($\sigma$ and $\delta$) are retrieved from standard fuel models, assuming uniform fuel parameters in a grid map element. Using standard fuel models is an effective procedure, however, may not fully depict the characteristics of the real fuel distribution due to low map resolution, low variety of fuel models (e.g., the NFFL standard (Anderson, 1982) consists of 13 different fuel models) or low model accuracy in truly representing fuels of a certain category. To select the calibration parameters, a series of simulations were conducted where each input parameter within a certain interval (holding a physical meaning) was modified to obtain the parameters that bear more weight in the final simulation results. It was possible to conclude that the selected parameters have the

Copyright © FirEUrisk Consortium. All rights reserved. 

most impact on the final simulation results according to the experimental tests (which depend on the fuel types considered). Furthermore, these are the parameters that can have the most variability in real conditions. Moreover, the fire dynamic changes the environment near the fire front, decreasing the fuel moisture in the vicinity. In this sense, the fuel moisture $Mf$, both from the dead and the live fuels, should be calibrated because it is likely that the initially measured value does not represent the dynamic behaviour that it experiences during the fire. This strategy proved to effectively improve prediction results, using as metrics the results from a fitness function based on the symmetric difference between the corresponding simulated and real fire area.

The developed graphical user interface allows the user to quickly navigate to any area in the world, using a geographical information system style interface, and quickly place the fire ignition point, line or polygon. **Figure 27** shows a print screen of a wildfire simulation done in the IMFire online platform, with three different types of ignitions: point, line and polygon.

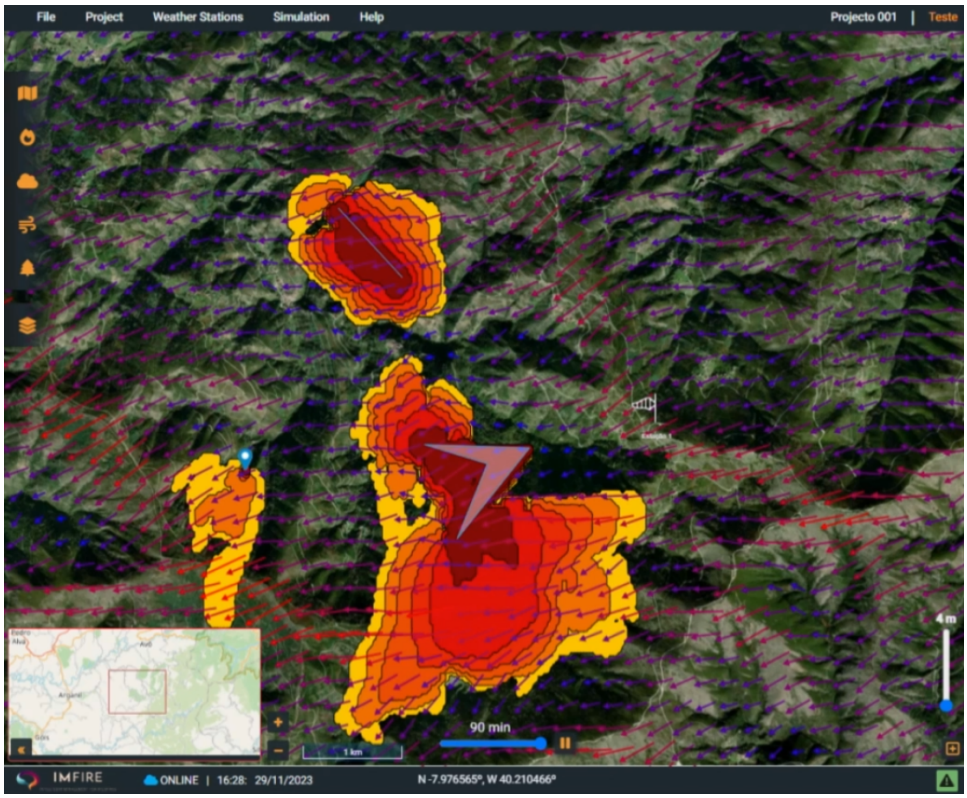


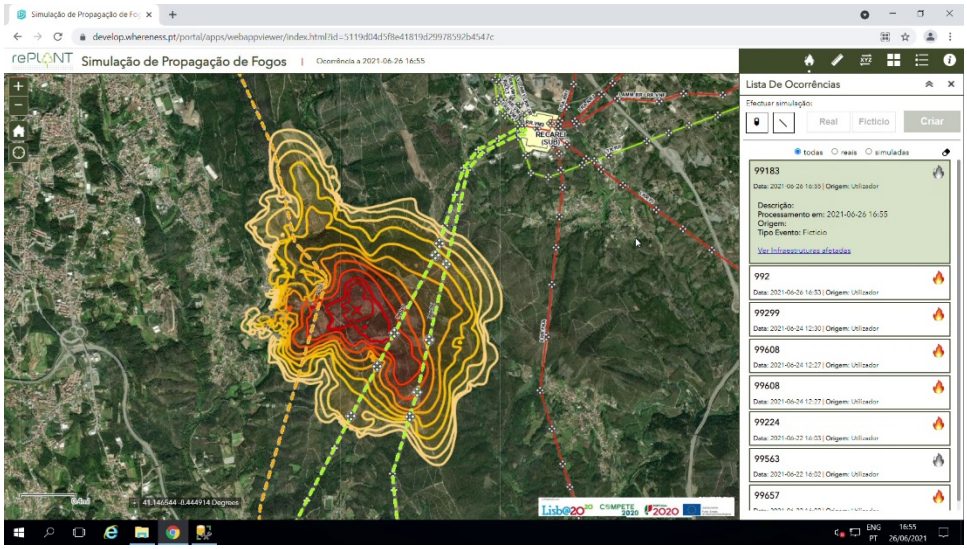

***Figure 27**. Print screen of a wildfire simulation in the IMFire online platform, with three types of ignitions: point, line and polygon.*

Each fire ignition source can easily be associated with a time reference. Then, the user can run the simulation, with the software automatically fetching the data concerning wind speed and direction for the set time and spatial references of the ignitions. The predicted propagation results are shown in less than

Copyright © FirEUrisk Consortium. All rights reserved. 

1 minute, in the form of isochronous lines, representing the fire perimeter every 15 minutes. The results can then be exported in the form of shapefiles or raster files. The platform assumes a set of standard parameters for the simulation, which can be customized by more experienced users in the simulation menu. However, the goal was to make the process accessible to any user without experience in wildfires, to quickly and with less than 5 mouse clicks, simulate a fire on a certain location. Information about local infrastructures can also be imported, as well as custom fuel or topography maps.

An API was also developed to allow users with existing digital decision support platforms to import the fire spread prediction results (see **Figure 28**). The API receives information about the fire ignition coordinates and time, and, optionally, local weather information. In return, it gives the predicted fire spread in the form of raster or shapefiles, to be visualized in the client's platform. This whole process is fully automated and is available 24/7. In the context of the national projects RePlant and CentroDec, the Portuguese Gas and Electrical Distribution Infrastructure Management company REN is using IMFire's API together with their digital infrastructure management platform, to predict if and when real fires might impact their infrastructure.




(dashed lines – gas and power transport infrastructure)

***Figure 28.*** *Print screen of REN's infrastructure management platform with IMFire's API integrated (predicted fire spread and time and point of fire impact in the gas and power transport infrastructure).*

Currently, within the FirEUrisk project, ADAI and UAveiro teams are integrating the DISPERFIRE smoke emissions and dispersion model into the IMFire platform, providing it with another invaluable tool for wildfire management. The DISPERFIRE model relies on the results of the fire propagation, namely the fire intensity and residence time, as well as the information about the local fuels, to produce smoke dispersion and concentration maps. These maps can then be translated to other meaningful parameters such as health hazard or visibility maps, crucial for the fire management efforts.

Copyright © FirEUrisk Consortium. All rights reserved. 

## 5.2 DISPERFIRE-CHIMERE

The DISPERFIRE-CHIMERE modelling system aims at simulating smoke behaviour at local and mesoscales. The system consists of a local model, DISPERFIRE, that based on fire progression simulations estimates emissions and simulates the smoke dispersion. It relies on a simple algebraic model for the emission component and a fast lagrangean algorithm for the dispersion as described in section 3.3. The emissions are then interpolated into a larger mesoscale domain used by CHIMERE. The latter is a comprehensive air quality model that, coupled with the meteorological WRF model, simulates emissions from multiple sources and atmospheric chemistry, as described in section 4.3.1. A detailed diagram containing all inputs and outputs of the system is shown in **Figure 29**.

Copyright © FirEUrisk Consortium. All rights reserved.

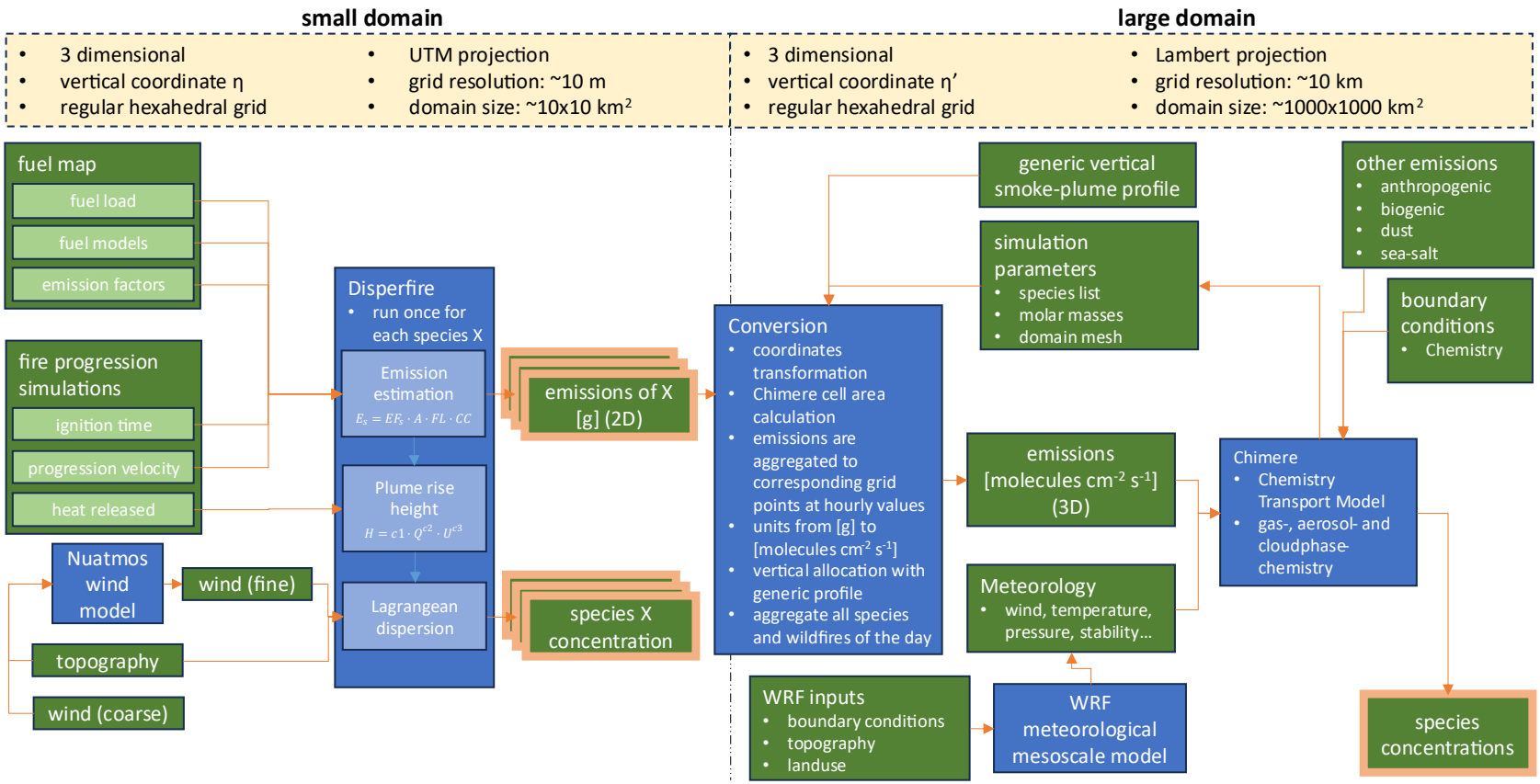



***Figure 29**. Diagram of the Disperfire-Chimere integration. (Green boxes: data. Blue boxes: programs.)*

This project has received funding from the European Union's Horizon 2020 research and innovation programme under grant agreement No 101003890.

DISPERFIRE works on a small domain spanning hundreds of meters to tens of kilometres divided into cells small enough to accurately resolve both the fire progression and the dispersion, typically no larger than twenty by twenty meters. Over this domain it requires elevation, fuel-model, and fuel-load data. The fuel-models are associated through a table with known emission factors for the species being modelled. Furthermore, wind-speed and direction must be specified at each cell as an input. This is computed using the NUATMOS model.

NUATMOS is a meteorological diagnostic model that takes as input the topography of the domain and a single value of wind magnitude and direction. This value is then interpolated over the whole domain. Based on this first rough estimate the model quickly finds a solution of the flow field that ensures mass continuity over the prescribed topography. The input wind direction and magnitude of NUATMOS comes from the WRF mesoscale meteorological model.

The remaining inputs for the DISPERFIRE model must be provided by a fire-progression simulation that should be run on the same grid to avoid the computation of interpolations. At each ground cell that burned the inputs contain ignition-time, progression-velocity and heat released.

After reading the necessary inputs DISPERFIRE calculates, one species at a time, the mass emitted by each cell that burned according to the equations described in section 3.2.1 creates an output file containing, in netCDF file format, the mass emitted by each cell along with a field for the ignition times, and the domain cell coordinates. This is later used as an input by CHIMERE.

The Lagrangean dispersion component of DISPERFIRE that follows models smoke emissions as emissions of virtual particles whose change in position due to the wind is updated at each time-step. The concentration of the species being considered can be estimated based on the amount of particles within each cell. At ten-minute intervals, an output of the concentrations of the whole domain is saved in netCDF file format. These output files contain the relevant information for local stakeholders, such as firefighters, regarding the forecast of concentrations of air-pollutants in the area surrounding the fire.

The local scale simulations run by DISPERFIRE provide the necessary wildfire emission for CHIMERE to run. However, for each species and wildfire simulation a different netCDF file was created. The fire emissions accounted for by CHIMERE, on the other hand, are stored in a single daily file with hourly emissions of all relevant species in the whole computational domain. Being a mesoscale model CHIMERE uses a much coarser cell resolution and different vertical levels than the ones found used in DISPERFIRE. To bridge these gaps an interpolation procedure is first performed.

Firstly, information about the CHIMERE parameters being used such as the list of required species, their molar masses, its coordinate reference system, and the mesh coordinates is obtained. Based on this an empty CHIMERE netCDF emissions file for the required day is created. A unit conversion is then performed from mass (used by DISPERFIRE) to molecules (used by CHIMERE), based on the molar mass of each species.

Next, for each DISPERFIRE simulation a coordinate reference system transformation to CHIMERE is carried out. Thus, both the coarse regional domain (CHIMERE) and the fine local domain (DISPERFIRE) are on the same reference system. A correspondence between cells from both domains is performed, assigning to each cell in the fine domain an index of a cell in the coarse domain, based on the shortest Euclidean distance. All hours of the day are then iterated upon. DISPERFIRE cells emitting within half-hour

This project has received funding from the European Union's Horizon 2020 research and innovation programme under grant agreement No 101003890.

of the time of day being considered are added to the corresponding cell in the CHIMERE domain. This ensures that the total emitted mass is never altered except by numerical precision errors. Next the emissions now in the CHIMERE cells that represent the molecules of a given species emitted during that hour are converted to molecules $s^{-1}$. CHIMERE requires as input not molecules $s^{-1}$ but a flux of molecules $cm^{-2}$ $s^{-1}$. The unit conversion makes use of functions found in the CHIMERE source code that first calculate the position of the cell corners in 3D and then the area of the surface connecting them. Finally, vertical allocation of the CHIMERE emissions is based on a general plume rise profile. A text file with the fraction of emissions to be allocated at each vertical level must be provided which is applied throughout the whole domain.

In addition to the wildfire emissions interpolated from DISPERFIRE, the CHIMERE simulations also consider anthropogenic, mineral dust, biogenic and sea salt emissions. WRF-CHIMERE is then run in forecast mode. It outputs daily files with the 3D concentrations of all considered species with hourly resolution. The ground level concentration forecast can then be used to assess the health impact of wildfire smoke along with other pollution sources. This can be particularly relevant information for municipalities, civil protection agencies, hospitals.

As a means of assessing the functionalities of the DISPERFIRE-CHIMERE coupling a case study was carried out. A controlled burn that had been previously performed in Portugal for which ample data was available was chosen for this purpose.

The prescribed fire was carried out on the 1$^{st}$ of March 2019 in the North of Portugal near Vila Real. During the experiment meteorological data was obtained, with a mobile monitoring station, as well as the characteristics of the fuel, based on aerial imagery. With this input the fire-line progression was estimated using the FARSITE model. The data from the meteorological station was used to run NUATMOS, providing the wind field within the computational domain. The fuel consisted of shrubland and was estimated to have an averaged load of 5 $kg.m^{-2}$, while the averaged emission factor for PM10 was 20 g/kg of fuel burned, and a burn efficiency of 100% due to the nature of the shrubland was assumed.

The DISPERFIRE domain was set to 5 m × 5 m resolution spanning 600 m × 400 m. The fire progression simulations contained progression velocity, heat released and the time that the cell started burning. The fuel map developed specifically for this case study was converted to the input format of DISPERFIRE. Thereafter the emission estimation was carried out as described in section 3.2.1 resulting in a total emission of 2643 kg of PM10.

Once the emission outputs of DISPERFIRE were available, the conversion of the PM10 fields to the CHIMERE requirements was carried out using the algorithm previously described and assuming that all emissions were injected at the lowest pressure level. This last assumption is reasonable in the case of small fires. CHIMERE was then run with the newly created emission files for one day. The WRF input datasets were the same ones as those used in the case-study of section 4.3 as was the case of the CHIMERE chemical boundary conditions and emissions, excluding wildfires. To maintain a low computational load a domain with a 5 km resolution was chosen solely over continental Portugal.

The results for the most critical hours of the simulation are shown in **Figure 30**. It can be seen that the plume of PM10 follows quite closely what is to be expected during a small fire when comparing this

Copyright © FirEUrisk Consortium. All rights reserved. 

one with the case-study of Greece in section 4.3 during which smaller fires could also be seen. The maximum concentration achieved was of 590 µg $m^{-3}$ directly over the controlled burn at 13:00. This quickly decreased during the next hour to 65 µg $m^{-3}$.

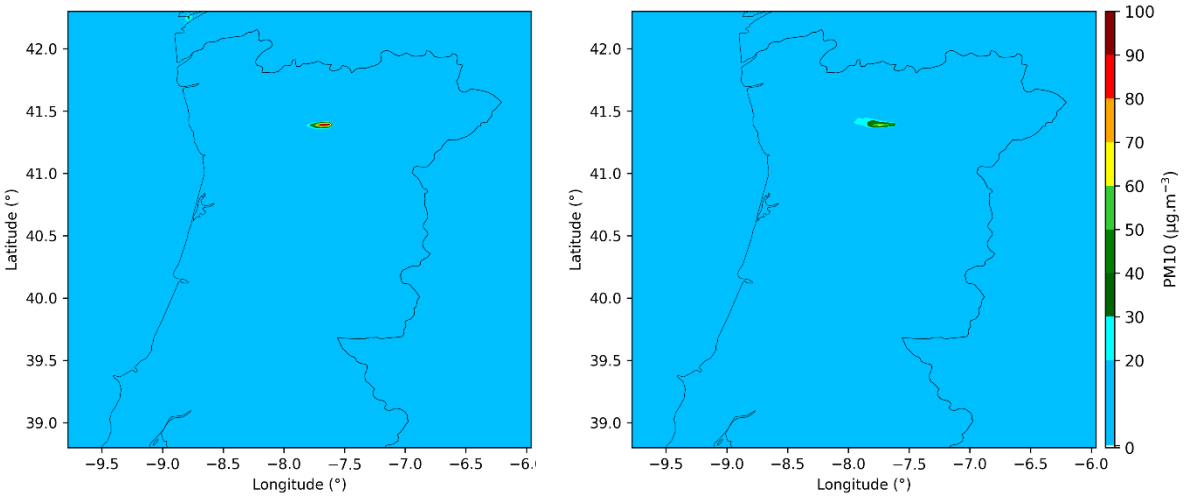



***Figure 30**. DISPERFIRE-CHIMERE PM10 concentrations during a controlled burn in Portugal.*

Copyright © FirEUrisk Consortium. All rights reserved.

# 6 Conclusions and final comments

In FirEUrisk fire progression and smoke modelling activities were developed aimed at improving our modelling practices. Available fire progression, as well as fire emissions and smoke dispersion models were reviewed to identify modelling approaches adequate to be part of FirEUrisk. The selected models and approaches were applied on FirEUrisk DS and PS to more accurately assess their features and efficacy. The successful application of modelling tools to FirEUrisk case studies, such as Ukraine (DA15), Portugal (PS3) and Greece (PS5) allowed identifying their main potentialities and to adapt them to be integrated in the FirEUrisk smoke modelling system.

The application of the selected models and approaches, carefully chosen for their relevance and potential impact, was undertaken to gain deeper insights into their characteristics and to evaluate their performance. The outcome of this exercise has provided valuable feedback, essential in refining these systems for future implementations and integration, ensuring that they are optimally tailored to the needs of the FirEUrisk project.

Finally, a local scale fire progression and smoke dispersion modelling system – IMFIRE-DISPERFIRE - was developed and its integration in an online platform is nowadays under conclusion. This system could be very useful to simulate fire behaviour during small fires (one example is its application to better prepare prescribed burnings). Moreover, and considering that smoke is a multi-scale process, a modelling system – DISPERFIRE-CHIMERE - composed of a local scale dispersion model and a regional scale chemical transport model was build and tested with a very simple and well-known case. This system will be operationally tested for 2024 summer season and, in the meanwhile, its inclusion in the FirEUrisk platform will start to be done.

With these modelling developments, FirEUrisk is contributing to the state-of-the-art on modelling tools able to simulate and forecast fire progression, emissions and smoke dispersion in a spatial and temporal scale adequate to national, regional and local stakeholders needs. Thus, FirEUrisk is promoting the improvement of the response to reduce the risk of high-impact fires, and upgrading fire behaviour modelling tools to better address extreme fire behaviour, including smoke emission and dispersion.

Copyright © FirEUrisk Consortium. All rights reserved.

## References

ADAI: Associação para o Desenvolvimento da Aerodinâmica Industrial. 2019. Análise dos Incêndios florestais ocorridos a 15 de Outubro de 2017. CEIF, Universidade de Coimbra.

Ager, A.A., Palaiologou, P., Evers, C.R., Day, M.A., Ringo, C., Short, K., 2019. Wildfire exposure to the wildland urban interface in the western US. Appl. Geogr. 111, 102059. https://doi.org/10.1016/j.apgeog.2019.102059

Akagi, S.K., Burling, I.R., Mendoza, A., Johnson, T.J., Cameron, M., Griffith, D.W.T., Paton-Walsh, C., Weise, D.R., Reardon, J., Yokelson, R.J., 2014. Field measurements of trace gases emitted by prescribed fires in southeastern US pine forests using an open-path FTIR system. Atmos. Chem. Phys. 14, 199–215. https://doi.org/10.5194/acp-14-199-2014

Akagi, S.K., Yokelson, R.J., Wiedinmyer, C., Alvarado, M.J., Reid, J.S., Karl, T., Crounse, J.D., Wennberg, P.O. 2011. Emission factors for open and domestic biomass burning for use in atmospheric models. Atmospheric Chemistry and Physics 11, 4039–4072. https://doi:10.5194/acp-11-4039-2011.

Albini, F.A. 1982. Response of Free-Burning Fires to Nonsteady Wind. Combustion Science and Technology 29, 225–241. https://doi:10.1080/00102208208923599.

Alexander, M.E. 1985. Estimating the length-to-breadth ratio of elliptical forest fire patterns. pp. 287-304 Proc. 8th Conf. Fire and Forest Meteorology.

Alves, C., Vicente, A., Nunes, T., Gonçalves, C., Fernandes, A.P., Mirante, F., Tarelho, L., Sánchez de la Campa, A.M., Querol, X., Caseiro, A., Monteiro, C., Evtyugina, M., Pio, C., 2011. Summer 2009 wildfires in Portugal: Emission of trace gases and aerosol composition. Atmos. Environ. 45, 641–649. https://doi.org/10.1016/j.atmosenv.2010.10.031

Anderson, H.E. 1982. Aids to Determining Fuel Models For Estimating Fire Behavior. (Gen. Tech. Rep. INT-GTR-122. Ogden, Utah: U.S. Department of Agriculture, Forest Service, Intermountain Forest and Range Experiment Station. 22p. https://doi:10.2737/INT-GTR-122.

Anderson, H.E. 1983. Predicting wind-driven wild land fire size and shape. Res. Pap. INT -305. Ogden, UT: U.S. Department of Agriculture, Forest Service, Intermountain Forest and Range Experiment Station; 26 p.

Anderson, G.K., Sandberg, D.V., Norheim, R.A. 2004. Fire Emission Production Simulator (FEPS) User's Guide. www.fs.fed.us/pnw/fera/feps/

Copyright © FirEUrisk Consortium. All rights reserved. 

Andreae, A.O., Merlet, P., 2001. Emission of trace gases and aerosols from biomass burning. Global Biogeochem. Cycles 15, 955–966. https://doi.org/10.1029/2000GB001382

Ansari, M., Ehrampoush, M.H., 2019. Meteorological correlates and AirQ+ health risk assessment of ambient fine particulate matter in Tehran, Iran. Environ. Res. 170, 141–150. https://doi.org/10.1016/J.ENVRES.2018.11.046

Apte, J.S., Brauer, M., Cohen, A.J., Ezzati, M., Pope, C.A., 2018. Ambient PM2.5 Reduces Global and Regional Life Expectancy. Environ. Sci. Technol. Lett. 5, 546–551. https://doi.org/10.1021/acs.estlett.8b00360

Arregocés, H.A., Rojano, R., Restrepo, G., 2023. Health risk assessment for particulate matter: application of AirQ+ model in the northern Caribbean region of Colombia. Air Qual. Atmos. Heal. 16, 897–912. https://doi.org/10.1007/S11869-023-01304-5/FIGURES/5

Asgari, G., Khoshniyat, R., Karimi, F., Ebrahimi, K., Habibzadeh, K., Rahimnejad, S., 2021. Assessment of Health Impacts of PM2.5 by AirQ+ Software in the City of Sanandaj, Iran (2018-2019). J. Adv. Environ. Heal. Res. 9, 45–56. https://doi.org/10.32598/JAEHR.9.1.1200

Baldassarre, G., Pozzoli, L., Schmidt, C. C., Unal, A., Kindap, T., Menzel, W. P., Whitburn, S., Coheur, P.-F., Kavgaci, A., Kaiser, J. W. 2015. Using SEVIRI fire observations to drive smoke plumes in the CMAQ air quality model: a case study over Antalya in 2008, Atmos. Chem. Phys., 15, 8539–8558, https://doi.org/10.5194/acp-15-8539-2015.

Bayat, R., Ashrafi, K., Shafiepour Motlagh, M., Hassanvand, M.S., Daroudi, R., Fink, G., Künzli, N., 2019. Health impact and related cost of ambient air pollution in Tehran. Environ. Res. 176, 108547. https://doi.org/10.1016/J.ENVRES.2019.108547

Beresford, N.A., Barnett, C.L., Gashchak, S., Maksimenko, A., Guliaichenko, E., Wood, M.D., Izquierdo, M. 2021. Radionuclide transfer to wildlife at a 'Reference site' in the Chernobyl. Journal of Environmental Radioactivity https://doi.org/10.1016/j.jenvrad.2018.02.007

Beresford, N.A., Barnett, C.L., Gashchak, S., Maksimenko, A., Guliaichenko, E., Wood, M. D., Izquierdo, M. 2018. Radionuclide transfer to wildlife at a 'Reference Site' in the Chernobyl Exclusion Zone and resultant radiation exposures. Journal of Environmental Radioactivity, in press. 10.1016/j.jenvrad.2018.02.007

Copyright © FirEUrisk Consortium. All rights reserved. 

Benali, A.; Russo, A.; Sá, A.C.L.; Pinto, R.M.S.; Price, O.; Koutsias, N.; Pereira, J.M.C. 2016. Determining Fire Dates and Locating Ignition Points With Satellite Data. *Remote Sens. 8*, 326. https://doi.org/10.3390/rs8040326

Berlad, A.L., Yang, C.H. 1959. On the existence of steady state flames. Combustion and Flame 3, 447–452. https://doi:10.1016/0010-2180(59)90049-5.

Bessagnet, B., Pirovano, G., Mircea, M., Cuvelier, C., Aulinger, A., Calori, G., Ciarelli, G., Manders, A., Stern, R., Tsyro, S., García Vivanco, M., Thunis, P., Pay, M.-T., Colette, A., Couvidat, F., Meleux, F., Rouïl, L., Ung, A., Aksoyoglu, S., Baldasano, J. M., Bieser, J., Briganti, G., Cappelletti, A., D'Isidoro, M., Finardi, S., Kranenburg, R., Silibello, C., Carnevale, C., Aas, W., Dupont, J.-C., Fagerli, H., Gonzalez, L., Menut, L., Prévôt, A. S. H., Roberts, P., White, L. 2016. Presentation of the EURODELTA III intercomparison exercise – evaluation of the chemistry transport models' performance on criteria pollutants and joint analysis with meteorology, Atmos. Chem. Phys., 16, 12667–12701, https://doi.org/10.5194/acp-16-12667-2016

Black, C., Tesfaigzi, Y., Bassein, J.A., Miller, L.A., 2017. Wildfire smoke exposure and human health: Significant gaps in research for a growing public health issue. Environ. Toxicol. Pharmacol. 55, 186–195. https://doi.org/10.1016/j.etap.2017.08.022

Bond, T.C., Doherty, S.J., Fahey, D.W., Forster, P.M., Berntsen, T., Deangelo, B.J., Flanner, M.G., Ghan, S., Kärcher, B., Koch, D., Kinne, S., Kondo, Y., Quinn, P.K., Sarofim, M.C., Schultz, M.G., Schulz, M., Venkataraman, C., Zhang, H., Zhang, S., Bellouin, N., Guttikunda, S.K., Hopke, P.K., Jacobson, M.Z., Kaiser, J.W., Klimont, Z., Lohmann, U., Schwarz, J.P., Shindell, D., Storelvmo, T., Warren, S.G., Zender, C.S., 2013. Bounding the role of black carbon in the climate system: A scientific assessment. J. Geophys. Res. Atmos. 118, 5380–5552. https://doi.org/10.1002/jgrd.50171

Borsuk Oleksandr Anatoliyovych. 2020. Comprehensive assessment of the fire hazard of forests in the exclusion zone [Text] : Diss. cand. agr sciences : 06.03.03 / Oleksandr Anatoliyovych Borsuk; National University of Life and Environmental Sciences of Ukraine. - Kiev, 2020. - 188 p.

Bowman, D.M.J.S., Williamson, G.J., Abatzoglou, J.T., Kolden, C.A., Cochrane, M.A., Smith, A.M.S. 2017. Human exposure and sensitivity to globally extreme wildfire events. Nature Ecology and Evolution. https://doi:10.1038/s41559-016-0058.

Brito, J., Bernardo, A., Gonçalves, L.L., 2022. Atmospheric pollution and mortality in Portugal: Quantitative assessment of the environmental burden of disease using the AirQ+ model. Sci. Total Environ. 815, 152964. https://doi.org/10.1016/J.SCITOTENV.2022.152964

Copyright © FirEUrisk Consortium. All rights reserved. 

Bytnerowicz, A., Cayan, D., Riggan, P., Schilling, S., Dawson, P., Tyree, M., Wolden, L., Tissell, R., Preisler, H., 2010. Analysis of the effects of combustion emissions and Santa Ana winds on ambient ozone during the October 2007 southern California wildfires. Atmos. Environ. 44, 678–687. https://doi.org/10.1016/j.atmosenv.2009.11.014

Byram, B. 1959. Combustion of forest fuels. In 'Forest Fire: Control and Use'. pp. 61–89. ( New York, NY)

Carvalho, A., Monteiro, A., Flannigan, M., Solman, S., Miranda, A.I., Borrego, C., 2011. Forest fires in a changing climate and their impacts on air quality. Atmos. Environ. 45, 5545–5553. https://doi.org/10.1016/j.atmosenv.2011.05.010

Cascio, W.E., 2018. Wildland fire smoke and human health. Sci. Total Environ. 624, 586–595. https://doi.org/10.1016/j.scitotenv.2017.12.086

Chuvieco, E., Yebra, M., Martino, S., Thonicke, K., Gómez-Giménez, M., San-Miguel, J., Oom, D., Velea, R., Mouillot, F., Molina, J.R., Miranda, A.I., Lopes, D., Salis, M., Bugaric, M., Sofiev, M., Kadantsev, E., Gitas, I.Z., Stavrakoudis, D., Eftychidis, G., Bar-Massada, A., Neidermeier, A., Pampanoni, V., Pettinari, M.L., Arrogante-Funes, F., Ochoa, C., Moreira, B., Viegas, D., 2023. Towards an Integrated Approach to Wildfire Risk Assessment: When, Where, What and How May the Landscapes Burn. Fire 6. https://doi.org/10.3390/fire6050215

Chuvieco, E., Yue, C., Heil, A., Mouillot, F., Alonso-Canas, I., Padilla, M., Pereira, J.M., Oom, D., Tansey, K. 2016. A new global burned area product for climate assessment of fire impacts. Global Ecology and Biogeography 25, 619–629. https://doi:10.1111/geb.12440.

Clinton, N.E., Gong, P., Scott, K., 2006. Quantification of pollutants emitted from very large wildland fires in Southern California, USA. Atmos. Environ. 40, 3686–3695. https://doi.org/10.1016/j.atmosenv.2006.02.016

Colette, A., Andersson, C., Manders, A., Mar, K., Mircea, M., Pay, M.-T., Raffort, V., Tsyro, S., Cuvelier, C., Adani, M., Bessagnet, B., Bergström, R., Briganti, G., Butler, T., Cappelletti, A., Couvidat, F., D'Isidoro, M., Doumbia, T., Fagerli, H., Granier, C., Heyes, C., Klimont, Z., Ojha, N., Otero, N., Schaap, M., Sindelarova, K., Stegehuis, A. I., Roustan, Y., Vautard, R., van Meijgaard, E., Vivanco, M. G., Wind, P. 2017. EURODELTA-Trends, a multi-model experiment of air quality hindcast in Europe over 1990–2010, Geosci. Model Dev., 10, 3255–3276, https://doi.org/10.5194/gmd-10-3255-2017.

Copyright © FirEUrisk Consortium. All rights reserved. 

Costa, S., Ferreira, J., Silveira, C., Costa, C., Lopes, D., Relvas, H., Borrego, C., Roebeling, P., Miranda, A.I., Paulo Teixeira, J., 2014. Integrating health on air quality assessment - Review report on health risks of two major european outdoor air pollutants: PM and NO<inf>2</inf> J. Toxicol. Environ. Heal. - Part B Crit. Rev. 17. https://doi.org/10.1080/10937404.2014.946164

Crutzen, P.J., Heidt, L.E., Krasnec, J.P., Pollock, W.H., Seiler, W., 1979. Biomass burning as a source of atmospheric gases CO, H2, N2O, NO, CH3Cl and COS. Nature 282, 253–256. https://doi.org/10.1038/282253a0

Cruz, M.G., Alexander, M.E. 2013. Uncertainty associated with model predictions of surface and crown fire rates of spread, Environmental Modelling & Software, Volume 47, Pages 16-28, https://doi.org/10.1016/j.envsoft.2013.04.004.

Darmenov A, da Silva A.M. 2015. The Quick Fire Emissions Dataset (QFED) - Documentation of versions 2.1, 2.2 and 2.4.

De Marco, A., Garcia-Gomez, H., Collalti, A., Khaniabadi, Y.O., Feng, Z., Proietti, C., Sicard, P., Vitale, M., Anav, A., Paoletti, E., 2022. Ozone modelling and mapping for risk assessment: An overview of different approaches for human and ecosystems health. Environ. Res. 211, 113048. https://doi.org/10.1016/J.ENVRES.2022.113048

Dennekamp, M., Straney, L.D., Erbas, B., Abramson, M.J., Keywood, M., Smith, K., Sim, M.R., Glass, D.C., Del Monaco, A., Haikerwal, A., Tonkin, A.M., 2015. Forest fire smoke exposures and out-of-hospital cardiac arrests in Melbourne, Australia: A case-crossover study. Environ. Health Perspect. 123, 959–964. https://doi.org/10.1289/ehp.1408436

DGT, (Direção Geral do Território), 2018. Cartografia de Uso e Ocupação do Solo (COS, CLC e Copernicus) [WWW Document]. URL https://snig.dgterritorio.gov.pt/rndg/srv/por/catalog.search#/metadata/b498e89c-1093-4793-ad22-63516062891b (accessed 10.19.18).

Dold, J.W., Zinoviev, A., Weber. 2006. Nonlocal flow effects in bushfire spread rates. http://eprints.maths.manchester.ac.uk/.

Draxler, R., Hess, G. 1998. An overview of the HYSPLIT_4 modelling system for trajectories. Aust. Meteorol. Mag.. 47.

Copyright © FirEUrisk Consortium. All rights reserved. 

Dupuy, J.L., Maréchal, J., Portier, D., Valette, J.C. 2011. The effects of slope and fuel bed width on laboratory fire behaviour. International Journal of Wildland Fire 20, 272–288. https://doi:10.1071/WF09075.

ECMWF: European Centre for Medium-Range Weather Forecast (2022) ERA5 hourly data on pressure levels from 1979 to present. Copernicus Climate Change Service (C3S) Climate Data Store (CDS). [Accessed March 2022]

EEA, (European Environment Agency), 2019. EMEP/EEA air pollutant emission inventory guidebook 2019. 11.B Forest Fires.pdf. EA Report No 13/2019. doi:10.2800/293657.

EFFIS (2022) Rapid Damage Assessment – MODIS Burnt Areas. (European Forest Fire Information System) Available at https://effis.jrc.ec.europa. eu/about-effis/technical-background/rapid-damage-assessment

Egerstrom, N., Rojas-Rueda, D., Martuzzi, M., Jalaludin, B., Nieuwenhuijsen, M., So, R., Lim, Y.H., Loft, S., Andersen, Z.J., Cole-Hunter, T., 2023. Health and economic benefits of meeting WHO air quality guidelines, Western Pacific Region. Bull. World Health Organ. 101, 130. https://doi.org/10.2471/BLT.22.288938

Elliott, C.T., Henderson, S.B., Wan, V., 2013. Time series analysis of fine particulate matter and asthma reliever dispensations in populations affected by forest fires. Environ. Heal. A Glob. Access Sci. Source 12, 1–9. https://doi.org/10.1186/1476-069X-12-11

EMEP/Centre on Emission Inventories and Projections database (2021) EMEP gridding 2021/2019. Available at https://webdab01. umweltbundesamt.at/download/gridding2021/2019/ [retrieved March 2022]

Fernandes, A.P., Lopes, D., Sorte, S., Monteiro, A., Gama, C., Reis, J., Menezes, I., Osswald, T., Borrego, C., Almeida, M., Ribeiro, L.M., Viegas, D.X., Miranda, A.I., 2022. Smoke emissions from the extreme wildfire events in central Portugal in October 2017. Int. J. Wildl. Fire 1–13. https://doi.org/10.1071/WF21097

Finney, M.A. 1998. FARSITE: Fire Area Simulator-model development and evaluation. Res. Pap. RMRS-RP-4, Revised 2004, Ogden, UT: U.S. Department of Agriculture, Forest Service, Rocky Mountain Research Station. 47 p.

Copyright © FirEUrisk Consortium. All rights reserved. 

Finney, M.A. 2004. FARSITE: Fire Area Simulator–model development and evaluation. Research Paper RMRS-RP-4 Revised. Ogden, UT: U.S. Department of Agriculture, Forest Service, Rocky Mountain Research Station. (1,667 KB; 47 pages)

Finney, M.A., Cohen, J.D., Forthofer, J.M., McAllister, S.S., Gollner, M.J., Gorham, D.J., Saito, K., Akafuah, N.K., Adam, B.A., English, J.D., Dickinson, R.E. 2015. Role of buoyant flame dynamics in wildfire spread. Proceedings of the National Academy of Sciences of the United States of America 112, 9833–9838. https://doi:10.1073/pnas.1504498112.

Freeborn, P.H., Wooster, M.J., Hao, W.M., Ryan, C.A., Nordgren, B.L., Baker, S.P., Ichoku, C., 2008. Relationships between energy release, fuel mass loss, and trace gas an aerosol emissions during laboratory biomass fires. J. Geophys. Res. Atmos. 113, 1–17. https://doi.org/10.1029/2007JD008679

Garcia-Menendez, F., Hu, Y., Mehmet T., Odman, M.T. 2014. Simulating smoke transport from wildland fires with a regional-scale air quality model: Sensitivity to spatiotemporal allocation of fire emissions, Science of The Total Environment, Volume 493, Pages 544-553, https://doi.org/10.1016/j.scitotenv.2014.05.108.

Giannaros, T.M., Papavasileiou, G., Lagouvardos, K., Kotroni, V., Dafis, S., Karagiannidis, A., Dragozi, E. 2022. Meteorological analysis of the 2021 extreme wildfires in Greece: lessons learned and implications for early warning of the potential for pyroconvection. Atmosphere 13, 475. https://doi:10.3390/atmos13030475

Gifford, F. 1982. Horizontal diffusion in the atmosphere: A Lagrangian-dynamical theory, Atmospheric Environment, Volume 16, Issue 3, Pages 505-512, https://doi.org/10.1016/0004-6981(82)90159-7.

Giglio, L., van der Werf, G.R., Randerson, J.T., Collatz, G.J., Kasibhatla, P.S. (2006) Global estimation of burned area using MODIS active fire observations, Atmos. Chem. Phys., 6, 957–974.

Giglio, L., Boschetti, L., Roy, D.P., Humber, M.L., Justice, C.O. 2018. The Collection 6 MODIS burned area mapping algorithm and product, Remote Sensing of Environment, Volume 217, Pages 72-85, https://doi.org/10.1016/j.rse.2018.08.005.

Giglio, L., Hall, J.V., Schroeder, W., Justice, C.O. 2021. MODIS/Terra thermal anomalies/fire 5-min L2 swath 1km. doi:10.5067/MODIS/ MOD14.NRT.061 [retrieved March 2021]

Haikerwal, A., Akram, M., Monaco, A. Del, Smith, K., Sim, M.R., Meyer, M., Tonkin, A.M., Abramson, M.J., Dennekamp, M., 2015. Impact of fine particulate matter (PM2.5) exposure during

Copyright © FirEUrisk Consortium. All rights reserved. 

wildfires on cardiovascular health outcomes. J. Am. Heart Assoc. 4, 1–10. https://doi.org/10.1161/JAHA.114.001653

Haikerwal, A., Akram, M., Sim, M.R., Meyer, M., Abramson, M.J., Dennekamp, M., 2016. Fine particulate matter (PM2.5) exposure during a prolonged wildfire period and emergency department visits for asthma. Respirology 21, 88–94. https://doi.org/10.1111/resp.12613

Hellenic Fire Service (2021) Event log - forest fires 2021. Available at https://www.fireservice.gr/en US/synola-dedomenon [retrieved June 2022]

Héroux, M.-E., Anderson, H.R., Atkinson, R., Brunekreef, B., Cohen, A., Forastiere, F., Hurley, F., Katsouyanni, K., Krewski, D., Krzyzanowski, M., Künzli, N., Mills, I., Querol, X., Ostro, B., Walton, H., 2015. Quantifying the health impacts of ambient air pollutants: recommendations of a WHO/Europe project. Int. J. Public Health 60, 619–627. https://doi.org/10.1007/s00038-015-0690-y

Hodzic, A., Madronich, S., Bohn, B., Massie, S., Menut, L., and Wiedinmyer, C. 2007. Wildfire particulate matter in Europe during summer 2003: meso-scale modeling of smoke emissions, transport and radiative effects, Atmos. Chem. Phys., 7, 4043–4064.

Holiaka, D.M., Levchuk, S.E., Kashparov, V.A., Holiaka, M.A., Yoschenko, L.V., Otreshko, L.N., Kosarchuk, O.V., Lazarev, N.M. 2020a. Vertical distribution of 90sr in soil profiles and its uptake by scots pine (Pinus sylvestris l.) wood growing within the Chernobyl exclusion zone. Nuclear Physics and Atomic Energy, 21(2), 157–165. https://doi.org/10.15407/jnpae2020.02.157

Holiaka, D.M., Levchuk, S.E., Yoschenko, V.I., Kashparov, V.A., Yoschenko, L.V., Holiaka, M.A., P avliuchenko, V.V., Diachuk, P.P., Zadorozhniuk, R.M., Morozova, V.S. 2020b. 90SR and 137CS inventories in the depots and biogenic fluxes of the typical forest stands in the chernobyl exclusion zone. In Nuclear Physics and Atomic Energy (Vol. 21, Issue 3, pp. 256–264). https://doi.org/10.15407/JNPAE2020.03.256

Hopke, P.K., Nazari, S.S.H., Hadei, M., Yarahmadi, M., Kermani, M., Yarahmadi, E., Shahsavani, A., 2018. Spatial and Temporal Trends of Short-Term Health Impacts of PM2.5 in Iranian Cities; a Modelling Approach (2013-2016). Aerosol Air Qual. Res. 18, 497–504. https://doi.org/10.4209/AAQR.2017.09.0325

Ichoku, C. Ellison, L. 2014. Global top-down smoke-aerosol emissions estimation using satellite fire radiative power measurements. Atmospheric Chemistry and Physics 14, 6643–6667. https://doi:10.5194/acp-14-6643-2014.

Copyright © FirEUrisk Consortium. All rights reserved. 

Ichoku, C., Ellison, L.T., Yue, Y., Wang, J., Kaiser, J.W., 2016. Fire and Smoke Remote Sensing and Modeling Uncertainties, in: Natural Hazard Uncertainty Assessment. American Geophysical Union (AGU), pp. 215–230. https://doi.org/https://doi.org/10.1002/9781119028116.ch14

IAEA, 2010. Handbook of parameter values for the prediction of radionuclide transfer in terrestrial and fresh-water environments. Vienna: IAEA-TRS-472, 194p. http://www-pub.iaea.org/MTCD/publications/PDF/trs472_web.pdf

ICNF, (Instituto da Conservação da Natureza e das Florestas), 2019. IFN6 - Inventário Florestal Nacional 6 [WWW Document]. URL https://www.icnf.pt/florestas/flestudosdocumentosestatisticasindicadores (accessed 12.5.19).

Jaffe, D., Chand, D., Hafner, W., Westerling, A., Spracklen, D., 2008. Influence of fires on O3 concentrations in the western U.S. Environ. Sci. Technol. 42, 5885–5891. https://doi.org/10.1021/es800084k

Jariwala, N., Kapadia, D., 2022. Estimation of health impact using AirQ+ model attributed to surface ozone in sub-regions of Surat city, India. J. Air Pollut. Heal. 7, 247–260. https://doi.org/10.18502/JAPH.V7I3.10539

Johnston, F.H., Henderson, S.B., Chen, Y., Randerson, J.T., Marlier, M., DeFries, R.S., Kinney, P., Bowman, D.M.J.S., Brauer, M., 2012. Estimated global mortality attributable to smoke from landscape fires. Environ. Health Perspect. 120, 695–701. https://doi.org/10.1289/ehp.1104422

Kaiser, J.W., Heil, A., Andreae, M.O., Benedetti, A., Chubarova, N., Jones, L., Morcrette, J.J., Razinger, M., Schultz, M.G., Suttie, M., van der Werf, G.R., 2012. Biomass burning emissions estimated with a global fire assimilation system based on observed fire radiative power. Biogeosciences 9, 527–554. https://doi.org/10.5194/bg-9-527-2012

Kashparov, V., Levchuk, S., Zhurba, M., Protsak, V., Beresford, N.A., Chaplow, J.S., 2020. Spatial radionuclide deposition data from the 60 km radial area around the Chernobyl Nuclear Power Plant: Results from a sampling survey in 1987. Earth Syst. Sci. Data 12, 1861–1875. https://doi.org/10.5194/essd-12-1861-2020

Keywood, M., Cope, M., Meyer, C.P.M., Iinuma, Y., Emmerson, K., 2015. When smoke comes to town: The impact of biomass burning smoke on air quality. Atmos. Environ. 121, 13–21. https://doi.org/10.1016/j.atmosenv.2015.03.050

Copyright © FirEUrisk Consortium. All rights reserved. 

Kliengchuay, W., Srimanus, W., Srimanus, R., Kiangkoo, N., Moonsri, K., Niampradit, S., Suwanmanee, S., Tantrakarnapa, K., 2022. The association of meteorological parameters and AirQ+ health risk assessment of PM2.5 in Ratchaburi province, Thailand. Sci. Rep. 12, 12971. https://doi.org/10.1038/S41598-022-17087-1

Knorr, W., Lehsten, V., Arneth, A., 2012. Determinants and predictability of global wildfire emissions. Atmos. Chem. Phys. 12, 6845–6861. https://doi.org/10.5194/acp-12-6845-2012

Kochanski, A.K., Jenkins, M. A., Yedinak, K., Mandel, J., Beezley, J., Lamb, B. 2016. Toward an integrated system for fire, smoke and air quality simulations. International Journal of Wildland Fire. 25(5):534–546.

Kochanski, A. K., Mallia, D. V., Fearon,M. G., Mandel, J., Souri, A. H., Brown, T. 2019. Modeling wildfiresmoke feedback mechanisms using a coupled fire-atmosphere model with a radiatively active aerosol scheme. Journal of Geophysical Research: Atmospheres,124, 9099–9116. https://doi.org/10.1029/2019JD030558

Kukkonen, J., Olsson, T., Schultz, D. M., Baklanov, A., Klein, T., Miranda, A. I., Monteiro, A., Hirtl, M., Tarvainen, V., Boy, M., Peuch, V.-H., Poupkou, A., Kioutsioukis, I., Finardi, S., Sofiev, M., Sokhi, R., Lehtinen, K. E. J., Karatzas, K., San José, R., Astitha, M., Kallos, G., Schaap, M., Reimer, E., Jakobs, H., Eben, K. 2012. A review of operational, regional-scale, chemical weather forecasting models in Europe, Atmos. Chem. Phys., 12, 1–87, https://doi.org/10.5194/acp-12-1-2012.

Langmann, B., Duncan, B., Textor, C., Trentmann, J., van der Werf, G.R., 2009. Vegetation fire emissions and their impact on air pollution and climate. Atmos. Environ. 43, 107–116. https://doi.org/10.1016/j.atmosenv.2008.09.047

Lee, B., Seungwan, C., Seung-Kii, L., Choongshik, W., Joowon, P. 2019. Development of a Smoke Dispersion Forecast System for Korean Forest Fires. Forests. 10. 219. 10.3390/f10030219.

Liousse, C., Guillaume, B., Grégoire, J.M., Mallet, M., Galy, C., Pont, V., Akpo, A., Bedou, M., Castéra, P., Dungall, L., Gardrat, E., Granier, C., Konaré, A., Malavelle, F., Mariscal, A., Mieville, A., Rosset, R., Serça, D., Solmon, F., Tummon, F., Assamoi, E., Yoboué, V., Van Velthoven, P., 2010. Updated African biomass burning emission inventories in the framework of the AMMA-IDAF program, with an evaluation of combustion aerosols. Atmos. Chem. Phys. 10, 9631–9646. https://doi.org/10.5194/acp-10-9631-2010

Liu, Y., Kochanski, A.K., Baker, K.R., Mell, W.E., Linn, R.R.; Paugam, R., Mandel, J., Fournier, A., Jenkins, M.A, Goodrick, S.L., Achtemeier, G.L.; Zhao, F., Ottmar, R.D.; French, N.H.F., Larkin, N.K., Brown,

Copyright © FirEUrisk Consortium. All rights reserved. 

T.J., Hudak, A.T., Dickinson, M.B., Potter, B.E., Clements, C.B., Urbanski, S.P., Prichard, S.J., Watts, A.C., McNamara, D. 2019. Fire behaviour and smoke modelling: model improvement and measurement needs for next-generation smoke research and forecasting systems. International Journal of Wildland Fire 28(8):570-588.

Li, Y., Tong, D., Ngan, F., Cohen, M., Stein, A., Kondragunta, A., Zhang, S., Ichoku, X., Hyer, C., Kahn, E., Ralph. 2020. Ensemble PM 2.5 Forecasting during the 2018 Camp Fire Event Using the HYSPLIT Transport and Dispersion Model. Journal of Geophysical Research: Atmospheres. 125. 10.1029/2020JD032768.

Lopes, A.M.G., M.G. Cruz, M.G., Viegas, D.X. 2002. FireStation — an integrated software system for the numerical simulation of fire spread on complex topography, Environmental Modelling & Software, Volume 17, Issue 3, Pages 269-285,

Martins, V., Miranda, A.I., Carvalho, A., Schaap, M., Borrego, C., Sá, E., 2012. Impact of forest fires on particulate matter and ozone levels during the 2003, 2004 and 2005 fire seasons in portugal. Sci. Total Environ. 414, 53–62. https://doi.org/10.1016/j.scitotenv.2011.10.007

Mandel, J., Beezley, J.D., Kochanski, A.K. 2011. Coupled atmosphere-wildland fire modeling with WRF 3.3 and SFIRE 2011. Geoscientific Model Development. 4(3):591–610.

Matsala, M., Cornelius, S., Andrii, B., Petro, D., Roman, Z., Maksym, B., Rupert, S. 2021. The impact of radioactive contamination on tree regeneration and forest development in the Chernobyl Exclusion Zone. Applied Vegetation Science. 25. 10.1111/avsc.12631.

Mendes-Lopes, J.M.C., Ventura, J.M.P., Amaral, J.M.P. 2003. Flame characteristics, temperature - time curves, and rate of spread in fires propagating in a bed of Pinus pinaster needles. International Journal of Wildland Fire 12, 67. doi:10.1071/WF02063.

Menut, L., Flamant, C., Turquety, S., Deroubaix, A., Chazette, P., Meynadier, R. 2018. Impact of biomass burning on pollutant surface concentrations in megacities of the Gulf of Guinea. Atmospheric Chemistry and Physics 18, 2687–2707. https://doi:10.5194/acp-18-2687-2018

Mieville, A., Granier, C., Liousse, C., Guillaume, B., Mouillot, F., Lamarque, J.F., Grégoire, J.M., Pétron, G. 2010. Emissions of gases and particles from biomass burning during the 20th century using satellite data and an historical reconstruction. Atmospheric Environment 44, 1469–1477. https://doi:10.1016/j.atmosenv.2010.01.011.

Copyright © FirEUrisk Consortium. All rights reserved. 

Miranda, A.I., 2004. An integrated numerical system to estimate air quality effects of forest fires. Int. J. Wildl. Fire 13, 217–226. https://doi.org/10.1071/WF02047

Miranda, A.I., Amorim, J.H., Martins, V., Pimentel, C., Rodrigues, R., Tavares, R., Borrego, C., 2008. Numerical modelling of the impact of wildland-urban interface fires on Coimbra air quality, in: WIT Transactions on Ecology and the Environment. pp. 333–342. https://doi.org/10.2495/FIVA080331

Miranda, A.I., Borrego, C., Martins, H., Martins, V., Amorim, J.H., Valente, J., Carvalho, A., 2009. Forest Fire Emissions and Air Pollution in Southern Europe., in: Chuvieco, E. (Ed.), Earth Observation of Wildland Fires in Mediterranean Ecosystems. Springer, Berlin, Heidelberg, pp. 171–187. https://doi.org/10.1007/978-3-642-01754-4_12

Miranda, A.I., Coutinho, M., Borrego, C., 1994. Forest fire emissions in Portugal: A contribution to global warming? Environ. Pollut. 83, 121–123. https://doi.org/https://doi.org/10.1016/0269-7491(94)90029-9

Miranda, A.I., Ferreira, J., Valente, J., Santos, P., Amorim, J.H., Borrego, C., 2005. Smoke measurements during Gestosa-2002 experimental field fires. Int. J. Wildl. Fire 14, 107–116. https://doi.org/10.1071/WF04069

Miranda, Ana Isabel, Marchi, E., Ferretti, M., Millán, M.M., 2008. Chapter 9 Forest Fires and Air Quality Issues in Southern Europe, in: Bytnerowicz, A., Arbaugh, M.J., Riebau, A.R., Andersen, C. (Eds.), Wildland Fires and Air Pollution, Developments in Environmental Science. Elsevier, pp. 209–231. https://doi.org/https://doi.org/10.1016/S1474-8177(08)00009-0

Miranda, A.I., Martins, V., Cascão, P., Amorim, J.H., Valente, J., Tavares, R., Borrego, C., Tchepel, O., Ferreira, A.J., Cordeiro, C.R., Viegas, D.X., Ribeiro, L.M., Pita, L.P., 2010. Monitoring of firefighters exposure to smoke during fire experiments in Portugal. Environ. Int. 36, 736–745. https://doi.org/10.1016/j.envint.2010.05.009

Miranda, A.I., Martins, V., Casco, P., Amorim, J.H., Valente, J., Borrego, C., Ferreira, A.J., Cordeiro, C.R., Viegas, D.X., Ottmar, R., 2012. Wildland smoke exposure values and exhaled breath indicators in firefighters. J. Toxicol. Environ. Heal. - Part A Curr. Issues 75, 831–843. https://doi.org/10.1080/15287394.2012.690686

Monks, S.A., Arnold, S.R., Chipperfield, M.P., 2012. Evidence for El Niño-Southern Oscillation (ENSO) influence on Arctic CO interannual variability through biomass burning emissions. Geophys. Res. Lett. 39, 1–6. https://doi.org/10.1029/2012GL052512

Copyright © FirEUrisk Consortium. All rights reserved. 

Monteiro, A., Vautard, R., Borrego, C., Miranda, A.I. 2005. Long-term simulations of photo oxidant pollution over Portugal using the CHIMERE model, Atmospheric Environment, Volume 39, Issue 17. Pages 3089-3101, https://doi.org/10.1016/j.atmosenv.2005.01.045.

Monteiro, A., Miranda, A.I., Borrego, C., Vautard, R. 2007. Air quality assessment for Portugal, Science of The Total Environment, Volume 373, Issue 1, Pages 22-31, https://doi.org/10.1016/j.scitotenv.2006.10.014.

Monteiro, A., Corti, P., San Miguel-Ayanz, J., Miranda, A.I., Borrego, C. 2013. The EFFIS forest fire atmospheric emission model: Application to a major fire event in Portugal. Atmospheric Environment 84, 355–362. https://doi:10.1016/j.atmosenv.2013.11.059.

Mota, B., Wooster, M. 2018. A new top-down approach for directly estimating biomass burning emissions and fuel consumption rates and totals from geostationary satellite fire radiative power (FRP), Remote Sensing of Environment, Volume 206, Pages 45-62, https://doi.org/10.1016/j.rse.2017.12.016.

Mouillot, F., Narasimha, A., Balkanski, Y., Lamarque, J.F., Field, C.B. 2006. Global carbon emissions from biomass burning in the 20th century. Geophysical Research Letters 33, 2–5. https://doi:10.1029/2005GL024707.

Nguyen, H.M., Wooster, M. 2020. Advances in the estimation of high Spatio-temporal resolution pan-African top-down biomass burning emissions made using geostationary fire radiative power (FRP) and MAIAC aerosol optical depth (AOD) data, Remote Sensing of Environment, Volume 248, 111971, https://doi.org/10.1016/j.rse.2020.111971.

Nguyen, H. M., He, J., Wooster, M. J. 2023. Biomass burning CO, PM and fuel consumption per unit burned area estimates derived across Africa using geostationary SEVIRI fire radiative power and Sentinel-5P CO data, Atmos. Chem. Phys., 23, 2089–2118, https://doi.org/10.5194/acp-23-2089-2023.

Nuryanto, D. 2015. Simulation of Forest Fires Smoke Using WRF-Chem Model with FINN Fire Emissions in Sumatera, Procedia Environmental Sciences, Volume 24, Pages 65-69, https://doi.org/10.1016/j.proenv.2015.03.010.

Oliveri Conti, G., Heibati, B., Kloog, I., Fiore, M., Ferrante, M., 2017. A review of AirQ Models and their applications for forecasting the air pollution health outcomes. Environ. Sci. Pollut. Res. 24, 6426–6445. https://doi.org/10.1007/s11356-016-8180-1

Copyright © FirEUrisk Consortium. All rights reserved. 

Osswald, T., Gama, C., Fernandes, A.P., Lopes, D., Varela, V., Miranda, A.I. 2023. Effects of the wildfires in August 2021 on the air quality of Athens through a numerical simulation. International Journal of Wildland Fire 32, 1633-1645. https://doi.org/10.1071/WF22148

Ostro, B., 2004. Outdoor Air Pollution: Assessing the Environmental Burden of Disease at National and Local Levels. Geneva,.

Ottmar, R.D., Miranda, A.I., Sandberg, D. V., 2008. Characterizing Sources of Emissions from Wildland Fires, in: Developments in Environmental Science. pp. 61–78. https://doi.org/10.1016/S1474-8177(08)00003-X

Pan, X., Ichoku, C., Chin, M., Bian, H., Darmenov, A., Colarco, P., Ellison, L., Kucsera, T., Da Silva, A., Wang, J., Oda, T., Cui, G., 2020. Six global biomass burning emission datasets: Intercomparison and application in one global aerosol model. Atmos. Chem. Phys. 20, 969–994. https://doi.org/10.5194/acp-20-969-2020

Parvez, F., Wagstrom, K., 2020. Impact of regional versus local resolution air quality modeling on particulate matter exposure health impact assessment. Air Qual. Atmos. Heal. 13, 271–279. https://doi.org/10.1007/S11869-019-00786-6/FIGURES/6

Paskevich Serhiy Anatoliyovych. 2005. Radiation weight of phytocenoses of meadows and fallows of the Chornobyl exclusion zone at the stage of the late phase of the accident [Text] : Diss. cand. biological sciences: 03.00.01 / Serhii Anatoliyovych Paskevich; National Academy of Sciences of Ukraine, Institute of Prob. NPP safety. - Chernobyl, 188 p.

Pastor, E., Zárate, L., Planas, E., Arnaldos, J. 2003. Mathematical models and calculation systems for the study of wildland fire behaviour. Prog Energy Combust Sci 29, 139–153. https://doi:10.1016/S0360-1285(03)00017-0.

Péré, J.C., Bessagnet, B., Mallet, M., Waquet, F., Chiapello, I., Minvielle, F., Pont, V. and Menut, L. 2014. Direct radiative effect of the Russian wildfires and its impact on air temperature and atmospheric dynamics during August 2010. Atmospheric Chemistry and Physics, 14(4), 1999-2013. https://doi.org/10.5194/acp-14-1999-2014

Pereira, G., Freitas, S.R., Moraes, E.C., Ferreira, N.J., Shimabukuro, Y.E., Rao, V.B., Longo, K.M., 2009. Estimating trace gas and aerosol emissions over South America: Relationship between fire radiative energy released and aerosol optical depth observations. Atmos. Environ. 43, 6388–6397. https://doi.org/10.1016/j.atmosenv.2009.09.013

Copyright © FirEUrisk Consortium. All rights reserved. 

Pereira, G., Siqueira, R., Rosário, N.E., Longo, K.L., Freitas, S.R., Cardozo, F.S., Kaiser, J.W., Wooster, M.J., 2016. Assessment of fire emission inventories during the South American Biomass Burning Analysis (SAMBBA) experiment. Atmos. Chem. Phys. 16, 6961–6975. https://doi.org/10.5194/acp-16-6961-2016

Pervin, T., Gerdtham, U.G., Lyttkens, C.H., 2008. Societal costs of air pollution-related health hazards: A review of methods and results. Cost Eff. Resour. Alloc. 6. https://doi.org/10.1186/1478-7547-6-19

Petrenko, M., Kahn, R., Chin, M., Soja, A., Kucsera, T., Harshvardhan, 2012. The use of satellite-measured aerosol optical depth to constrain biomass burning emissions source strength in the global model GOCART. J. Geophys. Res. Atmos. 117. https://doi.org/10.1029/2012JD017870

Pinto, M. M., Da Camara, C. C., Trigo, I. F., Trigo, R. M., and Turkman, K. F. 2018. Fire danger rating over Mediterranean Europe based on fire radiative power derived from Meteosat, Nat. Hazards Earth Syst. Sci., 18, 515–529, https://doi.org/10.5194/nhess-18-515-2018.

Pinto, P., Silva, Á. P., Viegas, D. X., Almeida, M., Raposo, J., & Ribeiro, L. M. (2022). Influence of Convectively Driven Flows in the Course of a Large Fire in Portugal: The Case of Pedrógão Grande. Atmosphere, 13(3). https://doi.org/10.3390/atmos13030414

PNAC, (Programa Nacional para as Alterações Climática), 2002. Floresta e Produtos Florestais, Cenário de Referência.

Prichard, S., Larkin, N.S., Ottmar, R., French, N.H.F., Baker, K., Brown, T., Clements, C., Dickinson, M., Hudak, A., Kochanski, A., Linn, R., Liu, Y., Potter, B., Mell, W., Tanzer, D., Urbanski, S., Watts, A., 2019. The Fire and Smoke Model Evaluation Experiment-A plan for integrated, large fire-atmosphere field campaigns. Atmosphere (Basel). 10. https://doi.org/10.3390/atmos10020066

Prichard, S.J., Kennedy, M.C., Wright, C.S., Cronan, J.B., Ottmar, R.D., 2017. Predicting forest floor and woody fuel consumption from prescribed burns in southern and western pine ecosystems of the United States. For. Ecol. Manage. 405, 328–338. https://doi.org/10.1016/j.foreco.2017.09.025

Prichard, S.J., O'Neill, S.M., Eagle, P., Andreu, A.G., Drye, B., Dubowy, J., Urbanski, S., Strand, T.M., 2020. Wildland fire emission factors in North America: Synthesis of existing data, measurement needs and management applications. Int. J. Wildl. Fire 29, 132–147. https://doi.org/10.1071/WF19066

Copyright © FirEUrisk Consortium. All rights reserved. 

Raposo, J., Viegas, D.X., Xie, X., Almeida, M., Naian, L. 2014. Analysis of the jump fire produced by the interaction of two oblique fire fronts: comparison between laboratory and field cases. 'Advances in forest fire research'. pp. 88–94. (Imprensa da Universidade de Coimbra) https://doi:10.14195/978-989-26-0884-6_8.

Raposo, J. 2016. Extreme Fire Behaviour Associated with the Merging of Two Linear Fire Fronts. University of Coimbra. http://hdl.handle.net/10316/31020.

Raposo, J.R., Viegas, D.X., Xie, X., Almeida, M., Figueiredo, A.R., Porto, L., Sharples, J. 2018. Analysis of the physical processes associated with junction fires at laboratory and field scales. International Journal of Wildland Fire 27, 52–68. https://doi:10.1071/WF16173.

Rappold, A.G., Reyes, J., Pouliot, G., Cascio, W.E., Diaz-Sanchez, D., 2017. Community Vulnerability to Health Impacts of Wildland Fire Smoke Exposure. Environ. Sci. Technol. 51, 6674–6682. https://doi.org/10.1021/acs.est.6b06200

Reddington, C.L., Spracklen, D. V., Artaxo, P., Ridley, D.A., Rizzo, L. V., Arana, A., 2016. Analysis of particulate emissions from tropical biomass burning using a global aerosol model and long-term surface observations. Atmos. Chem. Phys. 16, 11083–11106. https://doi.org/10.5194/acp-16-11083-2016

Reid, C.E., Brauer, M., Johnston, F.H., Jerrett, M., Balmes, J.R., Elliott, C.T., 2016. Critical review of health impacts of wildfire smoke exposure. Environ. Health Perspect. 124, 1334–1343. https://doi.org/10.1289/ehp.1409277

Reid, J.S., Westphal, D.L., Curtis, C.A., Richardson, K.A., Hyer, E.J., Prins, E.M., Schmidt, C.C., Hoffman, J.P., Zhang, J., Wang, J., Christopher, S.A., Eleuterio, D.P. 2009. Global Monitoring and Forecasting of Biomass-Burning Smoke: Description of and Lessons from the Fire Locating and Modeling of Burning Emissions (FLAMBE) Program. IEEE Journal of Selected Topics in Applied Earth Observations and Remote Sensing 2, 144–162. https://doi:10.1109/JSTARS.2009.2027443.

Rémy, S., Veira, A., Paugam, R., Sofiev, M., Kaiser, J.W., Marenco, F., Burton, S.P., Benedetti, A., Engelen, R.J., Ferrare, R., Hair, J.W., 2017. Two global data sets of daily fire emission injection heights since 2003. Atmos. Chem. Phys. 17, 2921–2942. https://doi.org/10.5194/acp-17-2921-2017

Ribeiro, C., Viegas, D.X., Raposo, J., Reis, L., Sharples, J. 2023. Slope effect on junction fire with two non-symmetric fire fronts. International Journal of Wildland Fire 32, 328–335. https://doi:10.1071/WF22152.

Copyright © FirEUrisk Consortium. All rights reserved. 

Ross, D. G., Smith, I.N., Manins, P.C., Fox, D.G. 1988. Diagnostic Wind Field Modeling for Complex Terrain: Model Development and Testing. Journal of Applied Meteorology (1988-2005), vol. 27, no. 7, pp. 785–96. JSTOR, http://www.jstor.org/stable/26183717.

Rothermel, R. 1972. A mathematical model for predicting fire spread in wildland fuels. Res. Pap. INT-115. Ogden, UT: U.S. Department of Agriculture, Intermountain Forest and Range Experiment Station. 40 p.

Rothermel, R. 1983. How to predict the spread and intensity of forest and range fires. Gen. Tech. Rep. INT-143. Ogden, UT: U.S. Department of Agriculture, Forest Service, Intermountain Forest and Range Experiment Station. 161 p.

Rovira, J., Domingo, J.L., Schuhmacher, M., 2020. Air quality, health impacts and burden of disease due to air pollution (PM10, PM2.5, NO2 and O3): Application of AirQ+ model to the Camp de Tarragona County (Catalonia, Spain). Sci. Total Environ. 703, 135538. https://doi.org/10.1016/J.SCITOTENV.2019.135538

Rückerl, R., Schneider, A., Breitner, S., Cyrys, J., Peters, A., 2011. Health effects of particulate air pollution: A review of epidemiological evidence. Inhal. Toxicol. https://doi.org/10.3109/08958378.2011.593587

San-Miguel-Ayanz, J., Durrant, T., Boca, R., Libertá, G., Branco, A., de Rigo, D., Ferrari, D., Maianti, P., Artés-Vivancos, T., Oom, D., Pfeiffer, H., Nuijten, D., Leray, T. 2019. Forest fires in Europe, Middle East and North Africa 2018, Publications Office of the European Union, Luxembourg, 2019, https://doi:10.2760/1128

San-Miguel-Ayanz, J., Durrant, T., Boca, R., Maianti, P., Libertá, G., Artés-Vivancos, T., Oom, D., Branco, A., de Rigo, D., Ferrari, D., Pfeiffer, H., Grecchi, R., Onida, M., Löffler, P. 2022. Forest Fires in Europe, Middle East and North Africa 2021, Publications Office of the European Union, Luxembourg, 2022, https://doi:10.2760/34094, JRC130846.

Scott, J. H., Burgan, R. E., 2005. Standard fire behavior fuel models: A comprehensive set for use with Rothermel's surface fire spread model (RMRS-GTR-153). U.S. Department of Agriculture, Forest Service, Rocky Mountain Research Station. https://doi.org/10.2737/RMRS-GTR-153

Sebastião, R., Sorte, S., Valente, J., Miranda, A.I., Fernandes, J.M., 2019. Detecting changes in the heart rate of firefighters to prevent smoke inhalation and health effects. Evol. Syst. 10, 295–304. https://doi.org/10.1007/s12530-018-9241-0

Copyright © FirEUrisk Consortium. All rights reserved. 

Seethaler, R.K., Künzli, N., Sommer, H., Chanel, O., Herry, M., Masson, S., Vernaud, J.-C., Filliger, P., Horak, F.J., Kaiser, R., Medina, S., Puybonnieux-Texier, V., Quénel, P., Schneider, J., Studnicka, M., Heldstab, J., 2003. Economic costs of air pollution-related health impacts: An impact assessment project of Austria, France and Switzerland. Clean Air Environ. Qual. 37, 35–43.

Seiler, W., Crutzen, P., 1980. Estimates of Gross and Net Fluxes of Carbon Between. Clim. Change 2, 207–247.

Silvani, X., Morandini, F., Dupuy, J.L. 2012. Effects of slope on fire spread observed through video images and multiple-point thermal measurements. Experimental Thermal and Fluid Science 41, 99–111. https://doi:10.1016/j.expthermflusci.2012.03.021.

Silvani, X., Morandini, F., Dupuy, J.L., Susset, A., Vernet, R., Lambert, O. 2018. Measuring velocity field and heat transfer during natural fire spread over large inclinable bench. Experimental Thermal and Fluid Science 92, 184–201. https://doi:10.1016/j.expthermflusci.2017.11.020.

Silveira, C., Ferreira, J., Miranda, A.I., 2024. Health impact pathways related to air quality changes: testing two health risk methodologies over a local traffic case study. Air Qual. Atmos. Heal. https://doi.org/10.1007/s11869-024-01504-7

Silveira, C., Roebeling, P., Lopes, M., Ferreira, J., Costa, S., Teixeira, J.P., Borrego, C., Miranda, A.I., 2016. Assessment of health benefits related to air quality improvement strategies in urban areas: An Impact Pathway Approach. J. Environ. Manage. 183. https://doi.org/10.1016/j.jenvman.2016.08.079

Smith, H. 2021. 'Apocalyptic' scenes hit Greece as Athens besieged by fire. The Guardian, 7 August 2021. Available at https://www. theguardian.com/world/2021/aug/07

Sofiev, M., Ermakova, T., Vankevich, R. 2012. Evaluation of the smoke injection height from wildland fires using remote-sensing data. Atmospheric Chemistry and Physics 12, 1995–2006. doi:10.5194/acp-12-1995-2012

Sofiev, M., Vankevich, R., Ermakova, T., Hakkarainen, J., 2013. Global mapping of maximum emission heights and resulting vertical profiles of wildfire emissions. Atmos. Chem. Phys. 13, 7039–7052. https://doi.org/10.5194/acp-13-7039-2013

Sofiev, M., Vankevich, R., Lotjonen, M., Prank, M., Petukhov, V., Ermakova, T., Koskinen, J., Kukkonen, J., 2009. An operational system for the assimilation of the satellite information on wild-land fires for the needs of air quality modelling and forecasting. Atmos. Chem. Phys. 9, 6833–6847. https://doi.org/10.5194/acp-9-6833-2009

Copyright © FirEUrisk Consortium. All rights reserved. 

Spracklen, D. V., Logan, J.A., Mickley, L.J., Park, R.J., Yevich, R., Westerling, A.L., Jaffe, D.A., 2007. Wildfires drive interannual variability of organic carbon aerosol in the western U.S. in summer. Geophys. Res. Lett. 34, 2–5. https://doi.org/10.1029/2007GL030037

Stohl, A., Hittenberger, M., & Wotawa, G. 1998. Validation of the Lagrangian particle dispersion model FLEXPART against large-scale tracer experiment data. Atmospheric Environment, 32(24), 4245-4264.

Storn, R., Price, K. 1997. Differential Evolution – A Simple and Efficient Heuristic for global Optimization over Continuous Spaces. Journal of Global Optimization 11, 341–359. https://doi.org/10.1023/A:1008202821328

Sullivan, A.L. 2009. Wildland surface fire spread modelling, 1990 - 2007. 1: Physical and quasi-physical models. International Journal of Wildland Fire 18, 349. https://doi:10.1071/wf06143.

Thomas, C.M., Sharples, J.J., Evans, J.P. 2017. Modelling the dynamic behaviour of junction fires with a coupled atmosphere-fire model. International Journal of Wildland Fire 26, 331–344. https://doi:10.1071/WF16079.

Turquety, S., Menut, L., Bessagnet, B., Anav, A., Viovy, N., Maignan, F., Wooster, M., 2014. APIFLAME v1.0: High-resolution fire emission model and application to the Euro-Mediterranean region. Geosci. Model Dev. 7, 587–612. https://doi.org/10.5194/gmd-7-587-2014

Turquety, S., Menut, L., Siour, G., Mailler, S., Hadji-lazaro, J., George, M., Clerbaux, C., Hurtmans, D., Coheur, P., Paris, U., Pierre, I., Laplace, S., Ipsl L, Université S (2020) APIFLAME v2 . 0 biomass burning emissions model : impact of refined input parameters on atmospheric concentration in Portugal in summer 2016. 2981–3009.

Urbanski, S.P., 2013. Combustion efficiency and emission factors for wildfire-season fires in mixed conifer forests of the northern Rocky Mountains, US. Atmos. Chem. Phys. 13, 7241–7262. https://doi.org/10.5194/acp-13-7241-2013

Valente, J., Miranda, A.I., Lopes, A.G., Borrego, C., Viegas, D.X., Lopes, M., 2007. Local-scale modelling system to simulate smoke dispersion. Int. J. Wildl. Fire 16, 196–203. https://doi.org/10.1071/WF06085

van der Werf, G.R., Randerson, J.T., Giglio, L., Collatz, G.J., Mu, M., Kasibhatla, P.S., Morton, D.C., Defries, R.S., Jin, Y., Van Leeuwen, T.T., 2010. Global fire emissions and the contribution of deforestation,

Copyright © FirEUrisk Consortium. All rights reserved. 

savanna, forest, agricultural, and peat fires (1997-2009). Atmos. Chem. Phys. 10, 11707–11735. https://doi.org/10.5194/acp-10-11707-2010

van der Werf, G.R., Randerson, J.T., Giglio, L., Van Leeuwen, T.T., Chen, Y., Rogers, B.M., Mu, M., Van Marle, M.J.E., Morton, D.C., Collatz, G.J., Yokelson, R.J., Kasibhatla, P.S., 2017. Global fire emissions estimates during 1997-2016. Earth Syst. Sci. Data 9, 697–720. https://doi.org/10.5194/essd-9-697-2017

van Drooge, B., Sicard, M., Stohl, A., Fontal, M., Bravo, N., Muñoz, A., Lange, D., Fernández, P., Grimalt, J.O. 2016. Detection and simulation of wildfire smoke impacting a Mediterranean urban atmosphere, Atmospheric Pollution Research, Volume 7, Issue 3, Pages 494-502, https://doi.org/10.1016/j.apr.2015.12.003.

van Marle, M.J.E., Kloster, S., Magi, B.I., Marlon, J.R., Daniau, A.-L., Field, R.D., Arneth, A., Forrest, M., Hantson, S., Kehrwald, N.M., Knorr, W., Lasslop, G., Li, F., Mangeon, S., Yue, C., Kaiser, J.W., van der Werf, G.R. 2017. Historic global biomass burning emissions for CMIP6 (BB4CMIP) based on merging satellite observations with proxies and fire models (1750–2015), Geosci. Model Dev., 10, 3329–3357, https://doi.org/10.5194/gmd-10-3329-2017.

Vicente, A., Alves, C., Monteiro, C., Nunes, T., Mirante, F., Cerqueira, M., Calvo, A., Pio, C., 2012. Organic speciation of aerosols from wildfires in central Portugal during summer 2009. Atmos. Environ. 57, 186–196. https://doi.org/10.1016/j.atmosenv.2012.04.030

Vicente, A., Calvo, A., Fernandes, A.P., Nunes, T., Monteiro, C., Pio, C., Alves, C., 2017. Hydrocarbons in particulate samples from wildfire events in central Portugal in summer 2010. J. Environ. Sci. (China) 53, 122–131. https://doi.org/10.1016/j.jes.2016.02.022

Veira, A., Kloster, S., Wilkenskjeld, S., Remy, S. 2015. Fire emission heights in the climate system – part 1: Global plume height patterns simulated by ECHAM6-HAM2. Atmospheric Chemistry and Physics 15, 7155–7171. https://doi:10.5194/acp-15-7155-2015

Viegas, D.X. 2002. Fire line rotation as a mechanism for fire spread on a uniform slope. International Journal of Wildland Fire 11, 11–23. https://doi:10.1071/WF01049.

Viegas. D.X. 2004. On the existence of a steady state regime for slope and wind driven fires. International Journal of Wildland Fire 13, 101–117. https://doi:10.1071/WF03008.

Viegas, D.X. 2005. A mathematical model for forest fires blowup. Combustion Science and Technology 177, 27–51. https://doi:10.1080/00102200590883624.

Copyright © FirEUrisk Consortium. All rights reserved. 

Viegas, D.X. 2006. Parametric study of an eruptive fire behaviour model. International Journal of Wildland Fire 15, 169–177. https://doi:10.1071/WF05050.

Viegas, D. X., & Rossa, C. (2009). Fireline rotation analysis. Combustion Science and Technology, 181(12), 1495–1525. https://doi.org/10.1080/00102200903228891

Viegas, D.X., Raposo, J.R., Davim, D.A., Rossa, C.G. 2012. Study of the jump fire produced by the interaction of two oblique fire fronts. Part 1. Analytical model and validation with no-slope laboratory experiments. International Journal of Wildland Fire 21, 843–856. https://doi:10.1071/WF10155.

Viegas, D., Raposo, J., Figueiredo, A. 2013. Preliminary analysis of slope and fuel bed effect on jump behavior in forest fires. In 'Procedia Eng', 1032–1039. (Elsevier Ltd) https://doi:10.1016/j.proeng.2013.08.158.

Viegas, D.X., Pita, L.P. 2004. Fire spread in canyons. International Journal of Wildland Fire 13, 253–274. https://doi:10.1071/WF03050.

Viegas, X., Raposo, J., Ribeiro, C., Reis, L., Abouali, A., & Viegas, C. (2021). On the non-monotonic behaviour of fire spread. International Journal of Wildland Fire, 30(9), 702–719. https://doi.org/10.1071/WF21016

Viegas, X., Raposo, J., Ribeiro, C., Reis, L., Abouali, A., Ribeiro, L. M., & Viegas, C. (2022). On the intermittent nature of forest fire spread – Part 2. *International Journal of Wildland Fire*, *31*(10), 967–981. https://doi.org/10.1071/WF21098

Viegas, X., Ribeiro, C., Almeida, M., Pinto, P., Ribeiro, L. M., & Silva, Á. (2023). Field and laboratory analysis of the junction fire process in the catastrophic fire of Pedrógão Grande in June 2017. International Journal of Wildland Fire. https://doi.org/10.1071/WF22161

Viegas, D. X., Ribeiro, C., Barbosa, T. F., Rodrigues, T., & Ribeiro, L. M. (2024). A Fireline Displacement Model to Predict Fire Spread. Fire, 7(4), 121. https://doi.org/10.3390/fire7040121

Wade, D.D., Ward, D.E., 1973. An analysis of the Air Force Bomb Range Fire. USDA Forest Service, Southeastern Forest Experiment Station, Research Paper SE-105. Asheville, NC.

Ward, D.E., Hardy, C.C., 1991. Smoke emissions from wildland fires. Environ. Int. 17, 117–134. https://doi.org/10.1016/0160-4120(91)90095-8

Wettstein, Z.S., Hoshiko, S., Fahimi, J., Harrison, R.J., Cascio, W.E., Rappold, A.G., 2018. Cardiovascular and cerebrovascular emergency department visits associated with wildfire smoke exposure in California in 2015. J. Am. Heart Assoc. 7. https://doi.org/10.1161/JAHA.117.007492

Copyright © FirEUrisk Consortium. All rights reserved. 

WHO, 2021. WHO global air quality guidelines: particulate matter (PM2.5 and PM10), ozone, nitrogen dioxide, sulfur dioxide and carbon monoxide. Geneva, Switzerland.

WHO, 2013a. New emerging risks to health from air pollution – results from the survey of experts, Health risks of air pollution in Europe – HRAPIE project. World Health Organization, Copenhagen.

WHO, 2013b. Recommendations for concentration–response functions for cost–benefit analysis of particulate matter, ozone and nitrogen dioxide, Health risks of air pollution in Europe – HRAPIE project. World Health Organization, Copenhagen.

WHO, 2013c. Health effects of particulate matter: Policy implications for countries in Eastern Europe, Caucasus and central Asia. World Health Organization.

WHO, n.d. AirQ+: software tool for health risk assessment of air pollution [WWW Document]. World Heal. Organ.

WHO, (World Health Organization), 1999. Health guidelines for vegetation fire events. Geneva, Switzerland.

Wiedinmyer, C., Akagi, S.K., Yokelson, R.J., Emmons, L.K., Al-Saadi, J.A., Orlando, J.J., Soja, A.J. 2011. The Fire INventory from NCAR (FINN): A high resolution glob<al model to estimate the emissions from open burning. Geoscientific Model Development 4, 625–641. https://doi:10.5194/gmd-4-625-2011.

Wiedinmyer, C., Kimura, Y., McDonald-Buller, E. C., Emmons, L. K., Buchholz, R. R., Tang, W., Seto, K., Joseph, M. B., Barsanti, K. C., Carlton, A. G., and Yokelson, R. 2023. The Fire Inventory from NCAR version 2.5: an updated global fire emissions model for climate and chemistry applications, Geosci. Model Dev., 16, 3873–3891, https://doi.org/10.5194/gmd-16-3873-2023

Wooster, M., Roberts, G.J., Giglio, L., Roy, D.P., Freeborn, P.H., Boschetti, L., Justice, C., Ichoku, C., Schroeder, W., Davies, D., Smith, A.M.S., Setzer, A., Csiszar, I., Strydom, T., Frost, P., Zhang, T., Xu, W., de Jong, M.C., Johnston, J.M., Ellison, L., Vadrevu, K., Sparks, A.M., Nguyen, H., McCarty, J., Tanpipat, V., Schmidt, C., San-Miguel-Ayanz, J. 2021. Satellite remote sensing of active fires: History and current status, applications and future requirements, Remote Sensing of Environment, Volume 267, 112694, https://doi.org/10.1016/j.rse.2021.112694.

Yao, J., Eyamie, J., Henderson, S.B., 2016. Evaluation of a spatially resolved forest fire smoke model for population-based epidemiologic exposure assessment. J. Expo. Sci. Environ. Epidemiol. 26, 233–240. https://doi.org/10.1038/jes.2014.67

Copyright © FirEUrisk Consortium. All rights reserved. 

Xanthopoulos, G., Athansasiou, M., Kaoukis, K. 2022. Suppression versus prevention: the disastrous forest fire season of 2021 in Greece. Wildfire, Quarter 2, 18–24.

Xiaodong, X., Naian, L., Viegas, D.X., Raposo, J.R. 2014. Experimental research on upslope fire and jump fire. In 'Fire Safety Science', 1430–1442. (International Association for Fire Safety Science) https://doi:10.3801/IAFSS.FSS.11-1430.

Zhang, H., Qi, P., Guo, G., 2014. Improvement of fire danger modelling with geographically weighted logistic model. Int. J. Wildl. Fire 23, 1130–1146.

Zhu, J., Zhang, Y., Xu, X., Yan, Y., Zhu, X., Li, X., 2022. Air Pollution and Health Impacts of Atmospheric PM: Application of AirQ+ Model to Jiangsu Province in China. Int. J. Environ. Res. 16, 1–11. https://doi.org/10.1007/S41742-022-00458-X/TABLES/5

Copyright © FirEUrisk Consortium. All rights reserved. 